PHYSICS-BASED 3D MULTI-DIRECTIONAL RELOADING ALGORITHM FOR DEEP BURN HTR PRISMATIC BLOCK SYSTEMS

A Dissertation

by

TOM GOSLEE LEWIS III

Submitted to the Office of Graduate Studies of
Texas A&M University
in partial fulfillment of the requirements for the degree of

DOCTOR OF PHILOSOPHY

August 2010

Major Subject: Nuclear Engineering

PHYSICS-BASED 3D MULTI-DIRECTIONAL RELOADING ALGORITHM FOR DEEP BURN HTR PRISMATIC BLOCK SYSTEMS

A Dissertation

by

TOM GOSLEE LEWIS III

Submitted to the Office of Graduate Studies of
Texas A&M University
in partial fulfillment of the requirements for the degree of

DOCTOR OF PHILOSOPHY

Approved by:

Chair of Committee,	Pavel Tsvetkov
Committee Members,	Yassin Hassan
	Sean McDeavitt
	Guergana Petrova
Head of Department,	Raymond Juzaitis

August 2010

Major Subject: Nuclear Engineering

ABSTRACT

Physics-Based 3D Multi-Directional Reloading Algorithm for Deep Burn HTR Prismatic Block Systems. (August 2010)

Tom Goslee Lewis III, B.S.; M.S., Texas A&M University

Chair of Advisory Committee: Dr. Pavel Tsvetkov

To assure nuclear power sustainability, ongoing efforts on advanced closed-fuel cycle options and adapted open cycles have led to investigations of various strategies involving utilization of Transuranic (TRU) nuclides in nuclear reactors. Due to favorable performance characteristics, multiple studies are focused on transmutation options using High Temperature Gas-cooled Reactors (HTGRs). Prismatic HTGRs allow for 3-Dimensional (3D) fuel shuffling and prior shuffling algorithms were based on experimental block movement and/or manual block shuffle patterns. In this dissertation, a physics based 3D multi-directional reloading algorithm for prismatic deep burn very high temperature reactors (DB-VHTRs) was developed and tested to meet DB-VHTR operation constraints utilizing a high fidelity neutronics model developed for this dissertation. The high fidelity automated neutronics model allows design flexibility and metric tracking in spatial and temporal dimensions. Reduction of TRUs in DB-VHTRs utilizing full vectors of TRUs from light water reactor spent nuclear fuel has been demonstrated for both a single and two-fuel composition cores. Performance of the beginning-of-life and end-of-life (EOL) domains for multi-dimensional permutations were evaluated. Utilizing a two-fuel assembly permutation within the two-fuel system domain for a Single-Fuel vector, the developed shuffling algorithm for this dissertation has successfully been tested to meet performance objectives and operation constraints.

DEDICATION

I would like to dedicate this work to those who supported me through this process, both academically and in my personal life. I would like to thank my parents, Russelene and Tom Lewis, and sister, Andrea Black, who have always been available for the support needed to pursue this decade-long endeavor. Thanks also to my professor, Dr. Pavel Tsevetkov, for always pushing me to find my own solutions and for the guidance he gave through this research process. Thank you to my coworkers in 19a, Ayodeji Alajo, David Ames, and Megan Pritchard, who always served as a needed distraction. To my friends, Rachel Blaylock, Chris Parsons, Benjamin Wilson, Melissa Ghrist, and Josh Jarrel, that reminded me life has to be lived. I would also like to thank my Vegas friends, Claude Kabera, Alex Sulkowski, Matt & Sam Brenner, Tanya Sloma, and David Darling, for the great time we had there and the good times to come, and finally to my dog Shelly, for her loyal companionship.

ACKNOWLEDGEMENTS

I would like to express my full gratitude to all those who provide support to complete this dissertation. I am deeply indebted to my advisor Dr. Tsvetkov, whose broad knowledge, stimulating suggestions and encouragement was the leading force behind the research for and writing of this dissertation. I also would like to extend my gratitude to my committee members, Dr. Hassan, Dr. McDeavitt, and Dr. Petrova, for without their support and time, I would not have met success.

NOMENCLATURE

3-D	3 Dimensional
BOL	Beginning of Life
C/HM	Carbon to Heavy Metal
DB-VHTR	Deep Burn Very High Temperature Reactor
DOE	Department of Energy
EOL	End of Life
FP	Fission Product
GRF	Gas Cooled Fast Reactor
GWd/tHM	Gigawatt Day per Ton of Heavy Metal
HLW	High Level Waste
HTGR	High Temperature Gas-cooled Reactor
HTTR	High Temperature Test Reactor
LEU	Low Enriched Uranium
LFR	Lead Cooled Fast Reactor
LLW	Low Level Waste
LWR	Light Water Reactor
MA	Minor Actinide
MOX	Mix-Oxide
MSR	Molten Salt Reactor
MT	Metric Ton
MWth	Megawatt Thermal

MOP	Multi-Objective Problem
MSR	Molten Salt Reactor
NGNP	Next Generation Nuclear Plant
NRC	Nuclear Regulatory Commission
P&T	Partitioning and Transmutation
PyC	Pyro-Carbon
PWR	Pressurized Water Reactor
SCWCR	Super Critical Water Cooled Reactor
SFR	Sodium Cooled Fast Reactor
SNF	Spent Nuclear Fuel
TRISO	Tri-structural Isotropic
TRU	Transuranics
U.S.	United States
VHTR	Very High Temperature Reactor

TABLE OF CONTENTS

Page

LIST OF FIGURES

FIGURE Page

FIGURE Page

LIST OF TABLES

I. INTRODUCTION

The United States (U.S.) Congress mandated the disposal of high level waste (HLW) in a geological repository at Yucca Mountain. Difficulties in opening and safeguarding this facility have led to a reassessment of the U.S.'s long-term nuclear energy strategy. To assure nuclear power sustainability, ongoing efforts on advanced closed-fuel cycle options and adapted open cycles have led to investigations of various strategies involving utilization of TRU nuclides in nuclear reactors. Due to favorable performance characteristics, multiple studies are focused on transmutation options using HTGRs.

This section gives an overview of the current waste policy and possible adaptations to it. Gas reactors will be introduced, including experience and proposed systems such as the Next Generation Nuclear Plant (NGNP) and DB-VHTR. Finally an overview of multi-objective problems (MOPs) in respect to assembly shuffling will be discussed.

I.A Nuclear Waste Management

Nuclear reactors date back to 1943 and have operated commercially for over 40 years, demonstrating an excellent safety record. Currently there are over 400 nuclear power reactors operating in 31 countries, accounting for about one-fifth of the electrical generation worldwide [1]. In the U.S, commercial reactors operate under a once-through fuel cycle. At the end of this cycle, spent nuclear fuel (SNF) is considered as HLW when it is accepted for permanent disposal. This is due to the Nuclear Regulatory Commission (NRC) defining HLW as either [2]:

1. Spent reactor fuel when it is accepted for disposal.

2. Waste materials remaining after spent fuel are reprocessed.

This dissertation follows the style of the journal of *Nuclear Technology*.

The official U.S policy is for all HLW from SNF to be placed in the Yucca Mountain geological repository. The current President of the U.S., Barack Obama, has made significant endorsements of nuclear energy, most notably in the form of loan guarantees

for new power stations, and increased spending on basic research. In line with expected growth in the industry, problems with HLW are taking center stage in both federal policy and on Wall Street. The current administration is asking for a review of the once through geological repository approach. If it is decided that a geological repository can't be open, or requires TRU waste to be destroyed with a fuel cycle change, several technologies and reactors that might have been commercially prohibitive become attractive, requiring new fundamental research.

I.B Proposed Future Fuel Cycles

If it is decided that Yucca is no longer an option for all HLW, the U.S. will have to undergo a fuel cycle shift, most likely to one of the following three:

1. Partial recycling. In this scenario, a portion of the SNF is reprocessed, where a fraction of the actinide material is recovered and fabricated into new fuel, most likely in the form of mix-oxide (MOX) for thermal reactors.

2. Full fissile recycling. In this scenario all SNF is recovered and reprocessed for the extraction of Pu, U-233 and U-235 for fuel in both thermal and fast reactors. This process occurs several times over until recycling is no longer feasible.

3. Full actinide recycling. In this final scenario, all the SNF is processed and all the actinides are used as fuel in fast reactors capable of higher actinide destruction [3].

The removal of low level waste (LLW) and stable nuclides reduces the amount of nuclear waste requiring permanent disposal. Waste inventory estimates show that at the time of waste acceptance, there will be more than 70,000 tons of waste sitting at

domestic power reactor sites that are spread across 39 states [4]. This amount of waste is more than enough to completely fill the geological repository at the capacity mandated by the current U.S. law [5]. Most of this waste is a result of the operation of the U.S. light water reactor (LWR) fleet (~60% pressurized water reactors (PWR)).

An average PWR produces approximately 30 tones of SNF per year characterized by burnup levels of about 40 GWd/tHM. There are around 11.5 kg/SNF tone of TRUs composed of approximately 10 kg of Plutonium and 1.5 kg of minor actinides (MAs). The remainder consists of fission products (FPs) (~30kg) and depleted low enriched uranium (LEU) [6].

Elements labeled as TRUs have atomic numbers greater than 92 (Uranium) and are created in nuclear reactors from ^{238}U via neutron capture events and beta minus decays that result in the formation of higher elements. A subset of TRUs, MAs, is composed of Np, Am, and Cm. MAs have very different cross-sections when compared to U and Pu. For example, Np-237 and Am-241 have very large neutron capture cross-sections when compared to U-238. Furthermore, many of Np-237 and Am-241 daughter nuclides have very large fission cross-sections, thus causing the MAs to burn much faster than the U-238 found in LEU fuel [7].

TRUs are the major source of long-term radioactivity in SNF, while FPs are the major contributor to the short-term (500 years) decay heat, radioactivity and local (e.g. water table and topsoil) toxicity due to their ease of mobility in the environment (e.g. I-129) [8]. Figure 1, shows the reduction of normalized radiotoxicity over time for different LWR SNF handling approaches.

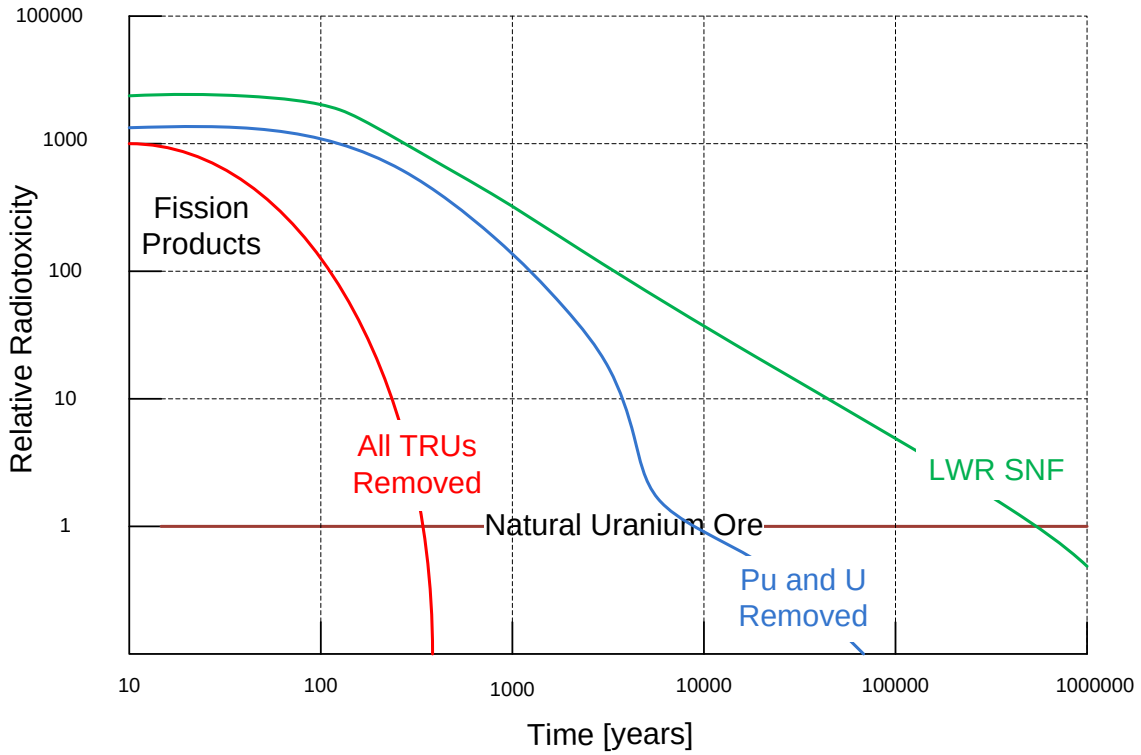

Fig. 1. Illustration of normalized SNF radiotoxicity reduction scenarios

If the SNF is “partitioned” and “transmutated” (P&T) the resulting fuel waste requires less than 1,000 years obtaining the emission levels of natural U [9]. Due to their high decay heat per unit mass and relative short half-lives, Am and Cm pose significant technological risks to the long term survivability of SNF engineered isolation systems and worker safety. Transmutation and fission destruction of these two nuclides alone has been suggested as a necessary step for any HLW isolation. Possible removal systems can be described in three categories, fast reactors, thermal reactors, and sub-critical external driven systems. Fast reactors offer the possibility of slow but complete destruction of TRUs, thermal reactors, most notably VHTRs, offer the possibility of destruction but incomplete creating in the process higher actinides such as Cm and Am, and finally external systems offer advantages similar to fast reactors but can’t maintain economic competiveness except under high government support. In all three systems, proper use of a shuffling scheme to rotate fuel assemblies/targets is needed to insure safe operation and the highest TRU destruction feasible in each scenario.

I.C Advanced Waste Management

A total of six generation IV systems were chosen for further study in 2002 by the Gen-IV Forum. Three of these systems (VHTR, super-critical water cooled reactor (SCWCR), molten salt reactor (MSR)) can operate with a thermal spectrum and the lead cooled fast reactor (LFR), gas cooled fast reactor (GFR), sodium cooled fast reactor (SFR), SCWCR, and MSR operate as fast reactor systems. The differences in design features and neutron spectra in these systems lead to drastically different options for TRU waste reduction scenarios if considered accounting for these systems.

Fast reactors, such as sodium cooled reactors, have the ability to completely burn TRUs due to the favorable fission to capture ratios at high neutron energies. Though a complete burn is possible, the small cross-section of Pu-Np-Am-Cm at high neutron energies lead to a slow burn process. This is further exacerbated by degradation of fuel structure as a result of fast neutron interactions. This degradation leads to a decrease in fuel life, thus requiring reprocessing of low burnup fuel. Several cycles would be required for a complete burn.

In the case of a thermal gas cooled reactor, these systems are incapable of complete burn due to the unfavorable fission to capture ratios at thermal neutron energies, but at these same energies large cross-sections and stable fuel forms allow for rapid and deep burns. Such abilities make VHTR economically favorable for initial TRU destruction. From these two systems, a two tier system employing a combination of partial but fast destruction in VHTRs and final destruction in SFR has been proposed as an eventual HLW inventory reduction method. A preliminary study at Idaho National Laboratory (INL) for the two tier approach compared the use of a DB-VHTR and MOX fueled VHTRs for first tier power plant fleet. The findings suggest that DB-VHTRs reduced the number of FRs per unit of tier one energy as well decreased reprocessing capacity [10]. The decrease in second tier and reprocessing footprint should lead to cost savings the consumer.

I.C.1 Very High Temperature Reactors

The Energy Policy Act of 2005 tasked the Department of Energy (DOE) with providing a demonstration of VHTR technology as a reliable and economical method to produce energy and hydrogen by 2021. The NGNP became a joint venture between INL and the private sector to develop the technology framework under which the plant will be constructed and operated. There are no commercial HTGRs currently operating in North America. However, the HTGR technology has been previously demonstrated beginning over four decades ago with Dragon in 1965. International interests in VHTRs have led South Africa, France, Japan, Russia, China, and South Korea to become key collaborators in VHTR technology development efforts. A timeline of HTGR operations is shown in Figure 2.

HTGRs are characterized for having better safety characteristics then LWRs. This is primarily due from the high heat capacity of the graphite core, high temperature resistant core components, inert coolant and moderator and chemical stability of the fuel. Generally HTGRs have inherent negative temperature coefficient of reactivity and passive heat transfer in off normal operations. Additionally EOL fuel has been predicted to have the highest survivability in a geological repository of all commercial fuels.

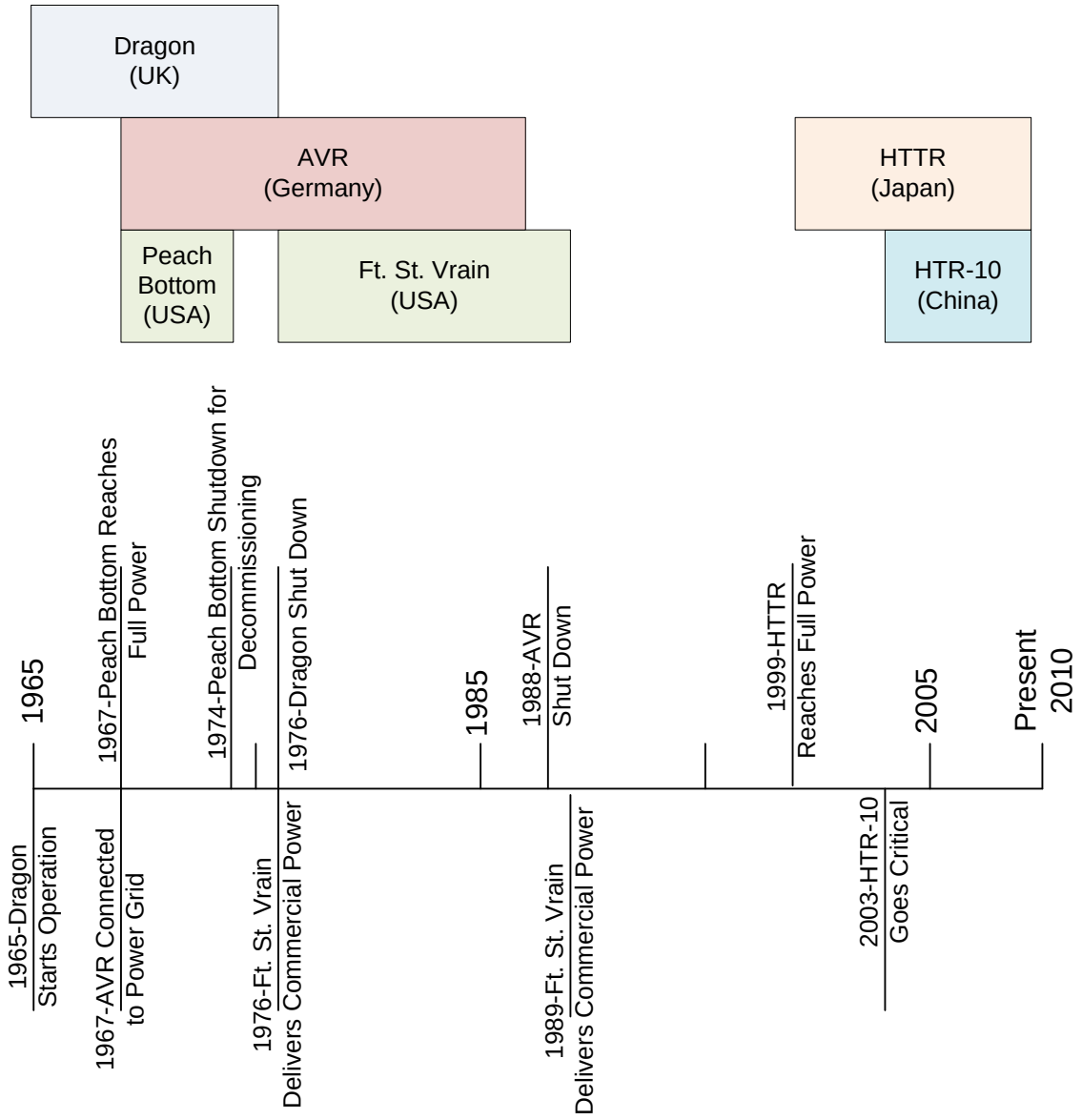

Fig. 2. HTGR operation experience

I.D Next Generation Nuclear Power Plant

The Next Generation Nuclear Power Plant (NGNP) will be a demonstration of the technical, licensing, operational, and commercial viability of HTGR technology for the production of process heat and electricity. The NGNP design requirements have not been finalized, but two requirements have been firmly defined. First the core should be

capable of producing outlet temperatures in excess of 1,000 K and second the core should maintain inherent safety under all transient and off-normal conditions. The latter requirement leads to the annular core design such that there is sufficient graphite mass in the inner reflector to maintain thermal energy during an active cooling loss.

NGNP can be built in two distinctive variations, one being the pebble bed design similar to Peach Bottom or as a prismatic core such as Ft. St. Vrain (FSVR), which is currently favored with announcement of South Africa abandoning their pebble bed program. The FSVR HTGR operated under a NRC license from 1974 to 1989 in Platteville, Colorado, as the nation's only HTGR to operate commercially. Due to the familiarity with the handling and numerous advantages of the FSVR prismatic block design, NGNP has already incorporated them into its design. FSVR fuel consists of small Tri-structural-isotropic (TRISO) fuel particles that are coated with multiple layers of pyrolitic carbon (PyC) and silicon carbide (SC) who together act as miniature pressure vessels to restrain fission products from escaping. The name for these fuel particles are a derivative of how cladding is applied to the fuel kernel. The cladding for TRISO particle consists of 4 layers starting with a porous PyC buffer layer, inner PyC layer, silicon carbide layer and outer PyC layer. Porous PyC acts as buffer and is approximately 50% void. The inner PyC Layer's main function is to prevent the reaction of chlorine produced during silicon carbide deposition with the kernel. The SC layer is the most significant of all the cladding layers where its main purpose is to provide the ability of the TRISO cladding to resist the high pressure generated during the fission reaction in the kernel as well as structural support to counteract stress induced dimensional changes in the PyC layers. The outer PyC layer's general function is to simply protect the SiC during the fabrication process. The unique arrangement of these coatings allow TRISO particles to withstand the high energy fluence encountered in high burnup cores, manipulation of coating thickness and/or arrangement can cause failure of fission product containment.

The fuel particles are then placed in a graphite matrix formed in a cylindrical geometry known as compacts. These compacts are stacked upon each other inside the graphite

blocks to make fuel rods. These large blocks are the physical form of the fuel that is handled in reactor loading and unloading operations.

The fuel block is hexagonal in cross section with dimensions of 36.0 cm across the flats by 79.3 cm high. The compacts are placed in an array of small-diameter hole; occupy alternating positions in a triangular array to the coolant channels in the block. The fuel holes are drilled from the top face of the element to within about 0.762 cm the fuel blocks bottom face. A graphite plug that is 1.27 cm tall is placed on the top of each fuel channel to immobilize the compacts. The fuel holes and coolant channels are distributed in a triangular array with a 1.88 cm pitch [11].

The control block is similar to the fuel block, but contains enlarged channels for the two control rods and the reserve shutdown absorber material in the original Ft. St. Vrain block, though the VHTR departs from this style block such that only one control rod channel is in each block. This can be seen in Figure 3. The control rod channels have 24.69 cm centerline spacing and a diameter of 10.16 cm. The reserve shutdown channel has a diameter of 9.525 cm. All of the active fuel element blocks including those with control rod holes have 1.27 cm diameter holes at each corners of the block for burnable poison rods. Burnable poison rods are 5.08 cm long and 1.143 cm in diameter. Prismatic block columns are held in place by a system of three graphite dowels located on the top face, while the bottom side has three dowel sockets for interlocking with the block underneath. A normal coolant channel passes through the center of each dowel. Height of the dowels measured from the block surface is 2.223 cm [11].

Several design requirements have been firmly set for NGNP, as a Generation IV system, a requirement was set forth that the core should maintain inherent safety under all transient and off-normal conditions. The latter requirement leads to the annular core design such that there is considerable graphite in the inner reflector to maintain thermal energy during active cooling loss. The NGNP prismatic core design program was jump started by borrowing heavily from the General Atomics GT-MHR design (Detailed in Fig. 3), producing an identical core layout [12].

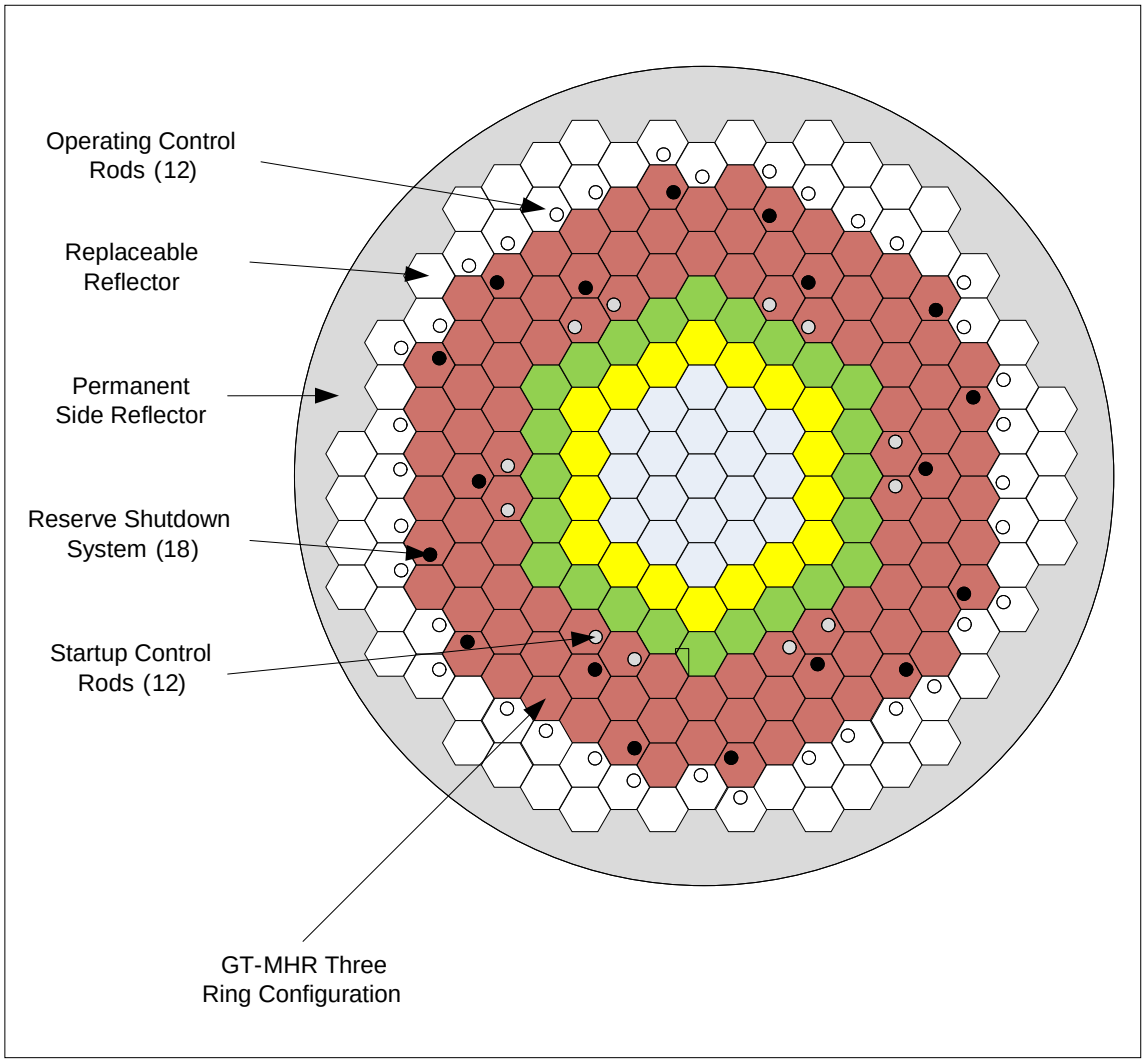

Fig. 3. Proposed GT-MHR core

The GT-MHR core is capable of 600 MWth and was developed under the framework of the July 1998 “Agreement between the government of the United States of America and the Government of the Russian Federation on Scientific and Technical Cooperation in the Management of Plutonium That Has Been Withdrawn from Nuclear Military Programs.” This reactor was chosen for its ideal high burnup fuel form, in addition to spent fuel degradation hesitance. Similar to the VHTR core, it has the recognizable annular core configuration of hexagonal graphite blocks. Graphite blocks come either as

solid reflector blocks, or blocks with holes bored into the top for the allowance of fuel, burnable poisons, and/or control rods. GA proposed the use of Er2O3 particles, much like the fuel particles to be used as the burnable poisons located in all fuel containing blocks. The “un-enriched” erbium is responsible for both reactivity compensation, and ensuring negative reactivity during transients. Erbium was chosen due to Er-167 capture resonance at 0.5 eV, which has a magnitude of nearly 10,000 barns, which shields Pu-239 reactions in the case of decreasing temperatures.

I.E Deep Burn Physics

Transmutation in thermal reactors generally employs multi-recycle approach because of neutron spectrum limitation to achieve the desirable transmutation efficiency in one path. The historical HTGRs and Gen IV VHTRs are well known for their flexibility to fuel cycle options. Recent studies have shown that efficient transmutation can be feasible in VHTRs under correct neutron spectrum condition. Dedicated transmuting reactors generally have variable fuel elements, with specialized transmutation fuel composed of TRUs oxides or metals, commonly with a high Pu composition. Reactors containing large quantities of Pu have a decrease in the negative reactivity temperature coefficient, requiring the addition of parasitic burnable poisons, but in an optimized DB core, the inventory increase of non-fissile TRUs pays the role of an “increased concentration” of burnable poisoned. This is accomplished via resonance absorbers to ensure prompt negative feedback and as a means to compensate for the large excess reactivity of fissile actinides [13]. The basis for DB-VHTRs is the use of thermalized neutrons and high burn up fuel forms (TRISO particles). This leads to a self-regulated balance of the fission and neutron capture-followed-by fission events that result in a controlled fuel consumption rate [14]. A VHTR core configured for DB, will readily burn TRUs while producing sustainable clean power for the electric grid and/or process heat for various industrial applications. With LWR SNF being used as the core fuel, the actinide inventory reduction when compared to a once through fuel cycles will actively decrease

the leading contributor to long term public dose from a geological repository, increasing the feasibility of such a project [13].

Neutron moderation in graphite in respect to the DB process produces more opportunities for thermal neutron interaction with fissionable isotopes and epithermal neutrons to interact with non-fissionable isotopes (i.e. neutron capture events for transmutation). This is primarily due to low parasitic capture and the reduction of energy loss per collision in graphite when compared to conventional light water moderation, which favorably increases the resonance reaction rate [13]. Neutrons in the epithermal range, when captured, provide a strong negative reactivity feedback effect with increasing fuel temperature [15]. The ceramic coated fuel particle's size can be adjusted to encourage such events. This is particularly true for fuel kernel diameters near the mean free path at resonance energies; such that neutrons traveling at or near resonance energies are drastically increase the chance of a compound nucleus reaction [13].

I.F DB-VHTR

As stated before, the DB core uses a full vector of actinides that ensure the same negative reactivity feedback. If the NGNP core is configured for transmutation as proposed by the DOE DB program, core reconfigurations could take place, including the addition of inner fuel rings. The ease in core rearrangement of NGNP allows for the core to take the form of a 3-ring annular core up to a limiting case of a core where the central reflector has been entirely replaced with fuel blocks, thus removing the characteristic annular arrangement, which would require additional safety evaluations to meet the NGNP design requirement of inherent core safety. Additional changes are proposed including a decrease of the kernel diameter between the ranges of 150-300 micrometers, increase of the TRISO buffer thickness to 150 micrometers, and decreasing the power density while keeping overall power to 600 MWth [14], which decreases the power density to 4.7 W/cc in the active core. Furthermore, in DB mode fuel will likely be in the form of a (TRU)O1.7 [14]. The actual dimensions of the fuel are highly dependent

on the isotopics and location of fuel inside the core. Many fuel feeds, fuel forms and fuel cycles have been proposed for a DB-VHTR, some of which are explored in Section IV.

In a 2005 report on the feasibility of DB, Argonne National Laboratory in close collaborations with General Atomics design team and Brookhaven National laboratory evaluation team proposed the four-ring and five ring active cores [13]. The four, five, and eight ring core could be nearly identical to the GT-MHR arrangement with the addition of inner rings of fuel blocks. Previous studies of the Pu-fueled GT-MHR physics features have shown important characteristics of this core arrangement. Three characteristics of noticeable concern for reactor safety are:

1. High power peaking occurs at the reflector and active core boundary due to the noticeably harder spectrum in the fuel blocks and the accumulation of thermal neutrons in the reflectors. This can be reduced by reducing fissile content near the reflectors or placing burnable poisons in the same region.

2. Control rod movement in the side reflector can significantly deform the power distribution in the core.

3. High Pu content cores can have a temperature reactivity coefficient near zero for temperatures near 400 Celsius. This temperature is close to startup conditions, but analysis has shown that even without operator intervention, safety is maintained due to the high fuel temperature failure limits [16].

Even with these concerns the DB-VHTR core remains stable, primarily because of:

1. The Doppler effect of even actinide isotopes.

2. Sensitivity of graphite slowing down efficiency to the neutron up-scattering.

3. The variation of the axial temperature profile [17].

I.G Shuffling Advancements for Nuclear Reactors

In a DB-VHTR, fuel assemblies are stacked in a honey comb pattern created radial rings and axial slices. Due to core neutronics, regions of the core have more preferential reaction rate densities then the average assembly location. These locations are known as hotspots and generally are not favorable for reactor operations due to safety concerns with component failure. In LWRs most assemblies experience low burnup, but in a DB-VHTR, some fuel assemblies can experience fuel destruction, were at EOL only having the TRU isotopes remains. Furthermore, LWR are known to have localized flux disruptions, while graphite moderated reactors experience region wide effects. This is due in fact to the mean free path of neutrons in graphite be upward of 10 times that of water moderated systems. Furthermore, these hotspots account to large amounts of excess reactivity, which will be needed at EOL to increase TRU destruction rates by increasing core life. This balance of minimizing power peaking but increasing core life, as well as minimizing and maximizing other system characteristics, requires the need of an intelligent robust balanced shuffling algorithm. Problems such as the above mentioned shuffling problem are referred to as MOP's.

MOPs are widely considered to be one of the most difficult optimization problems. In recent years several algorithms have been proposed for core shuffling including: [18-23]:

- Minimizing weighted sums of objective for Pareto set generation in multi-criteria optimization problems
- Evolving continuous Pareto regions, evolutionary multi-objective optimization
- Multi-objective programming, in multiple criteria decision analysis: state of the art surveys
- Search optimization using hybrid particle sub-swarms and evolutionary algorithms

- The normalized normal constraint method for generating the Pareto frontier, structural and multidisciplinary optimization

Generally, MOP algorithms use an iterative method to generate multiple points approximating the Pareto set. In order to improve core safety and operation characteristics, a nuclear reactor core undergoes a shuffling process every time the core has new fuel added to replace older fuel. In LWR, this happens every 18 months with approximately 1/3 of the core replaced.

Given a set of alternative shuffling locations for a set of fuel blocks, a change from one location to another that makes a fuel block parameter better without making any other individual worse off is called a Pareto improvement. A solution is said to be the Pareto optimal when no further Pareto improvements can be made. This Pareto optimal is the mathematical solution to the MOP. Pareto optimal for large Pareto sets come in multitude and thus are referred to as a Pareto optimal set. In continuous problems, the number of Pareto optimal solutions is usually infinite. Only in relatively simple cases the entire Pareto optimal set can be determined analytically, thus a separate criteria outside the MOP has be used to determine when an optimal set is robust enough to be called as a representative Pareto optimal set. This representative set criteria defines the quality of the solution to cover the whole minimal set evenly with the needed fidelity. For many MOPs, the cost of generating one Pareto optimum is high enough such that the designer can afford only to find a few Pareto optimal solutions, as it is for core shuffling patterns. Assuming 240 unique assembly locations, there are nearly 240 core configurations! Assuming a 10 year life span for a deep burn core with 10 shut down for core shuffling, the number of life-time configurations jumps to $240!^{10}$. This of course assumes no prior knowledge or restraint in the assembly shuffles, but emphasizes the need for an optimization strategy. It is from this large configuration set and reactor physics knowledge about shuffling objectives, the possible number of configurations can be vastly reduced to solve for the Pareto optimal set.

Several methods have been proposed for the solutions of such problems. Popular methods for solving multi-objective problems are classical methods such as weighted sum method, multi-objective evolutionary algorithms (MOEA), population based approaches, mixed-integer non linear programming (MINLP) [24], and simulated annealing based approaches (AMOSA) [25].

This dissertation proposes a unique multi-objective algorithm and ε-perturbation method for solving such a problem as the above discussed Pareto set. For example, boron can be used to reduce power peaking of fresh assemblies, but the parasitic absorption of neutrons is disadvantageous for neutron economy, furthermore placing higher burnt fuel in locations of power peaking reduces power peaking but decreases excess neutrons required for system excess reactivity of core life time. Thus a tradeoff between parasitic absorption of burnable poison (BP) and assembly rotation has to be made for preferential EOL metrics.

Significant computational challenges are posed by multi-objective optimization problems; the prior work focusing on the optimization of TRU-DB VHTR core shuffling is uniquely represented by two significant studies [26, 27] within the framework of the Deep Burn project. One of these studies proposed core optimization from the viewpoints of fuel management, TRISO fuel specification, and neutron spectrum. In this work a conventional radial shuffling scheme of fuel blocks is compared with an axial-only block-shuffling strategy in terms of the fuel burnup and core power distributions [26]. Results of this study showed that core power distributions can be controlled by zoning of TRISO fuel packing through the core, as well as TRU burnup in excess of 60% in a single irradiation pass. Major departures from this prior study and the proposed research for this dissertation is the complete 3-D optimization accounting for the entire system performance as wells as no fresh fuel additions during operation versus the prior study proposed additions during shuffling down times. Furthermore, the shuffling pattern proposed prior to this dissertation used a general, but well conceived, movement from one fuel ring to another, which represents a small subset of the possible

Pareto solution set. Furthermore, general reactor physics parameters, such as power peaking, TRU destruction, etc., were outside the scope of the study, rather the ring to ring shuffling was never deviated through the core life.

In the second study, control rod movement was investigated in conjunction with axial shuffling for americium and curium transmutation. Though objectives of this study were different then that discussed above, the conclusion of this work demonstrated the importance of control rod movement in the axial core power profile [27], this concept will be incorporated into this dissertation's DB-VHTR model.

I.H Research Objectives

The objective of this dissertation is to develop a physics based 3-D multi-directional reloading algorithm for the prismatic DB-VHTR. Additionally, TRU destruction will be evaluated for several compact and fuel block loading patterns, to determine a set of physical fuel block and compact design that will facilitate the analysis of the physics based shuffling algorithm. To accomplish this objective the following sub-research objectives will be accomplished:

1. Starting with available reference prismatic block design, as represented by the prismatic NGNP design, develop a high fidelity 3-D model of a DB-VHTR capable of tracking performance variables and allow for fuel block movement.

2. Taking advantage of the 3-D DB-VHTR model, develop a physics-based reloading algorithm and the corresponding computational sequence for shuffling fuel in prismatic HTRs. The reloading algorithm includes detailed mapping of the DB-VHTR performance domain of several fuel compact designs and fuel block loading patterns. It requires an automated sequence based on given constraints and nuclides vectors to meet defined performance objectives. Total TRU destruction and core life are accounted for as performance objectives.

3. Utilizing the high fidelity 3-D model of a DB-VHTR and the reloading algorithm, sample studies will be performed for DB-VHTR behavior under shuffling conditions to (a) demonstrate performance of the developed algorithm and (b) taking advantage of the algorithm, provide unique physics insight into DB-VHTRs and their ability to destroy TRUs recovered from LWR spent fuel.

I.I Outline

The high fidelity 3-D neutronics model capable of tracking prismatic blocks 3-dimensionally will be introduced in Section II. Section III will discuss how the high fidelity 3-D neutronics model can be vectorized to utilize a shuffling algorithm. The physics based 3-D DB-VHTR shuffling algorithm will be developed in this section; furthermore its implementation in the neutronics model will be explained. Section IV will discuss results produce to map the domain of DB-VHTRs when a full LWR TRU vector is used. Results of several shuffling schemes will be presented. At the end of section IV BOL results for an equilibrium DB-VHTR utilizing the developed shuffling algorithm will be presented. These results will demonstrate the shuffling algorithm's ability to destroy TRUs recovered for LWR SNF. Section V will summarize and draw conclusions from this dissertation's research.

II. DB-VHTR SYSTEM MODEL

II.A Robust Design Development and Optimization Philosophy

Robust design approaches allow developing new systems for intended applications accounting for: a large number of design parameters and performance characteristics, interdependence of various system parameters and characteristics, uncertainties in system data, models, performance characterization, anticipated performance conditions and operation environments. By its nature, the robust design development philosophy leads to improved system reliability characteristics for targeted applications and operation conditions.

Because of the focus on improvements in performance and reliability, the robust design optimization philosophy is broadly used in engineering for a variety of systems [28-31]. In recent years, it has been successfully applied for many aspects of nuclear energy systems including those related to advanced HTGRs [32-39]. The methodology used in this dissertation adopts multi-objective robust design optimization strategies for postulated system design envelops and performance domains.

The present effort follows this philosophy in development efforts towards an integrated comprehensive optimization methodology for DB-VHTRs. The methodology adopts multi-objective robust design optimization strategies for postulated system design envelops and performance domains.

To create advanced nuclear energy systems it is desirable to have a high fidelity modeling-based design development that relies on simulating features of the entire life cycle of the system before actual physical prototyping - from concept development to detailed design, prototyping, and safety analysis. A 3D whole-core exact-geometry model of a VHTR hexagonal-block configuration with a detailed component representation has been developed and implemented for calculations with MCNP/MCNPX. Figure 4 shows the MCNP Vised plot of this model.

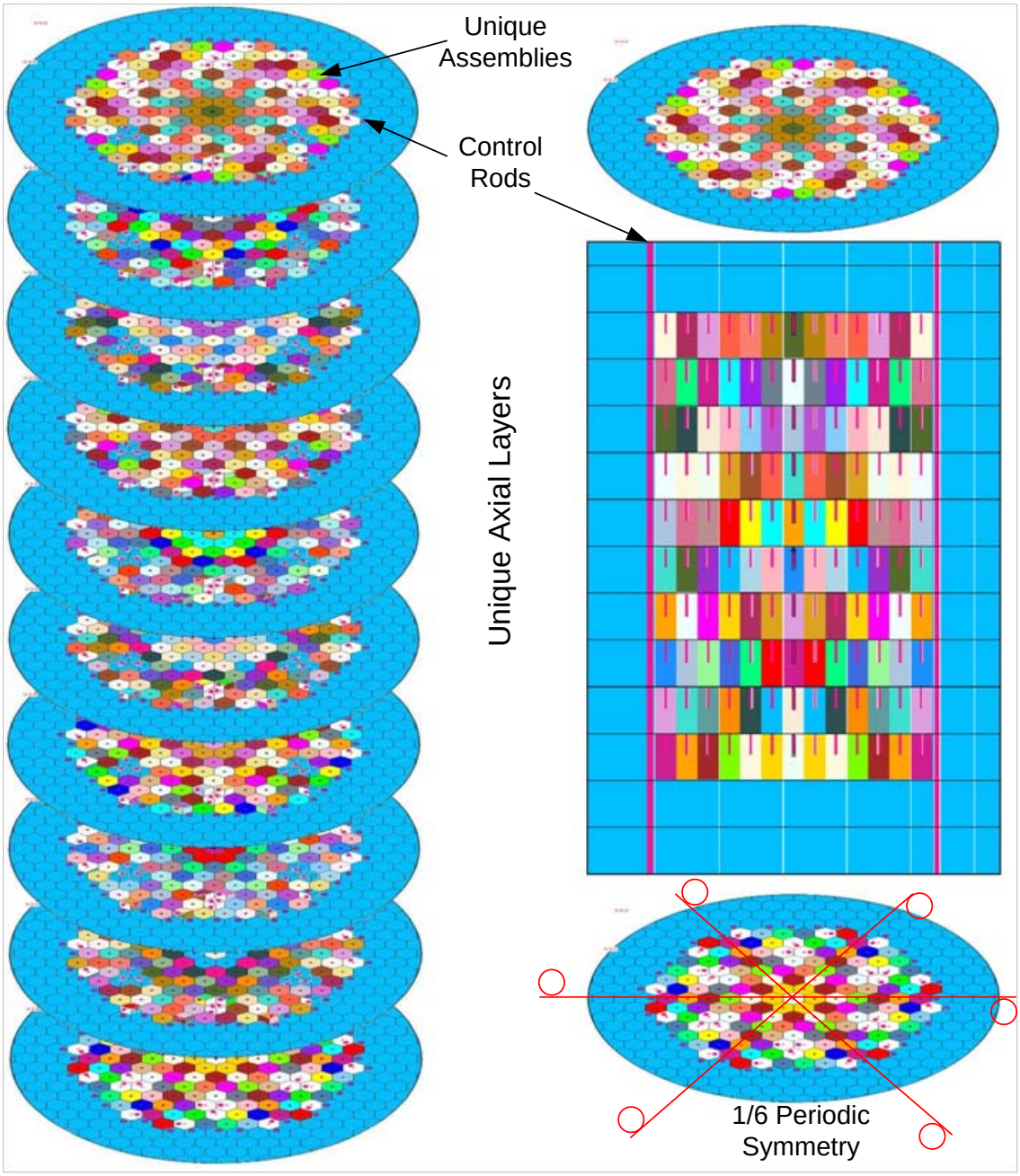

Fig. 4. Whole-core exact-geometry 3D representation of the VHTR hexagonal block configuration

II.B DB-VHTR Depletion Model for Multi-Directional Block Movement

In order to accurately account for both the multi-heterogeneity of a DB-VHTR and 3-D shuffle, a neutronics model had to be created that differentiates materials through time in 3-D space while preserving each level of heterogeneity correctly. From these requirements a large 3-D model for use with MCNPX has to be created, representing and accounting for the flexibility of a prismatic DB-VHTR fuel blocks. This model must be able to track nuclide changes through time.

The potential of any recycling and reprocessing of spent fuel involves partitioning and separating nuclides into various waste streams that can either be reused as fuel or placed with a geological repository. With the wide variety of UREX systems currently being researched, it has been assumed that a UREX or a UREX derivative system will be available when DB-VHTRs come online that will have the capability of near perfect efficiency at the separation of U, TRU, and FPs from LWR waste streams. For the basis of this dissertation a PWR with a fuel loading of 3.75% enriched uranium is burnt for 41,200 MWd/MTHM and cooled for 23 years is reprocessed. Table 1 gives the expected waste streams that can be produced from a UREX stream and are used in this dissertation as the basis of fuel compositions. This fuel composition was chosen because it represents an average composition of current U.S. commercial SNF.

Table I. Expected Waste Streams from PWR Reprocessing

Reactor Grade Plutonium (RGPu) Vector		
Element	**Nuclide**	**Composition (atom %)**
Plutonium	Pu-238	2.36
	Pu-239	61.453
	Pu-240	26.022
	Pu-241	4.877
	Pu-242	5.289
Total		100
Transuranic (TRU) Vector		
Element	**Nuclide**	**Composition (atom %)**
Neptunium	Np-237	6.121
Plutonium	Pu-238	1.986
	Pu-239	51.718
	Pu-240	21.899
	Pu-241	4.104
	Pu-242	4.451
Americium	Am-241	8.25
	Am-242m	0.02
	Am-243	1.23
Curium	Cm-243	0.003
	Cm-244	0.194
	Cm-245	0.021
	Cm-246	0.003
Total		100
Minor Actinide (MA) Vector		
Element	**Nuclide**	**Composition (atom %)**
Neptunium	Np-237	38.635
Americium	Am-241	52.079
	Am-242m	0.127
	Am-243	7.762
Curium	Cm-243	0.021
	Cm-244	1.225
	Cm-245	0.134
	Cm-246	0.017
Total		100

Starting at the lowest level of the MCNPX model, fuel vectors, a selection of the thousands of nuclides must be made to ensure proper depletion and reactivity feedback through core burnup. These nuclides and/or their decay daughters have large absorption cross-sections that significantly change the neutron economy of a system. A separate set of nuclides is required to accurately determine EOL radiotoxicity, these nuclides can be shared with those files required for the depletion process. These nuclides and/or decay daughters effect radiation emission after the fuel leaves the core.. These EOL nuclides that are not in the group of nuclides needed for depletion are excluded for tracking due the enormous computational time required during depletion. This subset of nuclides excludes all belonging to the fission product family. These nuclides mass at EOL can be estimated accurately based on fuel burnup, thus allowing for an accurate EOL radiotoxicity to be calculated.

Since criticality measurements are an important segment of nuclear research, a selection of known high reactivity worth nuclides has been compiled and ranked in several families based on independent research done at ORNL. For this dissertation 67 nuclides were chosen for depletion of each fuel, shown in Table II, with their corresponding MCNPX cross-section library. These nuclides are used for depletion in the MCNPX model and allow for accurate prediction of in-core metrics such as power production and excess reactivity. These in-core metrics will be used in the shuffling algorithm discussed at the end of Section IV. Nuclides are tracked in the model based on a unique composition number. The composition number remains constant throughout the model, a separate shuffling number is used to determine the location of the composition in the model. The these numbers are used inside the Matlab scripts discussed in Section IV.

Table II. Tracked Nuclides for Depletion Calculations

Nuclide	Library	Nuclide	Library	Nuclide	Library	Nuclide	Library
H-01	73c	Xe-131	73c	Sm-149	73c	U-236	73c
B-10	73c	Xe-135	73c	Sm-150	50c	U-238	73c
B-11	73c	Cs-133	73c	Sm-151	50c	Np-237	73c
C-12	50c	Cs-134	73c	Sm-152	50c	Pu-238	73c
N-14	73c	Cs-135	73c	Eu-151	73c	Pu-239	73c
O-16	73c	Cs-137	73c	Eu-153	73c	Pu-240	73c
Kr-83	73c	Ce-144	73c	Eu-154	50c	Pu-241	73c
Zr94	73c	Pr-143	73c	Eu-155	73c	Pu-242	73c
Nb-93	73c	Nd-143	73c	Gd-152	73c	Am-241	73c
Mo-95	50c	Nd-145	73c	Gd-154	73c	Am-242	73c
Tc-99	73c	Nd-146	73c	Gd-155	73c	Am-243	73c
Ru-106	73c	Nd-147	73c	Gd-156	73c	Cm-242	73c
Rh-103	73c	Nd-148	73c	Gd-157	73c	Cm-243	73c
Rh-105	50c	Pm-147	73c	Gd-158	73c	Cm-244	73c
Ag-109	73c	Pm-148	73c	Gd-160	73c	Cm-245	73c
Sn-126	73c	Pm-149	73c	U-234	73c	Cm-246	73c
I-135	73c	Sm-147	73c	U-235	73c		

For each of these nuclides reaction rates are calculated by MCNPX, then passed to CINDER for depletion. At each shuffling step, any other nuclides produced in the kernel are discarded due to their small contributions to reactivity changes. .

II.C 3D Whole-Core Exact Geometry DB-VHTR Model with Multi-Directional Block Movement

The method to model VHTRs and capture 3D block movement details requires the methodological tracking of material compositions. This method is described in detail in Section III.

With reactivity properly accounted for via nuclide selections, design of the core has to be representative of an actual physical model. The DB-VHTR is based on General Atomics prismatic block design, these blocks were used in the Ft. St. Vrain HTGR. Four core design arrangements, differing by the number of active fuel rings, were modeled. The

first model used three active core rings and was to the General Atomics GT-MHR configuration. The other three rings added fuel block rings by removing reflector block rings from the inner reflector. These four core arrangements are shown in Fig. 5. The active core is denoted with purple, control rod blocks without fuel in green, and reflector blocks with yellow.

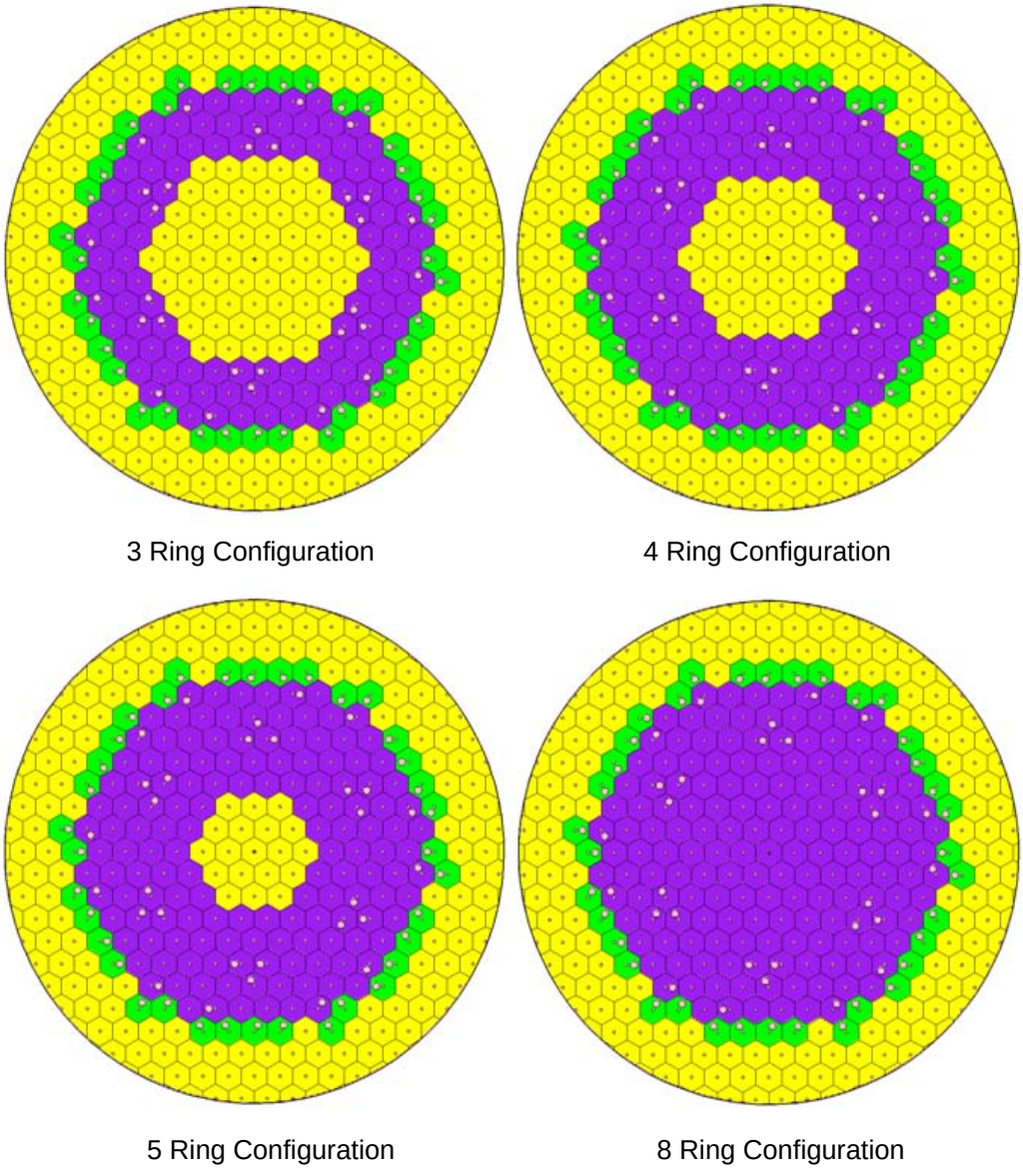

Fig. 5. MCNP VHTR active core arrangements

The bottom and top reflector blocks are identical to the active core blocks except for the fuel pins and burnable poison pins have been replaced with solid graphite. This was done to accommodate axial streaming. Fuel composition and burnable poison composition, generic values were used based on data obtained from the German HTTR program. Graphite blocks were based on Ft. St. Vrain blocks with a density of 1.72 g/cc. TRISO particle dimensions differ based on design selection criteria but a reference design and parameters are given below in Table III. The TRISO particle kernel dimension can greatly change the reaction rates and types in the kernel. Specifically, in terms of resonance mean free path, smaller kernels will favor resonance reactions, while larger favor non-resonance reactions [16].

Table III. TRISO Parameters

Parameter	**Dimensions [cm]**	**Mix Number**
Fuel Radius	0.030405	1
Coating 1 Thickness	0.00587	2
Coating 2 Thickness	0.00292	3
Coating 3 Thickness	0.00287	4
Coating 4 Thickness	0.00456	5
Compact Graphite Matrix	n/a	6
Name	**Mix Number**	**Atom Density [atom/barn-cm]**
Fuel (X-Dioxide)	1	Variable
Carbon	2	5.73E-02
Carbon	3	9.42E-02
Silicon	4	4.81E-02
Carbon	4	4.81E-02
Carbon	5	9.74E-02
Graphite	6	1.72 g/cc

Figure 6, shows the Monte Carlo model of a TRISO particle with the kernel and coating thicknesses. The particles are placed in the fuel rods by filling the rods with a body centered arrangement. Particles were not positioned to account for the fuel rod dimensions, such that some particles at the rod edges are only partial particles. This simplification eases the modeling without significantly effecting integral and non-integral parameters.

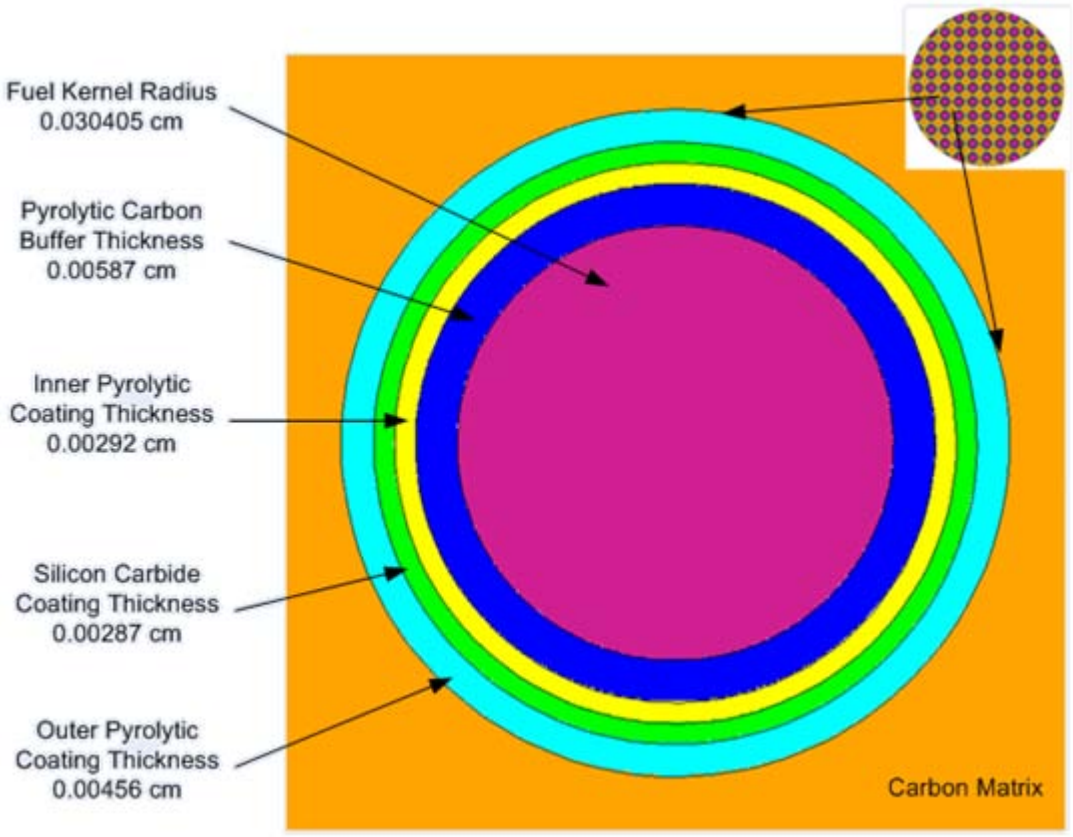

Fig. 6. Magnified TRISO particle

All other parameters are listed and referenced in Table IV. Figures following Table IV show the general core layout, and details on both the fuel blocks and control rod blocks with fuel. These blocks are compared with their corresponding FSVR sister block.

TRISO particles are not shown in these figures due the limitations of the packaged MCNPX visual editor (VISED). In each block, all voids, be it handling holes, coolant channel, or/and control rod holes are filed with He-4.

Table IV. MCNP Model Parameters

	Parameter	Unit	Measurement	Ref.
General	Active Core Height	m	7.93	14
	Top Reflector Height	cm	118.95	14
	Bottom Reflector Height	cm	158.6	14
	Number of columns	-	144	14
Fuel Column	Number of fuel pins (without control rod/with)	-	210/186	14
	Number of lumped BP	-	6	14
	Number of coolant holes (without control rod/with)	-	108/95	14
	Height	cm	79.3	14
Fuel Cell	Pitch of fuel cell	cm	1.8796	14
	Radius of fuel hole	cm	0.635	14
	Radius of fuel compact	cm	0.6223	14
	Radius of coolant hole	cm	0.79375	14
Control Mechanism	Control rods, start-up (inner ring)	-	12	40
	Control rods, operational (outer moderator reflector ring)	-	36	40
	Control rods, shutdown (central ring/outer ring)	-	6/12	40
	Control rods, hole radius	cm	5.05	40
	Control rods, distance from the center of the block	cm	9.75614	40
	Fuel blocks, burnable poison pins	-	6	40
Blocks	Length	cm	79.3	14
	Handling Hole Diameter	cm	3.5	14
	Flat to Flat Width	cm	36	14

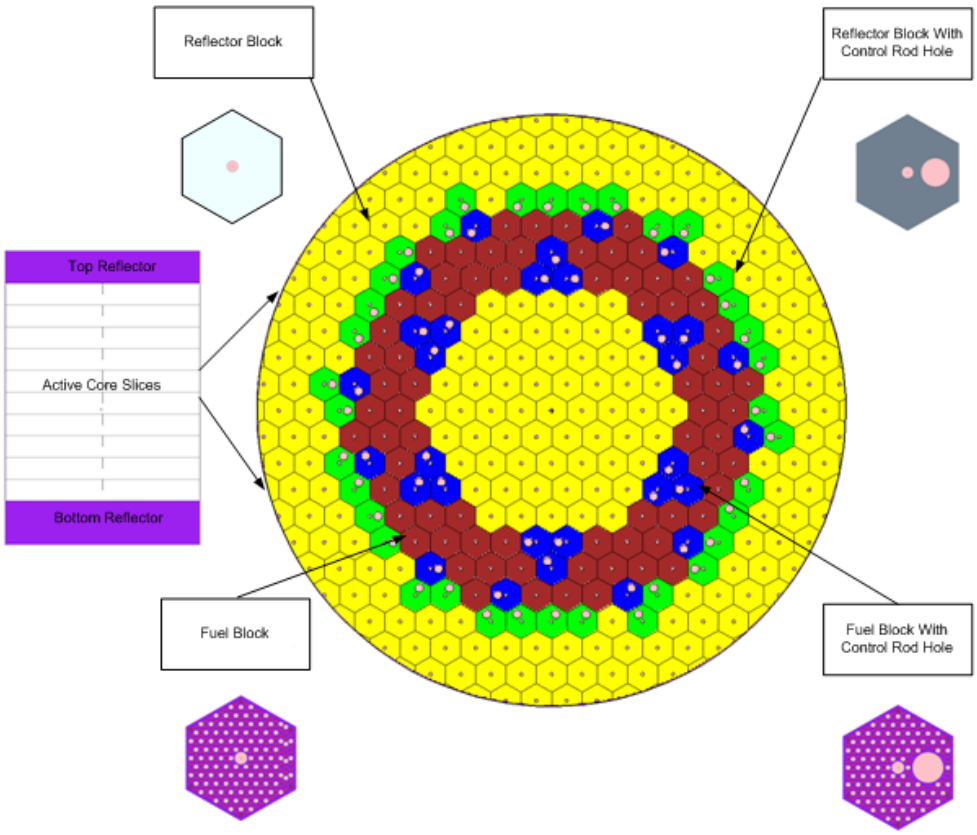

Fig. 7. Detailed 3-ring NGNP MCNP core layout

Fig. 7 shows the general layout of the NGNP core. Each axial slice has four basic blocks as shown. Furthermore, the core is modeled such that after a neutron leaves the core it can't reenter the system. Figures 8 and 9 were included to better show the fuel containing blocks and the locations of their components with respect to one another. Fuel placement in respect to coolant channels, handling hole, and control rod hole is based on the Ft StVrain block and can be adjusted if chosen. Fig, 6 demonstrates the change from FSVR control rod blocks to NGNP control rod style blocks.

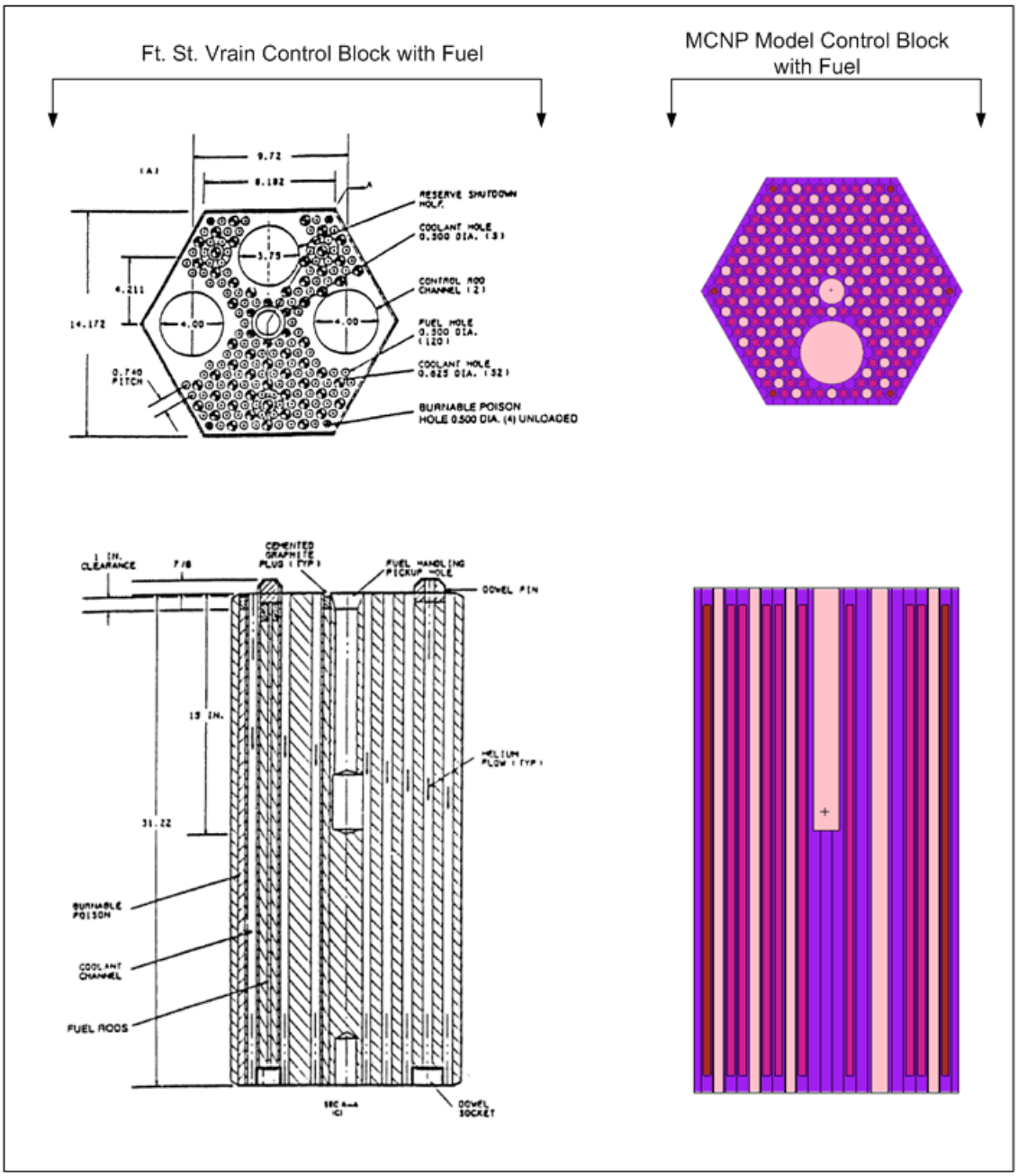

Fig. 8. Fuel containing control rod guide block as modeled and detailed Ft. St. Vrain block

A robust literature review has not given the decision as to why control rods where moved from one block to spread out between three separate blocks. It is presumed that the block gained durability from this change, furthermore control rod drive mechanism

could operations could play a role. By separation of these rods between several blocks, a decrease in non-control rod fuel block shuffle permutations and an increase in control rod block permutations.

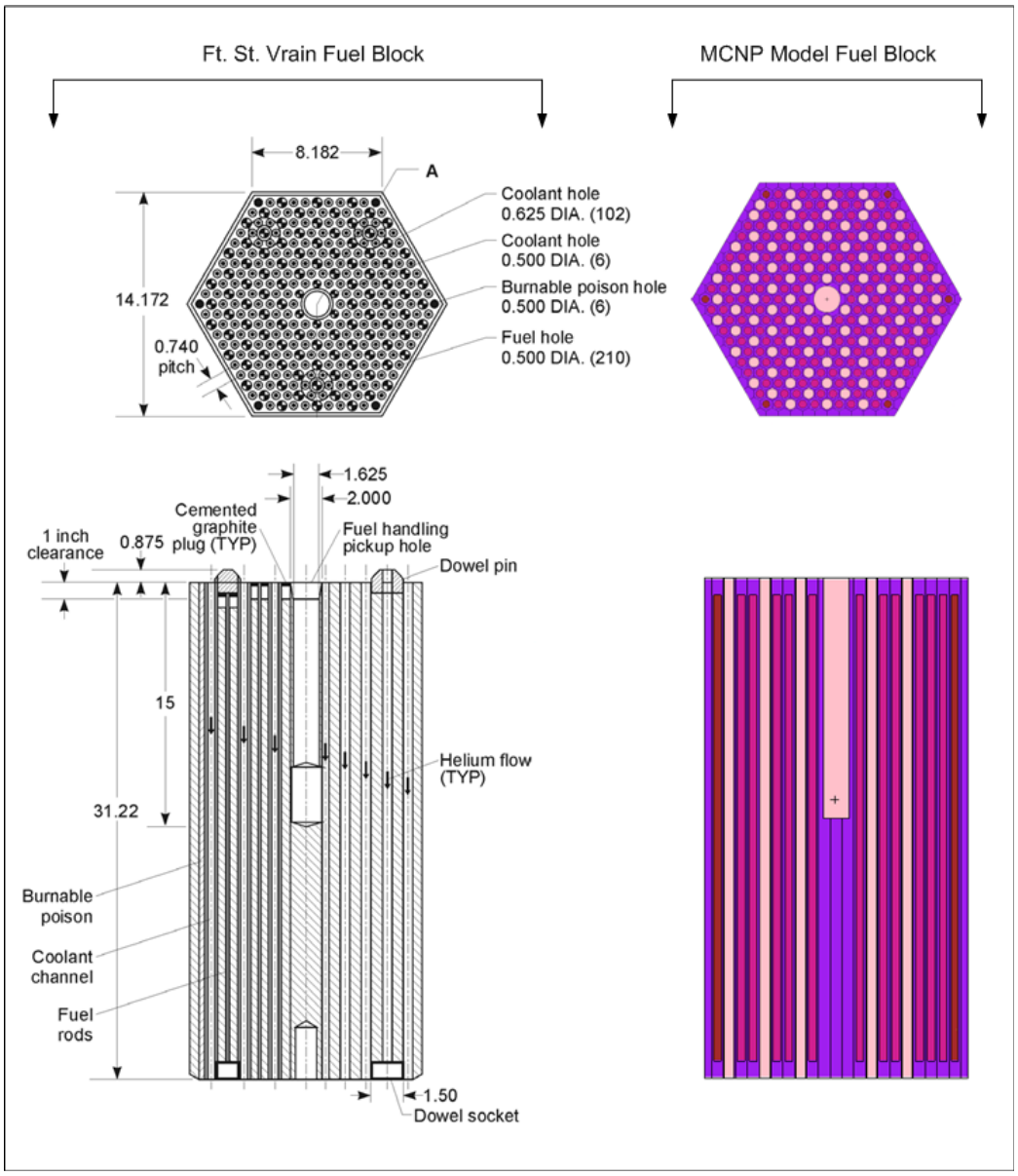

Fig. 9. Fuel block as modeled and detailed Ft. St. Vrain fuel block

III. METHODOLOGY AND APPLIED CODE FRAMEWORK IMPLEMENTATION

III.A Physical System Vectorization

The methods proposed here were developed for TRU fueled DB-VHTRs. With slight modifications to shuffling philosophies and constraints, this dissertations methodology and code framework can be applied to other reactor systems. The methodology aims at 3D in-core reloading/shuffling for hexagonal block systems. The design envelop is limited to the DB-VHTR configurations following their conceptualizations in preliminary studies, specifically – feasible families of MHR, Pu-MHR, and DB-MHR are used as the basis for developing the DB-VHTR configurations [36]. LEU- and TRU-systems are considered with the focus on TRU-systems, TRU compositions are derived from LWR used fuel vectors [6].

An attempt is made to assure system performance reliability in anticipated application environments by maximizing efficiency (TRU destruction) while searching for configurations exhibiting minimized sensitivity to fluctuations in system parameters and operation conditions. In particular, fluctuations in LWR used fuel vectors, and TRU vector effects on safety characteristics of TRU-fueled VHTR are taken into consideration. The impact of LWR used fuel vector fluctuations on TRU-fueled VHTRs has already been addressed in previous studies for general VHTR configurations based on HTTR fuel block design [16]. The results suggest importance of taking the effects into account for DB-VHTRs. From this, an optimization strategy was implemented in the code framework for engineered fuels that maximized selected performance criteria for any user defined initial fuel feed, thus ensuring an approximated peak performance throughout core life.

The comprehensive multi-directional 3D optimization and shuffling methodology evolves from historical developments for HTGRs and contemporary efforts for modern VHTRs and DB-VHTRs:

- Fort Saint Vrain – design, operating experience and decommissioning efforts of

Fort Saint Vrain Reactor (FSVR);[45-47]

- GT-MHR – development of the GT-MHR for Pu incineration;[48-49,16]
- DB-MHR – evaluations of the GT-MHR design modifications to accommodate TRU loadings and efforts on optimization of DB-MHRs for actinide incineration;[50,40,51]
- NGNP/VHTR – development of the initial NGNP point-design and the NGNP pre-conceptual design;[52-59]
- DB-VHTR – preliminary feasibility studies of the Deep-Burn concept;[41,60-62]
- DB-VHTR – contemporary efforts on optimization of axial fuel shuffling strategies.[63-64]

The up-to-date state-of-the-art accomplishments are mapped to the assumed design context flow for TRU-fueled VHTRs as shown in Figure 10. The operational domains and design features are used in the methodology development process to formulate optimization objectives and express them through postulated requirements and identified performance and design constraints. This representation approach is conceptually illustrated in Figure 10.

In the methodology, VHTRs are accounted for as integral components of the larger VHTR-based nuclear energy system. Consequently, this nuclear energy system consists of VHTRs and their associated fuel cycles. The specific VHTR unit representation in the system model and in the modeling framework is split into the “physics details” component and the “secondary side” component. These two components interact and influence each other and the overall system performance characteristics.

The unit design parameters and performance characteristics are also determined by associated fuel cycle features. Potential applications and environmental impact characteristics serve as connecting elements between these model groups. Figure 2 shows the noted interrelationship between various groups of design parameters and performance characteristics as they are accounted for and being developed in the high-fidelity system model.

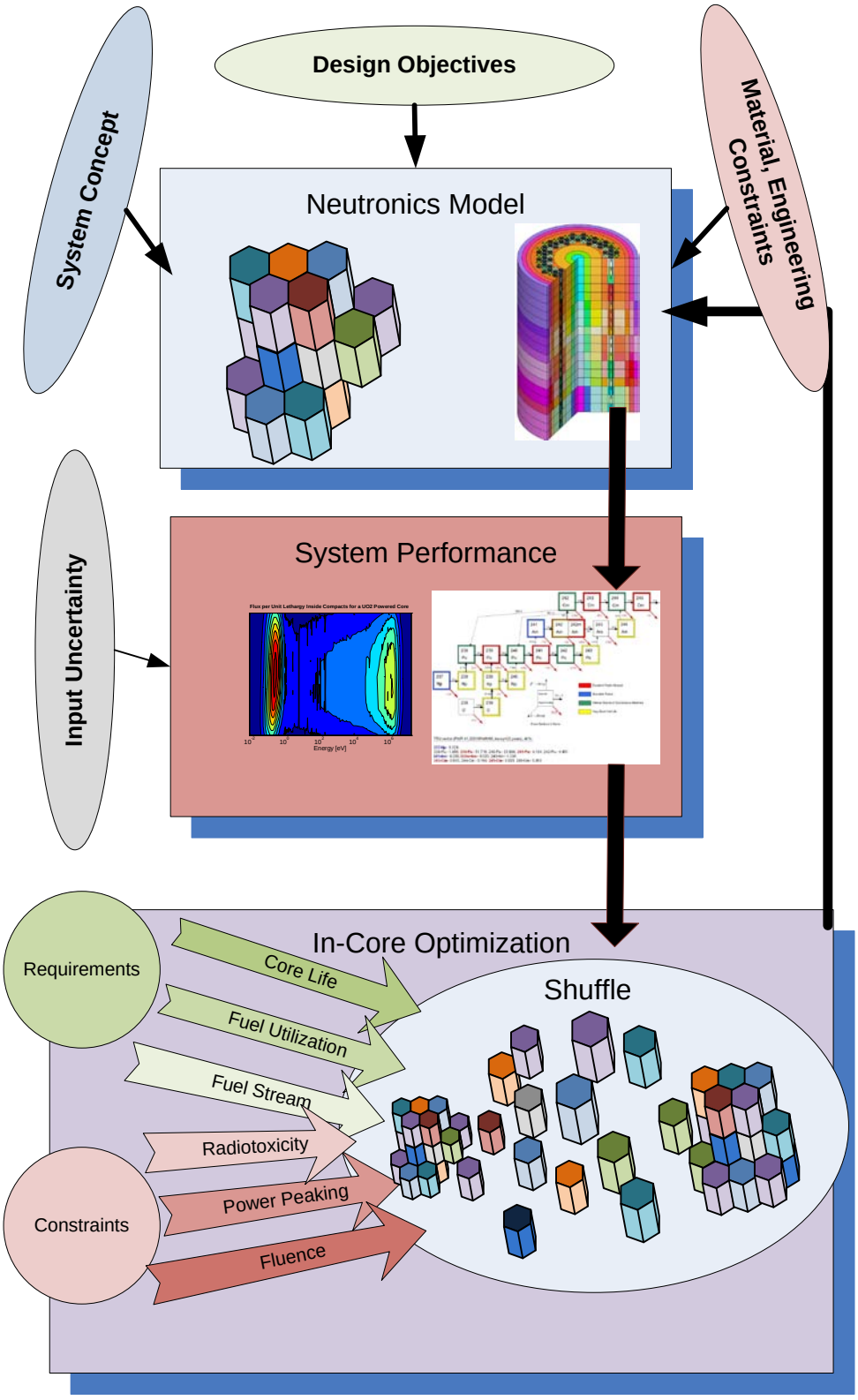

Fig. 10. Modeling framework

There are near countless designs possible with a system such as a DB-VHTR, but like all engineered products a selection process dwindles the possibilities to a few, with varying performance trade-offs. The speed at which one can remove non-adequate designs is related to both the knowledge of constraints and performance requests from the final product. In the case of the code framework here, a method was chosen that searched for optimal success through the whole design process. This starts with any given nuclide used fuel vector to the final shuffling method.

To realize the above described robust design optimization philosophy, the DB-VHTR system model is represented as an interrelated combination of two domains - domain of design parameters, D, and domain of performance characteristics, P. It readily follows that all data sets associated with the system have to be vectorized and classified to belong either to the system design domain (D) or to the performance domain (P).

The design domain is mapped to the performance domain by the functioning system itself:

$$P(D):\ D \xrightarrow{[S]} P \tag{1}$$

where $[S]$ is a mapping operator that simulates the system during its lifetime. In the context of the developed modeling framework, this $[S]$-mapping is provided by high-fidelity 3D Monte Carlo simulations. The data vectorization allows to classify the described robust design optimization problem as one belonging to the large class of vector optimization problems (VOP) [65-66].

Figure 3 shows multiple objectives to be reached in this problem because of performance requirements and constraints imposed on elements of the design and performance domains.

Because of the system data vectorization, the DB-VHTR system design parameters are formally represented by various vectors denoted as $\vec{d}$-vectors of the system design domain, D:

$$\forall \vec{d} \subset D .$$

Three types of $\vec{d}$-vectors capture design details of the DB-VHTR system in the developed methodology - geometrical vectors ($\vec{d}_G$), material vectors ($\vec{d}_M$), and fuel vectors ($\vec{d}_F$):

$$\forall \vec{d} \subset D = \left\{ \vec{d} \middle| \vec{d}_G \subset G,\ \vec{d}_M \subset M,\ \vec{d}_F \subset F :\ D = G \bigcap M \bigcap F \right\} \tag{2}$$

where G, M, and F are the corresponding design sub-domains. A graphical representation of this relationship is shown in Figure 11.

Geometrical vectors describe component structure, dimensions and arrangements. Structure and dimensions of the individual components are assumed to remain constant in optimization scenarios. In contrast, the dynamically-varying component arrangements determine shuffling scenarios as needed to maximize performance of DB-VHTRs in specific operational modes.

The optimization methodology uses their variability as an instrument to achieve optimization objectives. Material vectors carry composition details of structural materials and burnable absorbers. Because structural materials do not change their composition (unless they significantly degrade during operation), only burnable absorber data are accounted for as variable parameters. Fuel vectors are considered as a separate group because they directly affect performance characteristics of the DB-VHTR system design.

To account for these details, the simple representation by three vector types has to be

expanded to allow differentiating between static design parameters and those design parameters that change dynamically as a result of an optimization process to meet performance requirements:

- $\vec{d}_G$ are the $\vec{d}$-vectors accounting for all geometrical parameters in the DB-VHTR system model, $\vec{d}_G \subset G$:

$$\forall \vec{d}_G \subset G \Leftrightarrow G = \left\{ \vec{d}_G \middle| \vec{d}_G \subset G : \exists \vec{d}_G \subset D \right\},$$

where G is a geometry sub-domain of the DB-VHTR system design domain, D. In the present effort, it is convenient to divide $\vec{d}_G$-vectors into two categories:

$$\forall \vec{d}_G \subset G \Leftrightarrow G = \left\{ \vec{d}_G \middle| \exists \vec{d}_{G,S} \subset G,\ \exists \vec{d}_{G,O} \subset G \text{ but } \vec{d}_{G,S} \neq \vec{d}_{G,O} \Leftrightarrow G = G_S \bigcup G_O \right\} \qquad (3)$$

where:

1) Static geometrical parameters - $\vec{d}_{G,S}$ represents those $\vec{d}_G$-vectors that remain unchanged during operation, $\vec{d}_{G,S} \subset G_S$,

$$\forall \vec{d}_{G,S} \subset G_S \Leftrightarrow G_S = \left\{ \vec{d}_{G,S} \middle| \vec{d}_{G,S} \subset G_S : \exists \vec{d}_{G,S} \subset G \right\},$$

where G_S is a static geometrical sub-domain of the overall geometry sub-domain.

2) Dynamic geometrical parameters - $\vec{d}_{G,O}$ represents those $\vec{d}_G$-vectors that vary during operation, $\vec{d}_{G,O} \subset G_O$,

$$\forall \vec{d}_{G,O} \subset G_O \Leftrightarrow G_O = \left\{ \vec{d}_{G,O} \middle| \vec{d}_{G,O} \subset G_O : \exists \vec{d}_{G,O} \subset G \right\},$$

where G_O is a dynamic geometrical sub-domain of the overall geometry sub-domain.

- $\vec{d}_M$ are the $\vec{d}$-vectors accounting for all material parameters in the DB-VHTR system model except fuel composition data, $\vec{d}_M \subset M$:

$$\forall \vec{d}_M \subset M \Leftrightarrow M = \left\{ \vec{d}_M \middle| \vec{d}_M \subset M : \exists \vec{d}_M \subset D \right\},$$

where M is a material sub-domain of the DB-VHTR system design domain, D. According to the above-described approach, structural materials and burnable absorbers belong to different sub-domains,

$$\forall \vec{d}_M \subset M \Leftrightarrow M = \left\{ \vec{d}_M \middle| \exists \vec{d}_{M,S} \subset M,\ \exists \vec{d}_{M,O} \subset M \text{ but } \vec{d}_{M,S} \neq \vec{d}_{M,O} \Leftrightarrow M = M_S \bigcup M_O \right\} \quad (4)$$

where:

1) Static material parameters representing structural materials - $\vec{d}_{M,S}$ are those $\vec{d}_M$-vectors that remain unchanged during operation, $\vec{d}_{M,S} \subset M_S$,

$$\forall \vec{d}_{M,S} \subset M_S \Leftrightarrow M_S = \left\{ \vec{d}_{M,S} \middle| \vec{d}_{M,S} \subset M_S : \exists \vec{d}_{M,S} \subset M \right\},$$

where M_S is a static material sub-domain of the overall material sub-domain.

2) Dynamic material characteristics representing burnable absorbers - $\vec{d}_{M,O}$ are those $\vec{d}_M$-vectors that vary during operation, $\vec{d}_{M,O} \subset M_O$,

$$\forall \vec{d}_{M,O} \subset M_O \Leftrightarrow M_O = \left\{ \vec{d}_{M,O} \middle| \vec{d}_{M,O} \subset M_O : \exists \vec{d}_{M,O} \subset M \right\},$$

where M_O is a dynamic geometrical sub-domain of the overall material sub-domain.

- $\vec{d}_F$ are the $\vec{d}$-vectors of all beginning-of-life (BOL) fuel composition parameters in the DB-VHTR system model, $\vec{d}_F \subset F$:

$$\forall \vec{d}_F \subset F \Leftrightarrow F = \left\{ \vec{d}_F \middle| \vec{d}_F \subset F : \exists \vec{d}_F \subset D \right\},$$

where F is a BOL fuel sub-domain of the DB-VHTR system design domain, D.

As a collection of acceptable design parameters, the DB-VHTR system design domain, D, is an intersection of sub-domains, G, M, and F:

$$D = G \bigcap M \bigcap F \qquad (5)$$

This notation gives proper recognition of sub-domain interdependence resulting in the iterative nature of all design procedures.

The BOL fuel sub-domain, F, is the design side of the portal to the fuel cycle model parameters, characteristics and features. This is the design side of the interconnection point between design parameters (design domain) and performance characteristics (performance domain) that leads to the overall non-linearity of the high-fidelity DB-VHTR system model.

Following the above-developed $\vec{d}$-vector approach of the system design domain, D, the DB-VHTR system performance characteristics are formally represented by various vectors denoted as $\vec{p}$-vectors of the performance domain, P:

$$\forall \vec{p} \subset P .$$

It follows from Eq. (1) that the design domain, D, determines the corresponding DB-VHTR system performance domain, P:

$$P(D) = \left\{ \vec{p} \middle| \vec{p} \subset P,\ \vec{p} = \vec{p}(\vec{d}),\ \vec{d} \subset D \right\} \qquad (6)$$

Similarly to geometrical, material, and fuel vectors describing the DB-VHTR system design details, the DB-VHTR system performance domain, P, can be split into, at least, two sub-domains using the design context flow of Figure 2:

- $\vec{p}_A$ is the vector of all application-related performance characteristics in the DB-VHTR system model, $\vec{p}_A \subset A$:

$$\forall \vec{p}_A \subset A \Leftrightarrow A = \left\{ \vec{p}_A \middle| \vec{p}_A \subset A : \exists \vec{p}_A \subset P \right\},$$

where A is an application-related sub-domain of the DB-VHTR system performance domain, P;

- $\vec{p}_E$ is the vector of all environmental impact characteristics in the DB-VHTR system model, $\vec{p}_E \subset E$:

$$\forall \vec{p}_E \subset E \Leftrightarrow E = \left\{ \vec{p}_E \middle| \vec{p}_E \subset E : \exists \vec{p}_E \subset P \right\},$$

where E is an environmental impact sub-domain of the DB-VHTR system performance domain, P. The DB-VHTR environmental impact sub-domain, E, includes:

1) Used fuel vectors (end-of-life (EOL) fuel vectors as well as fuel vectors after some designated cooling/storage periods),

2) Spent fuel vectors,

3) Other environment-related fuel cycle characteristics and features accounted for in the DB-VHTR system model.

This is the performance side of the interconnection point between design parameters (design domain) and performance characteristics (performance domain). As above emphasized, this interconnection point leads to the overall non-linearity of the high-fidelity DB-VHTR system model.

To the contrary from Eq. (5) that provides the DB-VHTR system design domain, D as the three-sub-domain intersection; the corresponding system performance domain, P, is given by a sum of sub-domains, A and E:

$$P = A \bigcup E \tag{7}$$

Both, Eq. (5) for D and Eq. (7) for P are written under the assumption that their sub-domains do not share vectors – each sub-domain vector uniquely belongs to its own sub-domain. This assumption is self-evident for the system design sub-domains. However, it requires to be specifically defined for the system performance sub-domains.

Unless it is restricted, certainly, some environmental impact characteristics may also potentially be application-related characteristics. To avoid this confusion, in the present modeling methodology, vector-sub-domain distributions are assumed to be unique, and hence,

- For the system design domain:

$$\vec{d} = (\vec{d}_G \subset G, \vec{d}_M \subset M, \vec{d}_F \subset F) \subset D = G \bigcap M \bigcap F, \tag{8}$$

- For the system performance domain:

$$\vec{p} = (\vec{p}_A \subset A, \vec{p}_E \subset E) \subset P(D) = \begin{cases} A(D) \bigcup E(D) = A(G \bigcap M \bigcap F) \bigcup E(G \bigcap M \bigcap F), \\ A(D) \bigcap E(D) = \varnothing. \end{cases} \tag{9}$$

Table V summarizes the above-defined topology of the DB-VHTR system model. This model topology will be used throughout the project effort to develop and implement the robust design optimization methodology for the DB-VHTR system configurations with 3D in-core reloading/shuffling.

Table V. Topology of the Vectorized DB-VHTR System Model

<table>
<tr><td>Performance, P

$P = A \bigcup E$</td><td colspan="4">Design, D, $D = G \bigcap M \bigcap F$</td></tr>
<tr><td></td><td>Geometry, G

$G = G_S \bigcup G_O$</td><td colspan="2">Materials, M

$M = M_S \bigcup M_O$</td><td>BOL
Fuel, F</td></tr>
<tr><td>Applications, A

$A(G \bigcap M \bigcap F)$</td><td rowspan="4">$\vec{d}_G \pm \vec{\delta}_G$</td><td rowspan="2">$\vec{d}_{G,S} \pm \vec{\delta}_{G,S}$</td><td rowspan="2">$\vec{d}_M \pm \vec{\delta}_M$</td><td rowspan="2">$\vec{d}_{M,S} \pm \vec{\delta}_{M,S}$</td><td rowspan="4">$\vec{d}_F \pm \vec{\delta}_F$</td></tr>
<tr><td>$\vec{p}_A \pm \vec{\varepsilon}_A$</td></tr>
<tr><td>Environment, E

$E(G \bigcap M \bigcap F)$</td><td>$\vec{d}_{G,O} \pm \vec{\delta}_{G,O}$</td><td>$\vec{d}_{M,O} \pm \vec{\delta}_{M,O}$</td></tr>
<tr><td>$\vec{p}_E \pm \vec{\varepsilon}_E$</td></tr>
<tr><td>$\vec{p} \pm \vec{\varepsilon}$</td><td colspan="4">$\vec{d} \pm \vec{\delta}$</td></tr>
</table>

As given in Table IV, all vectors of applied design parameters and performance characteristics of the DB-VHTR system model have their corresponding vectors of uncertainties (“errors”) associated with individual vector component values:

- For the system design domain, $D = G \bigcap M \bigcap F$:

$$(\vec{d} \pm \vec{\delta}) = \left[(\vec{d}_G \pm \vec{\delta}_G) \subset G, \quad (\vec{d}_M \pm \vec{\delta}_M) \subset M, \quad (\vec{d}_F \pm \vec{\delta}_F) \subset F \right] \subset D \tag{10}$$

- For the system performance domain, $P = A \bigcup E$:

$$(\vec{p} \pm \vec{\varepsilon}) = \left[(\vec{p}_A \pm \vec{\varepsilon}_A) \subset A, \quad (\vec{p}_E \pm \vec{\varepsilon}_E) \subset E \right] \subset P \tag{11}$$

III.B Vectorized Objectives and Constraints

All performance characteristics dynamically vary in optimization scenarios as a function of variations of design parameters. They are subject to both performance requirements and constraints due to design parameter limitations (constraints on design parameters). Let's denote the corresponding domains of constraints due to design limitations and performance constraints as C_D and C_P, respectively:

$$\vec{d}_C \subset C_D \Leftrightarrow C_D = \left\{ \vec{d}_C \middle| \exists \vec{d}_C \subset D : \ \vec{d}_C \subset C_D \right\} \tag{12}$$

$$\vec{p}_C \subset C_P \Leftrightarrow C_P = \left\{ \vec{p}_C \middle| \exists \vec{p}_C \subset P : \ \vec{p}_C = \vec{p}(\vec{d} \subset C_D) \subset C_P, \ \vec{d} \subset D \right\} \tag{13}$$

For the DB-VHTR system, individual constraints on $\vec{d}$-vectors given by Eq. (12) are explicitly expressed as lower and upper bounds on individual elements of these vectors. Constraints given by Eq. (13) on performance characteristics can, certainly, be combined with performance requirements,

$$\vec{p}_R \subset R_P \Leftrightarrow R_P = \left\{ \vec{p}_R \middle| \exists \vec{p}_R \subset P : \ \vec{p}_R \subset R_P \right\} \tag{14}$$

to form the optimization objectives domain, $O_{P,D}$:

$$O_{P,D} = C_P \bigcap R_P ,$$

such that:

$$\vec{p}_O \subset O_{P,D} \Leftrightarrow O_{P,D} = \left\{ \vec{p}_O \middle| \exists \vec{p}_O \subset P : \ \vec{p}_O = \vec{p}(\vec{d} \subset C_D) \subset O_{P,D}, \ O_{P,D} = C_P \bigcap R_P, \ \vec{d} \subset D \right\} \tag{15}$$

III.C Optimization of the DB-VHTR System

Taking advantage of the developed vector representation approach for the DB-VHTR

system model, let's formulate the broad optimization problem in terms of $\vec{d}$- and $\vec{p}$-vectors of system data and domains of objectives and constraints, $O_{P,D}$ and C_D. Certainly, the robust design optimization approach for the vector optimization problem is unlikely to lead to a single optimal solution $\vec{d}_C^{\,opt.}$,

$$\exists!\vec{d}_C^{\,opt.} \subset C_D \subset D\,.$$

Some of the system performance objectives and constraints require trade-off decisions that result in deviations of $\vec{d}$-vectors from that unique solution (if even exists) to meet decided trade-off conditions. As a result, the domain-optimal solutions are more likely to meet the system performance requirements and constraints, $O_{P,D}$, under identified design limitations, C_D. This observation leads to considerations of global and local solutions with various dominance evaluations [65]. The formulated broad multi-objective multi-constraint vector optimization problem is given by Eq. (16).

$$\begin{aligned}
&P(D):\ D \xrightarrow{[S]} P \Leftrightarrow \left\{ \vec{p} \,\middle|\, \vec{p} \subset P,\ \vec{p} = \vec{p}(\vec{d}),\ \vec{d} \subset D \right\} \\
&\quad \text{Constraints:} \quad \exists \vec{d}_C \subset C_D \subset D \\
&\quad \text{Objectives:} \quad \exists \vec{p}_O = \vec{p}(\vec{d}_C \subset C_D) \subset O_{P,D} \subset P,\ O_{P,D} = C_P \bigcap R_P \\
&\text{Vector-optimal:} \quad \exists!\vec{d}_C^{\,opt.} \xleftarrow{[S]} \vec{p}_O^{\,opt.} \Leftrightarrow \left\{ \vec{d}_C^{\,opt.} \,\middle|\, \vec{p}_O^{\,opt.}(\vec{d}_C^{\,opt.}) \subset O_{P,D},\ \exists!\vec{d}_C^{\,opt.} \subset C_D \right\} \\
&\textit{.OR.} \\
&\text{Domain-optimal:} \quad \exists!D_C^{opt.} : \vec{d}_C \subset D_C^{opt.} \xleftarrow{[S]} P_O^{opt} \Leftrightarrow \left\{ P_O^{opt} \subset O_{P,D},\ \vec{d}_C \subset \exists!D_C^{opt.} \subset C_D \right\}
\end{aligned} \tag{16}$$

This optimization problem is the multi-objective multi-constraint vector optimization problem for the DB-VHTR system. Ultimately, once Pareto optimality criteria are met under the defined set of objectives, the end-system configuration can be finalized. In addition to Pareto-based techniques, multi-objective evolutionary algorithms are applied [37].

The design domain can be graphically represented as shown in Figure 11. Sub-domain

and DB-VHTR design domain interrelate as discussed above. The definition of these sub-domains and domain is discussed here.

$$D = G \bigcap M \bigcap F$$

Design Domain

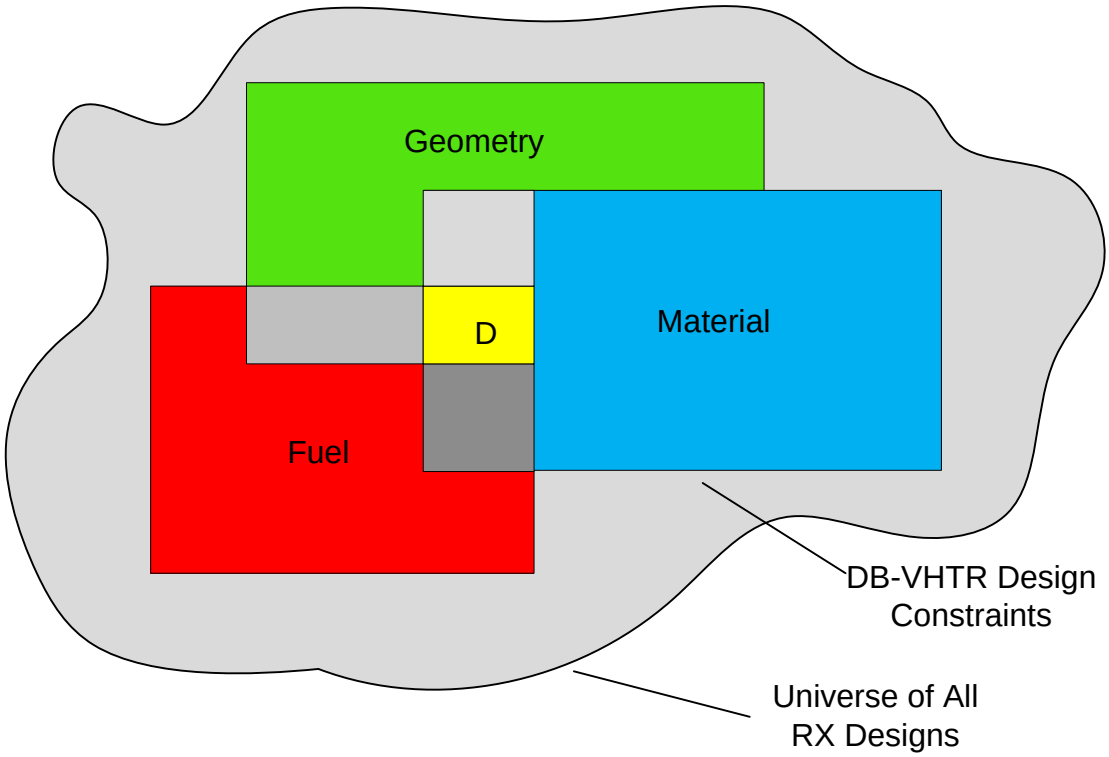

Fig. 11. DB-VHTR design domain

Beginning with the geometry design domain, G, static geometry vector, $\vec{d}_{G,S}$, can be formalized and hardcoded into mapping function $[S]$, while dynamic geometrical parameters, $\vec{d}_{G,O}$, can be left as both optimizable and/or user defined vectors. This simplification allows for generic DB-VHTR shell inputs to be created and decreases the complexity that a generalized reactor code would be needed, such that general geometry, shape, and arrangement of the core requires no user intervention. Geometry Domain, D, static geometry vector, $\vec{d}_{G,S}$, can be formalized and hardcoded into mapping function, $[S]$, while dynamic geometrical parameters, $\vec{d}_{G,O}$, can be left as both optimizable and/or user defined vectors. Table VI, shows VHTR geometry static or dynamic traits. Non-user defined dynamic geometrical parameters directly affect the core operation from in-core life to spent fuel behavior, these effects allow for the multi-objective optima search.

Table VI. Geometry Vector Classification

	Parameter	Type	Vector
General	Active Core Height	Static	$\vec{d}_{G,S} \subset D$
	Top Reflector Height	Static	$\vec{d}_{G,S} \subset D$
	Bottom Reflector Height	Static	$\vec{d}_{G,S} \subset D$
	External Core Radius	Static	$\vec{d}_{G,S} \subset D$
	Number of Active Fuel Rings	Dynamic	$\vec{d}_{G,D} \subset C_D \subset D$
Fuel Block	Number of Fuel Pins	Static	$\vec{d}_{G,S} \subset D$
	Number of PB Pins	Static	$\vec{d}_{G,S} \subset D$
	Number of coolant holes	Static	$\vec{d}_{G,S} \subset D$
	Fuel Isotopics and Designs	Dynamic	$\vec{d}_{M,D} \subset C_M \subset M$; $\vec{d}_{G,D} \subset C_D \subset D$
	Fuel Type Ratios	Dynamic	$\vec{d}_{G,D} \subset C_D \subset D$
	Pitch of Fuel Cell	Static	$\vec{d}_{G,S} \subset D$
	Radius of Fuel Hole	Static	$\vec{d}_{G,S} \subset D$
	Radius of Fuel Pin	Static	$\vec{d}_{G,S} \subset D$
	Height of Fuel Pin	Static	$\vec{d}_{G,S} \subset D$
	TRISO Packing Fraction	Dynamic	$\vec{d}_{G,D} \subset C_D \subset D$
	TRISO Layer Dimensions	Static	$\vec{d}_{G,S} \subset D$
	Kernel Radius	Dynamic	$\vec{d}_{G,D} \subset C_D \subset D$
BP Pin	Pitch of BP Pin Cell	Static	$\vec{d}_{G,S} \subset D$
	Radius of BP Pin Hole	Static	$\vec{d}_{G,S} \subset D$
	Radius of BP Pin	Static	$\vec{d}_{G,S} \subset D$
	Height of BP Pin	Static	$\vec{d}_{G,S} \subset D$
	BP Configuration	Dynamic	$\vec{d}_{G,D} \subset C_D \subset D$; $\vec{d}_{M,D} \subset C_M \subset M$
RX Control	Control rods, start-up (inner ring)	Static	$\vec{d}_{G,S} \subset D$
	Control rods, operational (outer moderator reflector ring)	Static	$\vec{d}_{G,S} \subset D$
	Control rods, shutdown (central ring/outer ring)	Static	$\vec{d}_{G,S} \subset D$
	Control rods, hole radius	Static	$\vec{d}_{G,S} \subset D$
	Control rods, distance from the center of the hexagon	Static	$\vec{d}_{G,S} \subset D$
	Control Rod Heights	Dynamic	$\vec{d}_{G,D} \subset C_D \subset D$
	Control Rod Configuration	Static	$\vec{d}_{G,S} \subset D$
Block	Flat to Flat Width	Static	$\vec{d}_{G,S} \subset D$
	Length	Static	$\vec{d}_{G,S} \subset D$
	Handling Hole Diameter	Static	$\vec{d}_{G,S} \subset D$

Generally all material properties are static, except for BP. BP is a dynamic material parameter, which mostly influences meeting in-core operation constraints, but additionally can be used to optimized fuel utilization optima when combined with a well informed shuffling algorithm. From this ability, BP is generally set as a dependent variable of core operation constraints (i.e. power peaking diminution). Effects of BP optimization are shown in Section IV.

Fuel design sub-domain is generally the largest influence on in-core and spent fuel objective optima search. Though fuel isotopics are a dynamic variable, a choice was made that initial fuel isotopics are generally constrained to initial LWR spent fuel feed, and will be either in the form of TRU-oxide or a subset of two oxides, one being PuNp-oxide, the other, AmCm-oxide. Recent research in the DB-VHTR suggest removal of AmCm from the fuel stream and use only a PuNp-oxide, since this is preliminary, this partial TRU fuel stream is not pursued here. With this vector constrained, a user can define initial the fresh fuel feed based on desire reprocessing technology and spent fuel breed. The design domain can thus be defined by both constraints of a universal DB-VHTR design, user selected fuel isotopics, and user elected geometrical criteria. Inside this design domain, dynamic design vectors allow for selection of acceptable performance domain.

Incorporation of constraints and prior knowledge of core neutronics, allow for a now defined DB-VHTR design domain to be reduced to a fraction of prior size as shown in Figure 12. In application, a user defined set of constraints and user supplied TRU vector, as well as user selected general core configuration provides a large possible universe of fuel block designs. By an iterative process on a Single-Fuel block using the mapping function S, MCNPX, initial whole core attributes, both during and at EOL can be estimated. From this estimation, fuel block selection occurs for desired traits thus reducing the design domain to a fraction of prior size. Several methods can be employed for selection reduction and search resolution, but generally computation time is low enough that a classical method can be utilized. General objectives that can be sought for at this stage is core life extension, TRU destruction rate, and power peaking within an element as well as preliminary BP requirements for in-core operation. This can be

written as:

$$G = G_{core} \bigcap G_{Assembly}; G_{Assembly} = G_{fuel} \bigcap G_{block}; G_{fuel} = G_{VF} \bigcap G_{TRISO}$$

$$\text{If } P_{obj} \subset D = G \bigcap F \bigcap M \simeq G \bigcap F \approx G_{Assembly} \bigcap F$$

$$\max P_{obj}, G_{Assembly} \subset C_G \bigcap F \subset C_F \xrightarrow{[S]} P \subset C_P$$

$$\because M_S >> M_D \ \& \ G_D \approx \bigcap G_{Assembly}$$

$$\text{DB-VHTR-optimal: } \exists! D_C^{opt.} : \vec{d}_C \subset G_{Assembly} \bigcap F_C^{opt.} \xleftarrow{[S]} P_{obj} \quad (18)$$

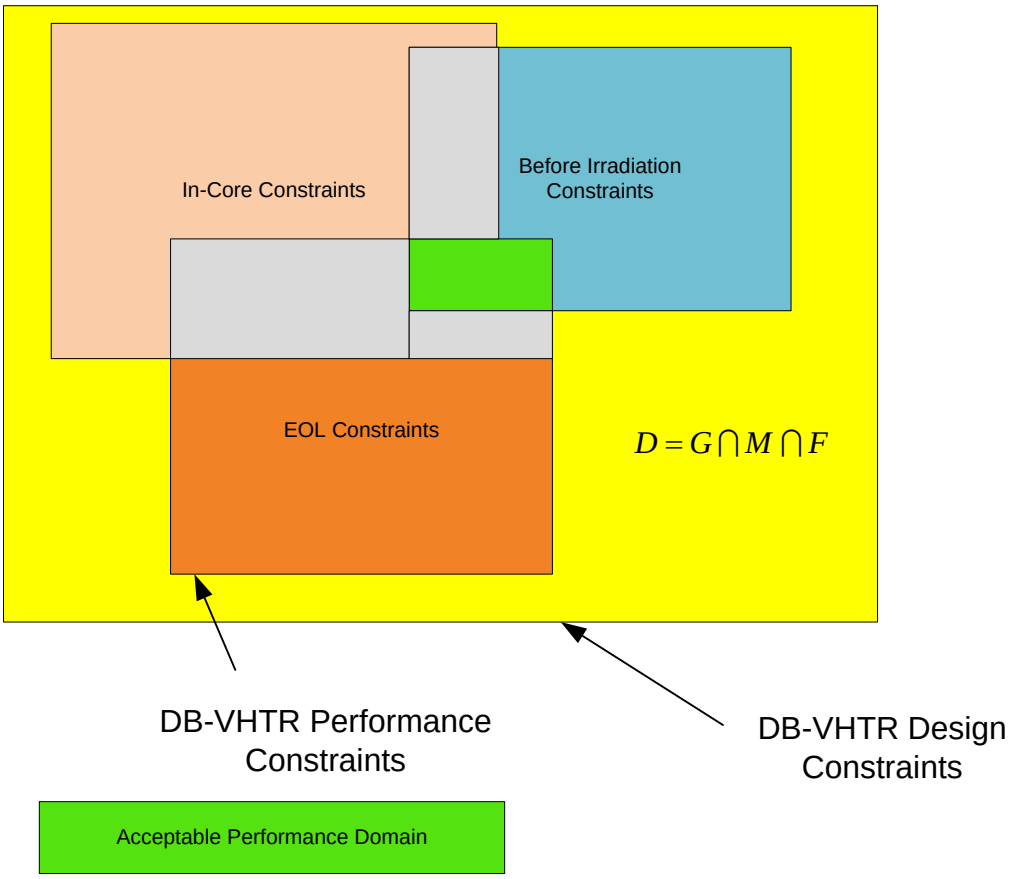

Fig. 12. Acceptable performance domain selection

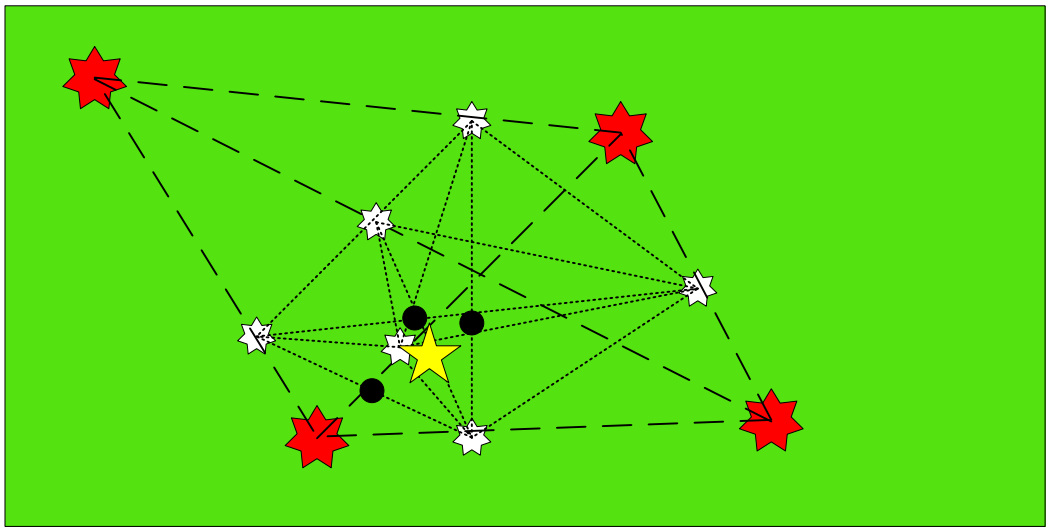

Fig. 13. Domain objective optima search

Figure 13 shows a representation of a MOP, where objective optima do not lend to a well defined domain objective optima, and thus tradeoffs between several desired objectives most be weighed and considered. In general before fuel is placed within the core, the tradeoff between maximum core life, and TRU destruction has been determined. Operational domain dictates that reach full domain objective within the operation of the DB-VHTR system will be dictated by operation and out of core constraints. These constraints are the formation of a complex MOP in terms of BP loading, equilibrium model, and 3D shuffling algorithm. This MOP is original in sense that general shuffling algorithms are for LWRs and take in only two dimension of possible fuel block movement. Furthermore, operational experience dictates general guidelines, and few things can be approved on. In the case of DB-VHTR guidelines are only hypothesized and there is no operational experience for meeting such objectives.

If the solution domain for TRU destruction is found separately from the optimal core reloading and 3D-Shuffling, then a two phase approach to search for the domain optima

for DB-VHTR can be developed as an effective two step approach. Step one is the search for an optimal compact design and fuel block loading to maximize TRU destruction. Step two is the maximization of core operation between core reloadings via optimal reload patterns (OTTO) and core shuffling pattern (equilibrium cycle) within operation constraints. Then the solution should unfold itself in several permutations, each similar to the other and within reach of the domain optima. Figure 14 show the second step to the solution process. Without an intelligent optimization process, the domain of possible core arrangements will unfold as a random distribution were the possibility of finding the domain optima without searching the entire space is remote. For demonstration, 20,000 random shuffles were calculated for a non-optimized design to demonstrate the futility of a brute force attack. Solutions were checked for predicted reactivity gain while tracking total block radial movement vs. axial movement. The product of this is shown in Figure 5. This demonstrates that taking on a small selection of possible permutation of the core reload pattern produces a distribution that appears to be unrelated to both radial and axial core movement. This random nature of the shuffling produces a 3D Gaussian distribution in terms of excess reactivity versus average fuel block radial and axial movement.

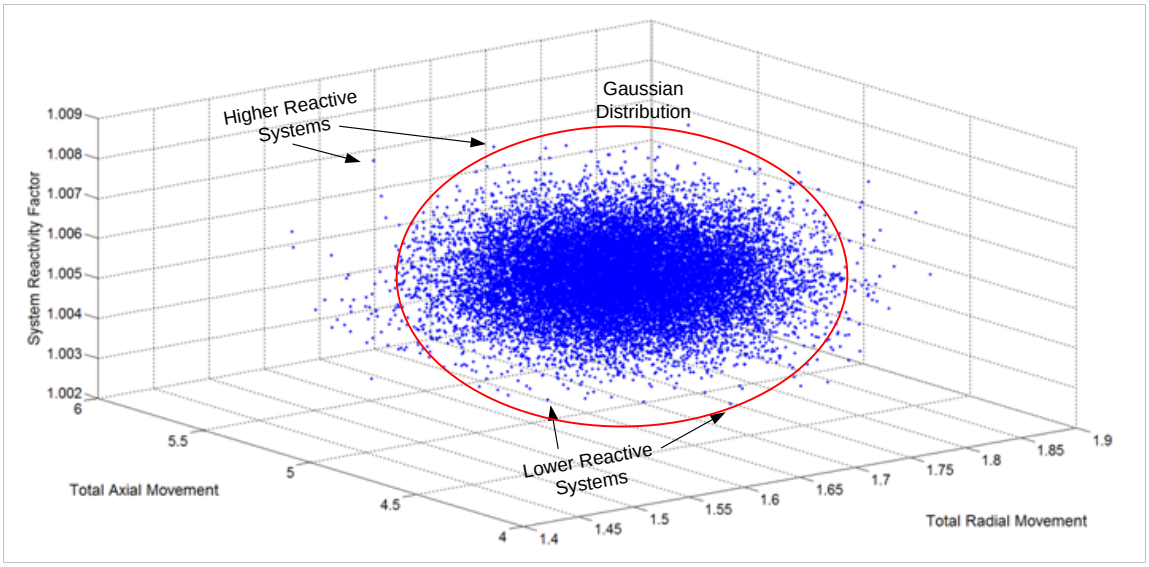

Fig. 14. Brute force domain search of a non-optimized shuffle

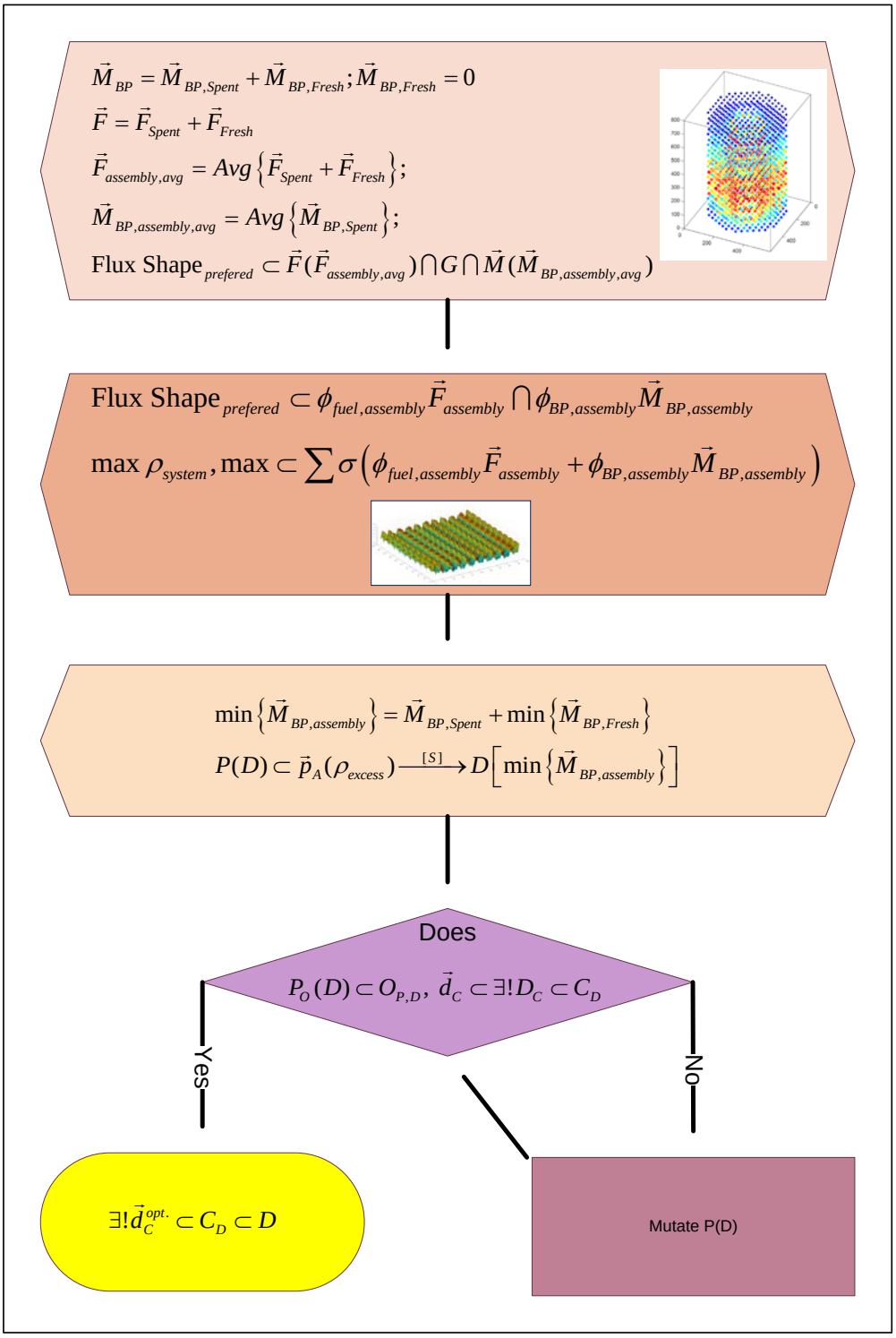

Fig. 15. Physics based shuffling algorithm

In the solution search method proposed here, shown in Figure 15, a simplified core model is used to determine preferred system neutronics. Preferred system neutronics refers to the core power profile. From this model, reaction rates are calculated based on a system wide average fuel and BP composition, where 2/3 of the fuel composition come from current fuel in the reactor and 1/3 from fresh fuel. The physical model's vectorized format is shown below for this process:

$\vec{M}_{BP}$ = Burnable Poison Material Vector

$$\vec{M}_{BP} = \vec{M}_{BP} + \vec{M}_{BP,Spent}; \qquad \vec{M}_{BP,Fresh} = 0$$

$\vec{F}_{assembly,avg}$ = The Average Fuel Compostion Vector

$$\vec{F}_{assembly,avg} = Avg\left\{\vec{F}_{Spent} + \vec{F}_{Fresh}\right\}$$

$\vec{M}_{BP,assembly,avg}$ = The Average BP Compostion Vector

$$\vec{M}_{BP,assembly,avg} = Avg\left\{\vec{M}_{BP,Spent}\right\}$$

$\phi(r)_{preffered}$ = 3D Preffered Flux Shape

$$\phi(r)_{preffered} \subset \vec{F}(\vec{F}_{assembly,avg}) \bigcap G \bigcap \vec{M}(\vec{M}_{BP,assembly,avg}) \tag{1}$$

Only BP from blocks destined to remain in the core is considered, with no fresh stream of BP. Generally BP, in the form of either Er-167 or B-10, will have insignificant concentrations at the end of cycle. By allowing for BP to be considered in the shuffling algorithm, the algorithm will remain accurate if the cycle length is reduced or more slowly burning BP are used. This method removes possible variation of core neutronics due variability of system fluxes due to resonance shielding via burnup induced nuclide concentration changes.

The next step requires individual nuclide compositions from each fuel block and known core power production fluxes to predict the best core reload arrangement. BP is then added to each fresh block to reduce BOL excess reactivity to operating constraints,

operation constraints on BOL excess reactivity are related to control rod worth and are a pre-programmed variable. At this point a core can be rerun again to calculate more accurate power production location preferences, predictive shuffling reactivity maximization occurs again.

Finally the algorithm determines if other constraints such as power peaking are being met and if so the core is burned. In the case the core is not acceptable; a ranking system is applied to each fuel block to determine excess reactivity. With a ranking of each fuel block known and power production location preferences already determined, the algorithm permutes the performance optimal solution to find P(D) optimal solution by cycling higher reactive assemblies to lower preferred power production locations, thus evolving the reload into an acceptable permutation. Furthermore, BP can be added to each fresh fuel block to also meet operation constraints. This permutation process is discussed at the end of this section and results in large changes in the initial core shuffling pattern found above.

III.D 3D Whole-Core Exact Geometry DB-VHTR Model with Multi-Directional Block Movement

To create advanced nuclear energy systems it is desirable to have a high fidelity modeling-based design development that relies on simulating features of the entire life cycle of the system before actual physical prototyping - from concept development to detailed design, prototyping, and safety analysis. A 3D whole-core exact-geometry model of a VHTR prismatic block configuration with a detailed component representation has been developed and implemented for calculations with MCNPX. This model is was developed to allow robust isotopic and physical metric changing on the fly. Such a model is not only favored but required for high fidelity depletion of full core models. Such a model allows the user to not only change isotopics, such as the addition of new fuel feeds, but also the 3D movement of fuel blocks, and if required, the addition of core physical parameter changes, including control rod movement and specialized fuel block addition and/or removal. With these abilities, a precise neutronic model can be evaluated.

III.E 3D DB-VHTR Performance Fuel Block Loading and Compact Based Search

With the knowledge that the EOL performance objective of TRU destruction for DB-VHTRSs is impacted by fuel block neutronics more than whole core neutronics, a search for an optimal compact and block loading can be performed for any given fuel vector before time is spent on a high fidelity model. In the case of a five ring design, an infinite assembly models has requires $1/400^{th}$ the time required for the full core high fidelity model. The use of an infinite assembly model is part of wider time management strategy to reduce computation time for this dissertation. With selection of a nuclide vector, an iteration process occurs that selects from a wide scope of possible fuel block designs based on design constraints and user input. This search is demonstrated in Figure 16.

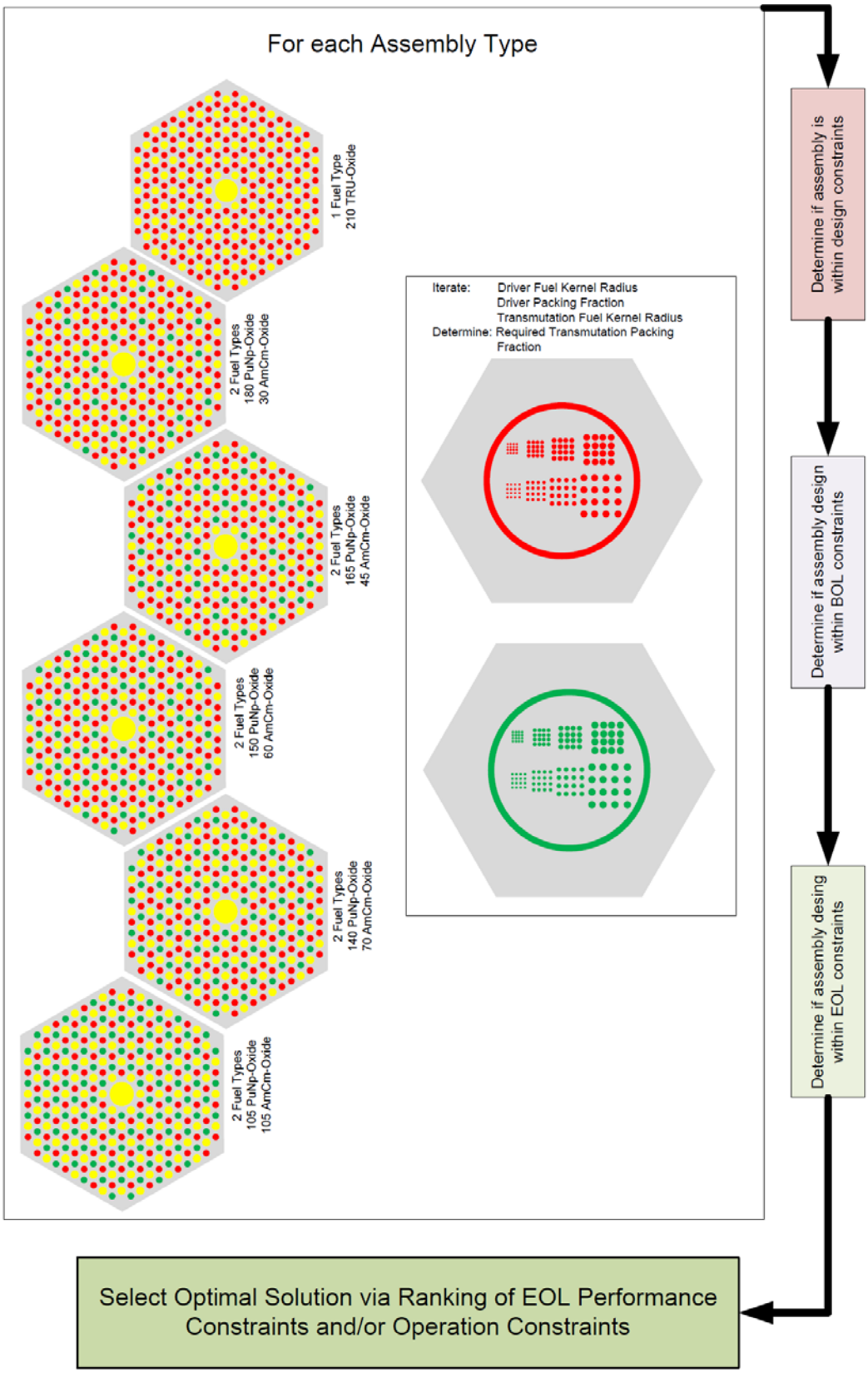

Fig. 16. Iterative fuel block search

III.F Modeling Approach to Capture 3D Whole-Core Exact Geometry DB-VHTR Features in Time

A high fidelity optimization algorithm requires neutronic calculations to assume 3D whole-core exact-geometry representations. This is accomplished through a series of codes and scripts created to manage and automate the enormous data handling requirements. The current code system is implemented through a Unix master command script that executes a subset of Matlab scripts, where optimization calculations occur and MCNPX, as the neutronics workhorse. The requirement of having the Unix master script was dictated by Unix/Matlab/MCNPX interactions that lead to unexpected crashing if MCNPX was executed within the Matlab environment for Unix. Figure 17 shows the basis of the Unix script. This file is a looping algorithm that reads information from Matlab to determine if the core has reached a subcritical state in the case of OTTO DB-VHTR, or if a reload and shuffle is required in a DB-VHTR equilibrium cycle.

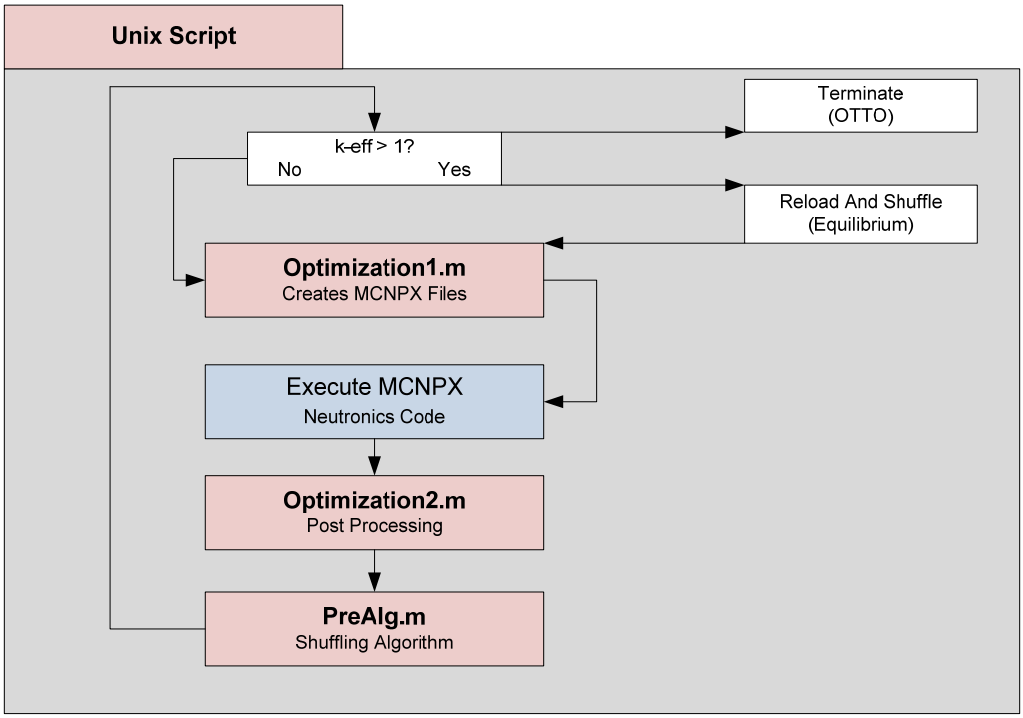

Fig. 17. Unix environment execution

User defined data is stored as hard coded variables in a Matlab script Optimization1.m. This data can also be read from an independent text file, if the user chooses show. The general execution of Optimization1.m is shown in Figure 18. Initially this script determines if any prior calculations have been completed, if there has been, saved data is used for the next step series, if this is the first calculation, user supplied information is used. At this point a shuffling pattern is implemented based on user definitions or on the shuffling algorithm developed for this dissertation. This information is fed into a Matlab function mcnpXburn.m, where the X stands for the number of fuel block rings in the active core. A simple flow of how mcnpXburn.m produces an input file for MCNPX is shown below in Figure 18.

The input files are optimized for flexibility in core configuration and subsequent output processing. This is paramount for not needing to create unique post processing for each core configuration, either being 3,4, or 8 core rings, or having several unique fuel types.

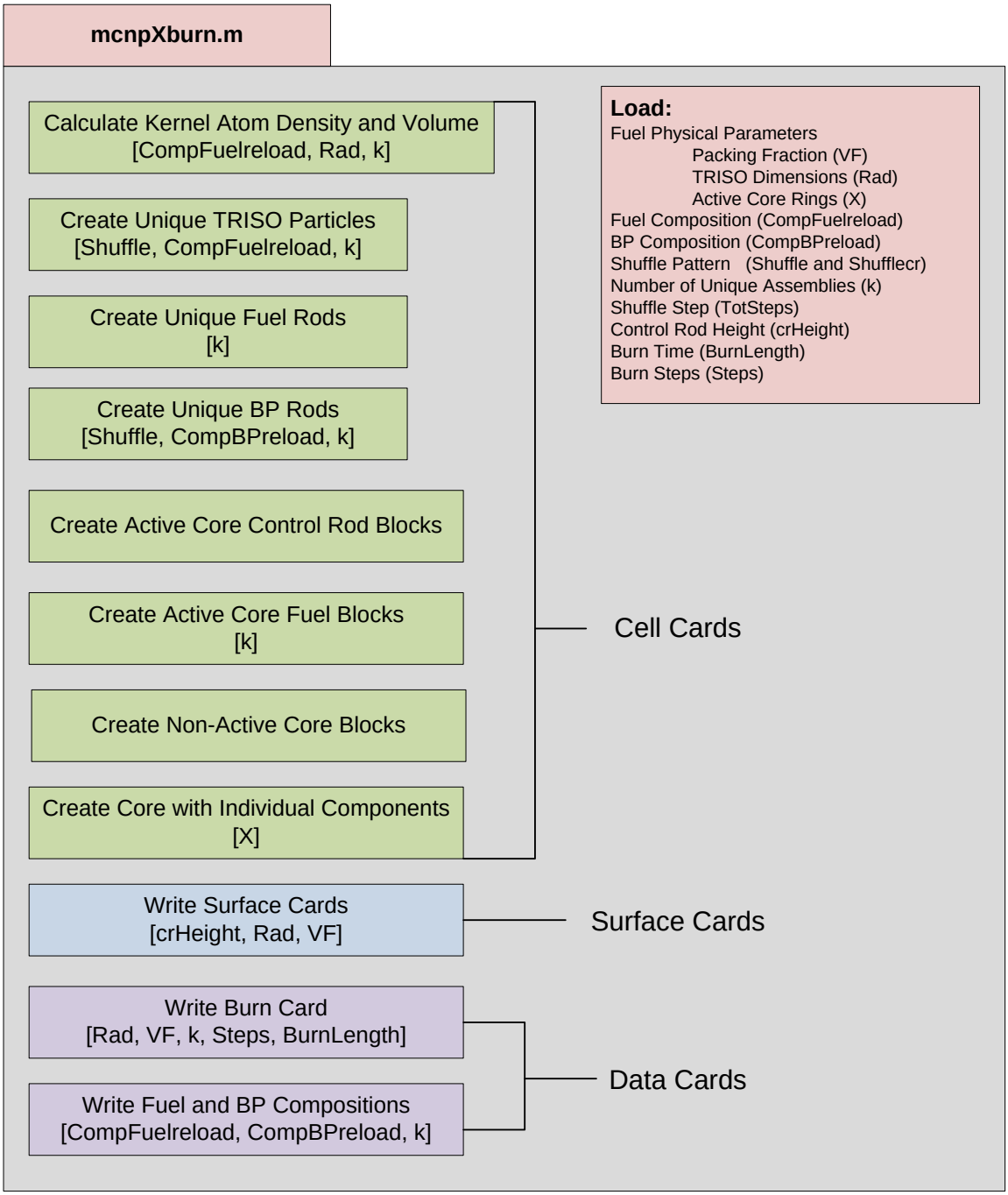

Fig. 18. Mcnpxburn.m

The shuffling algorithm is called upon prior to a new file creation by Optimization2.m. Currently there is a choice of a 3, 4, or 5 rings core configuration. Further information is imported into this function, such as isotopics, shuffling pattern, and core geometry. This function is the backbone of the high fidelity model. The next step creates an executable file containing commands to run MCNPX, including specified file names, and locations. Since there will be several output files created through the burning process, and these files are too large to be managed manually, thus a unique Perl file is created for each MCNPX output file, which extracts relevant information from the output files. This information is stored in smaller text files that can be later read in by the function matcard.m. Execution is ended by saving the Matlab workspace.

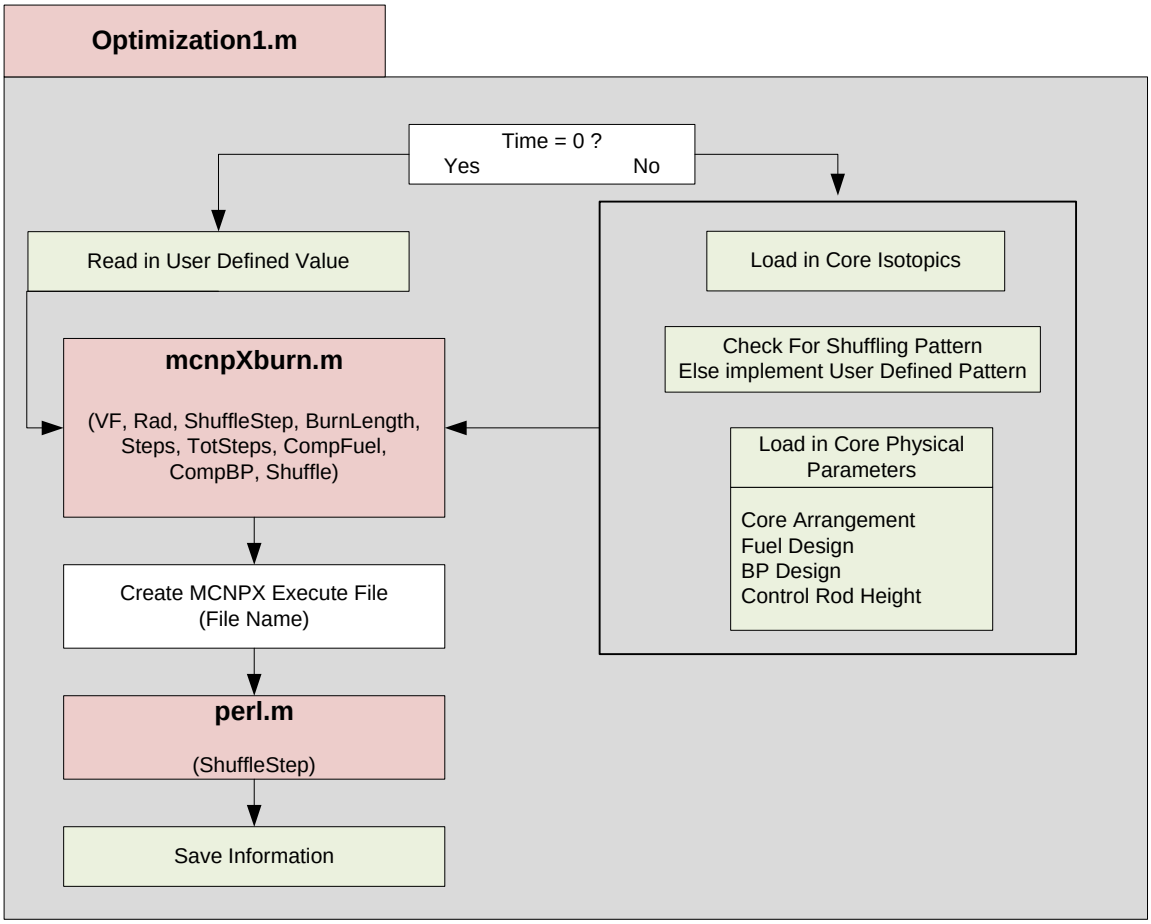

Fig. 19. Optimization1.m

After the Unix script executes MCNPX, a second Matlab script is ran. This script, Optimization2.m, is chiefly a data management subroutine. A general flow of how Optimization2.m operates is shown in Figure 20. Initially, saved data is retrieved and loaded into the Matlab workspace followed by the execution of the Perl file created by Perl.m. As mentioned above, Perl is chiefly used to extract data from the MCNPX output files. This data creates several text files that are read and manipulated by the Matlab function matcard.m, which eventually returns data to the workspace used by Optimization2.m. Additional data manipulation occurs next, including the use of data from prior burnup steps. The script terminates with the Matlab workspace being saved and the final k-eff of the burnup step to the Unix script.

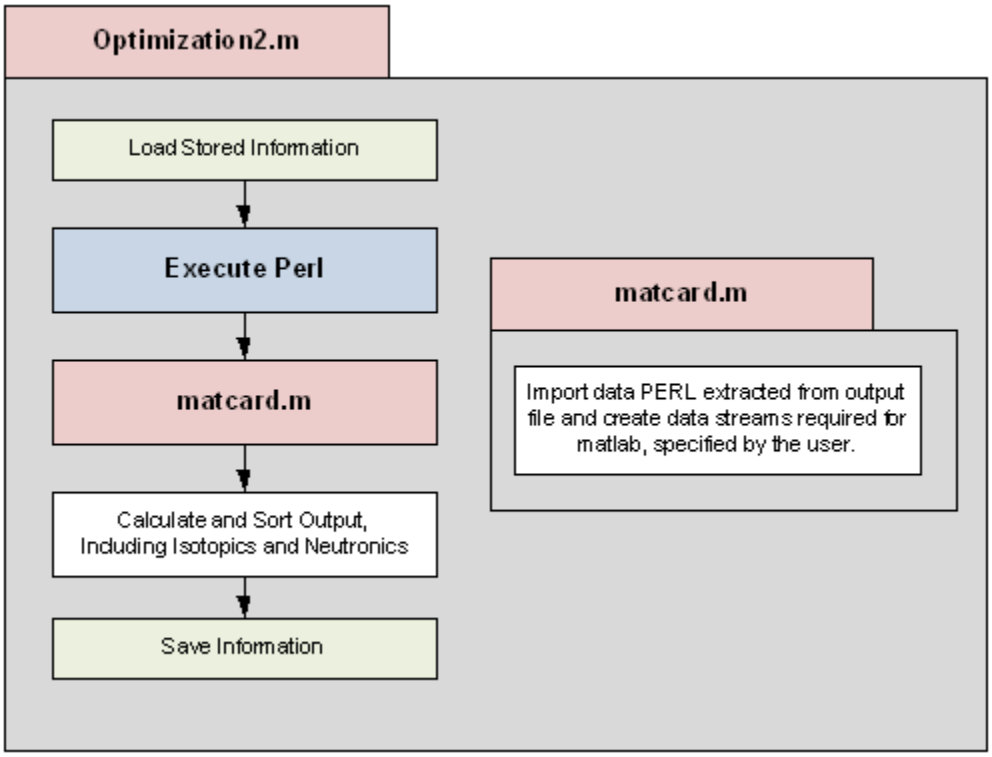

Fig. 20. Optimization2.m

III.G Operation and Performance Domain Mapping

MCNPX (MCNP eXtended) is a general purpose Monte Carlo radiation transport code designed to transport nearly all particles at nearly all energies. Starting with the release of MCNPX 2.6, several new features were added from the prior version, most important to this research, the ability of in-code depletion. The depletion/burnup capability is based on CINDER90 and MonteBurns. Currently, the depletion/burnup/transmutation capability is limited to criticality (KCODE) problems.

MCNPX depletion is a linked process involving steady-state flux calculations in MCNPX and nuclide depletion calculations in CINDER90. MCNPX runs a steady-state calculation to determine the system eigenvalue, 63-group fluxes, energy-integrated reaction rates, fission multiplicity (ν), and recoverable energy per fission (Q values). CINDER90 then takes those MCNPX-generated values and performs the depletion calculation to generate new number densities for the next time step. MCNPX takes these new number densities and generates another set of fluxes and reaction rates. The process repeats itself until after the final time step specified by the user.

MCNPX calculates parameters only for those materials listed on the MCNPX material cards, produced by the isotope generator algorithm, or selected by the specified fission-product tier. When the information is not specified from MCNPX, CINDER90 tracks the time-dependent reactions of 3400 isotopes using intrinsic cross-section and decay data inherent in the CINDER90 code. MCNPX is only capable of tracking energy-integrated reaction-rate information for those isotopes containing transport cross sections, for the following reaction rates: (n,gamma), (n,f), (n,2n), (n,3n), (n,alpha) and (n,proton). For those isotopes not containing transport cross-section information, MCNPX calculates a 63-group flux that is sent to CINDER90 and matched with a 63-group cross-section set inherent in CINDER90 to generate 63-group reaction rates. The 63-group cross sections in CINDER90 were collapsed over a generic spectrum that may or may not be representative of the system to be analyzed and thus may lead to large discrepancies in the isotope inventory of daughter products from these reactions. Those reaction rates are then energy integrated to determine the total reactions occurring. CINDER90 utilizes

decay and energy integrated reaction-rate probabilities along with fission yield information to calculate the temporal nuclide buildup and depletion. The library of data in CINDER90, residing in the CINDER.dat library file, includes isotope decay and interaction probability data for 3400 isotopes including, ~30 fission yield sets, and yield data for 1325 fission products. A flow of data is shown in Figure 21.

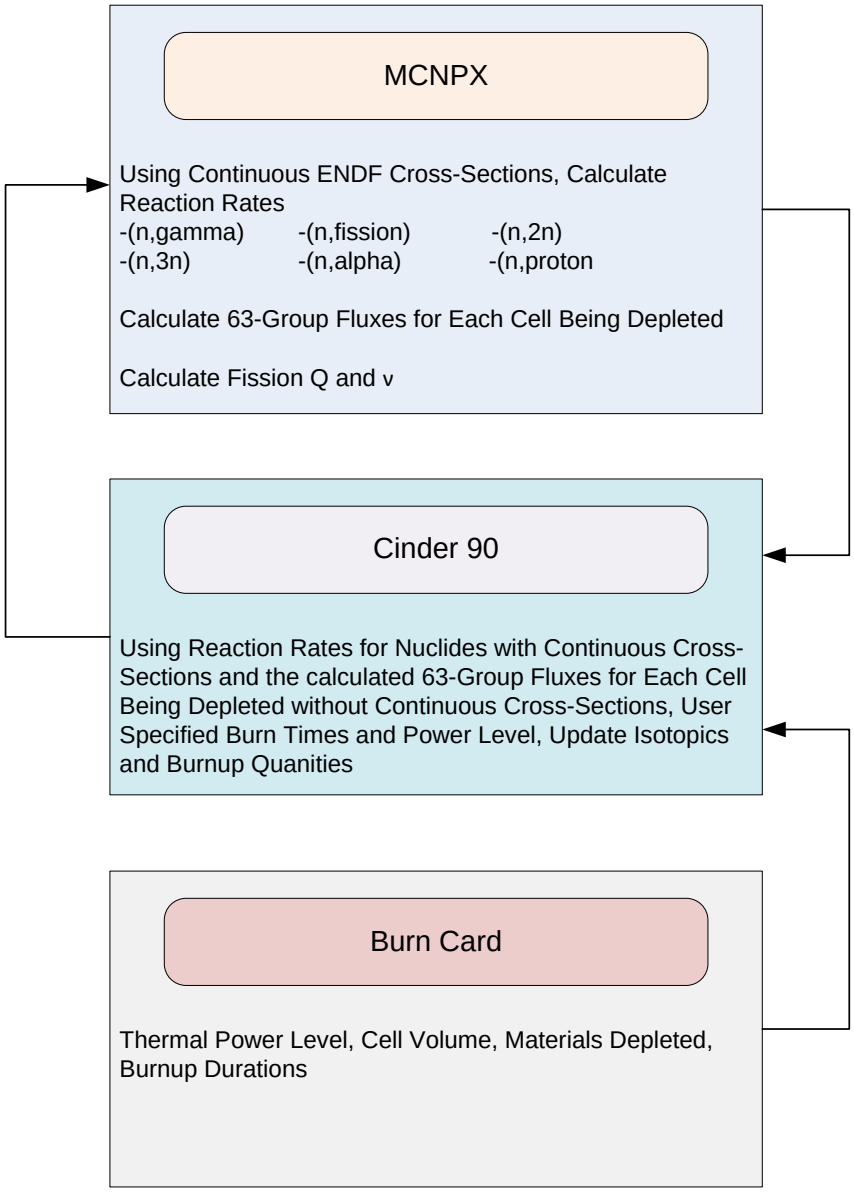

Fig. 21. Cinder 90, MCNPX, input file data flow

III.H 3D Core Operation Tracking with Block Movement (Reconfigurable Cores)

The ability to create high fidelity, 3-D burnable, reconfigurable cores is due to the mcnpXburn.m Matlab function. This function has the capability to create three, four, or eight ring configurations. There are currently three fuel block configuration options. The first option provides one unique fuel and one unique burnable poison per fuel block. The second option provides for a higher fidelity radial depletion model that includes seven unique fuel mixtures in assemblies without control rods and six fuels in assemblies that contain control rod guide holes, as well as one burnable poison in each fuel block. The final option allows for two unique TRISO particles to be modeled and inserted into assemblies in the form as special rods. The pattern of fuel loading for the second and third options are hardcoded in, but there is the ability to change the pattern by the user. At this date, the user must make changes within the code but by the addition of a few lines of code, a pattern change can be incorporated by auxiliary input formats such as a separate ACII file. This ability is embedded into Matlab and was a major reason for choosing Matlab as the primary core coding tool. Example of fuel block loading patterns can be seen in Figure 22.

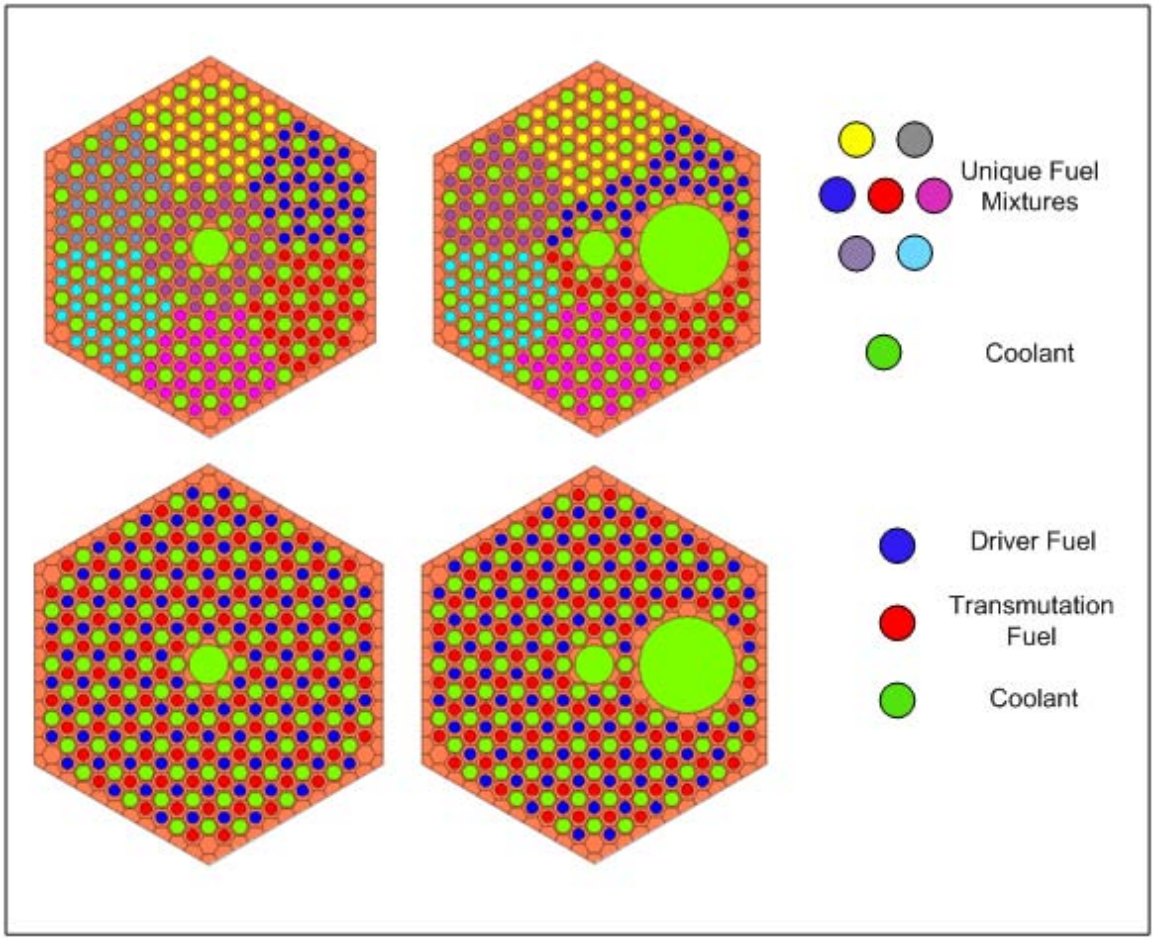

Fig. 22. Fuel block design example

All core options follow a general pattern of creation. Initially, the user supplies the core arrangement, while fuel block design can either be dictated by the user, or searched for based on performance objectives and design constraints. Next the code determines the number of unique TRISO particles to be designed. In an effort to maximize the efficiency of MCNPX for creation of high detailed cases, universe, material and cell numbers at all times must be tracked due to MCNPX placing limits on number lengths. The most limiting for this research is the maximum cell number of 999,999. Though this limit is large, to create one unique fuel rod, nine cell numbers are required. So far the maximum cell numbers needed has approached 25,000, though much less then the nearly one million allowed, if unique rods were modeled in all locations, approximately one million cells would be required.

Each input file follows a similar pattern; cells are grouped by type and combined into universe family sets. By doing so, input flows in a predictable pattern, this insures that a user with knowledge of the file flow will have the ability to debug and incorporate additional features, such as tallies. A general flow down of universe families can be seen in Figure 23. Files are designed with the emphasis on block movement. To ensure such a task can be accomplished without error, inputs were designed to be static geometrically and dynamic with respect of material properties.

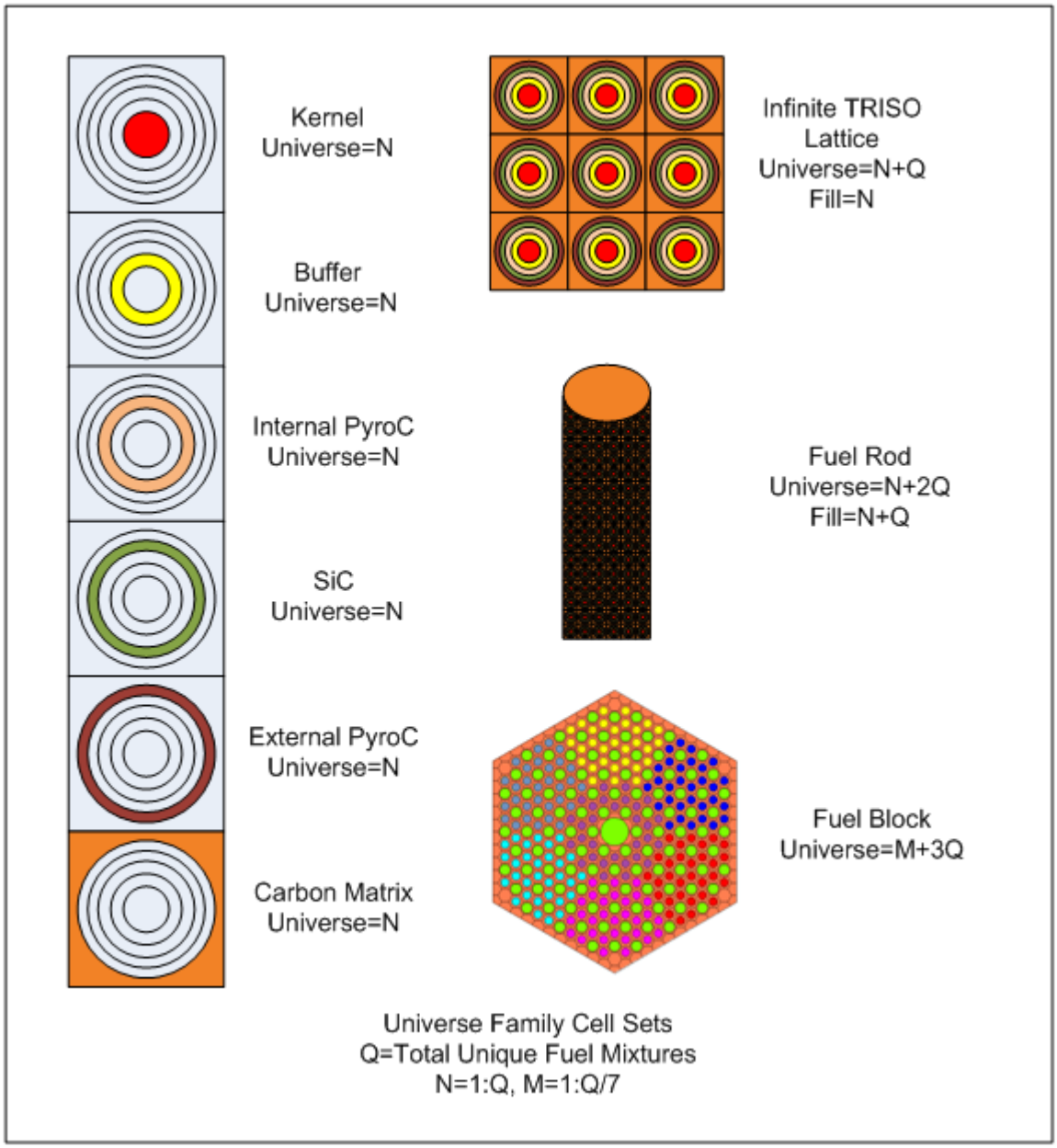

Fig. 23. Geometry domain vectorization

Essentially location throughout the core is determined by cell number. For example in a simple one fuel per fuel block 5 ring configuration, there are 240 unique blocks, 50 with control rod channels, 190 without. The simplest shuffled core optimization is an fuel block with only one unique fuel and one unique BP per fuel block and a random 3D shuffle. In this case the MCNP input file will define one unique TRISO kernel cell as:

10001 1000 7.2451E-02 -10 VOL=1.41372e-05 u=10 imp:n=1 $ Fuel kernel

The two values in bold, the material number and corresponding atom density, are the only numbers changed in the cell block of the MCNP file. This allows block movement to be reflected by changing only the material information in the model. In the case of this configuration, an array named Shuffle with dimensions of 240 by 1 is produced. In the cases of a 3D-random OTTO DB-VHTR model. This array is populated during each shuffle step as follows:

$$Shuffle\begin{bmatrix}1\\2\\.\\.\\.\\239\\240\end{bmatrix} \rightarrow Shuffle\begin{bmatrix}1 & rp(1:50)\\2 & rp(1:50)\\. & rp(1:50)\\. & rp(1:50)\\50 & rp(1:50)\\51 & rp(51:240)\\. & rp(51:240)\\. & rp(51:240)\\240 & rp(51:240)\end{bmatrix} \rightarrow Shuffle\begin{bmatrix}1 & rp(1:50) & rp(1:50)\\2 & rp(1:50) & rp(1:50)\\. & rp(1:50) & rp(1:50)\\. & rp(1:50) & rp(1:50)\\50 & rp(1:50) & rp(1:50)\\51 & rp(51:240) & rp(51:240)\\. & rp(51:240) & rp(51:240)\\. & rp(51:240) & rp(51:240)\\240 & rp(51:240) & rp(51:240)\end{bmatrix}$$

where rp=random # between X:Y, but not repeating in any one column

A separate array stores the material information for the fuel and another for BPs, as shown below.

$$
\begin{array}{c}
\\
isotope(i) \\
isotope(i+1) \\
. \\
. \\
. \\
isotope(i+n)
\end{array}
\begin{array}{c}
\begin{array}{ccccccc} & 1000 & . & . & . & 1239 \end{array} \\
\left[\begin{array}{ccccccc}
(i,j,k) & (i,j+1,k) & . & . & . & (i,j,k) \\
(i+1,j,k) & . & & & & . \\
. & . & & . & & . \\
. & . & & & . & . \\
. & . & & & & . \\
(i+n,j,k) & . & . & . & . & (i+n,j+239,k)
\end{array}\right]
\end{array}
$$

i, is the number of isotopes tracked

j, is the material number

k, is the number of times shuffled (2)

With these two arrays and the addition a final array that simply contains the x, y, and z of each cell, the core can be shuffled, while essentially maintaining track of the fuel material number inside this array. Additionally to a 3D random shuffle, the core can be shuffled 2D-randomly via axial or radial only movement.

With knowledge that fuel burnup behavior is dependent on core configuration changes during operation, a shuffling scheme that takes advantage of performance characteristics can increase/decrease desired final selected fuel characteristics.

III.I Core Shuffling Algorithm for Optimized DB-VHTR Bounded by Operational Constraints

The effect of switching two assemblies on total excess reactivity of the DB-VHTR system can be calculated, with relatively low error, the time required for using the system mapping function [S] is be greatly reduced. As mentioned prior, the number of possible shuffled core configurations cannot be possibly checked in the effort to find the domain optima. A search such as that shown in Figure 14 could be avoided while not having to use a neutronics code to determine excess reactivity for every core shuffle permutatoin; the system optima search range can be increased. Even with a reduction of computation time need for each shuffle configuration, the large number still poses an unworkable amount of computation time. In this effort, the Paretto set of possible combinations is attacked by a selection process in combination with a predictive excess reactivity model.

Knowing N_i, atom density for nuclide i, for each fuel and burnable poison, the following attributes can be calculated for each fuel and burnable poison:

$$\frac{RR_{\text{Reaction j, Nuclide i, Assembly k}}}{N_{i,k}} = \sum_E \phi_k(E)\sigma_{j,k,i}(E), \text{ for each assembly location}$$

$N_{i,k}$ = atom density for nuclide i, assembly k [atoms/cc]

$RR_{\text{Reaction j, Nuclide i, Assembly k}}$ = Reaction Rate for nuclide i, assembly k, Assembly k [Reactions]

$\phi_k(E)$ = Flux for location of assembly k [n/cm^{2}s]

$\sigma_{j,k,i}(E)$ = Microscopic Cross-Section for location of assembly k, nuclide i and Reaction j [cm^2] (3)

Nuclide vectors from any one fuel block can be used to predict reaction rates for possible relocation of the mentioned fuel block throughout the core. With these reactions rate predictions, a measurement of reactivity can be calculated for each possible fuel block re-location as shown below:

$$\frac{\sum_{i=1}^{I} \frac{RR_{\nu*\text{fiss,i,k1}}}{N_{i,k1}} N_{i,k2}}{\sum_{i=1}^{I}\left(\frac{RR_{\text{fiss,i,k1}}}{N_{i,k1}} N_{i,k2} + \frac{RR_{\alpha,\text{i,k1}}}{N_{i,k1}} N_{i,k2} + \frac{RR_{\gamma,\text{i,k1}}}{N_{i,k1}} N_{i,k2} + \ldots\right)} = \text{Reactivity Excess} \quad (4)$$

The calculated quantity, reactivity excess, is a dimensionless quantity and does not reflect the amount of material located in each fuel block. It is thus possible to assemblies with similar Reactivity Excess values but not share the same mass of fissile isotopes. Thus it must be weighted to known excess reactivity for an fuel block with closely related burnup. Further weighting of known spectral changes from core movement location can be added to account for increase of thermal neutrons from near reflector locations. Investigation into effects of using RRs produced from fresh fuel to calculate RRs for high burnup fuel showed minimal error in calculation of excess reactivity, while the opposite approach; using RRs from high burnup fuel on fresh fuel, produced large errors.

With excess reactivity for any one block in any one location calculated, a search of possible combinations can be calculated. This search is accomplished by producing two matrixes that are NxN and MxM. In the case of a five ring core, there are a total of 50 control rod block with fuel and 190 fuel blocks. This would produce a 190x190 array and a 50x50 array. Two arrays are produce to account for the fact that a fuel block and a control rod bock with fuel cannot swap locations. Figure 24 shows how location and material relate in such an array.

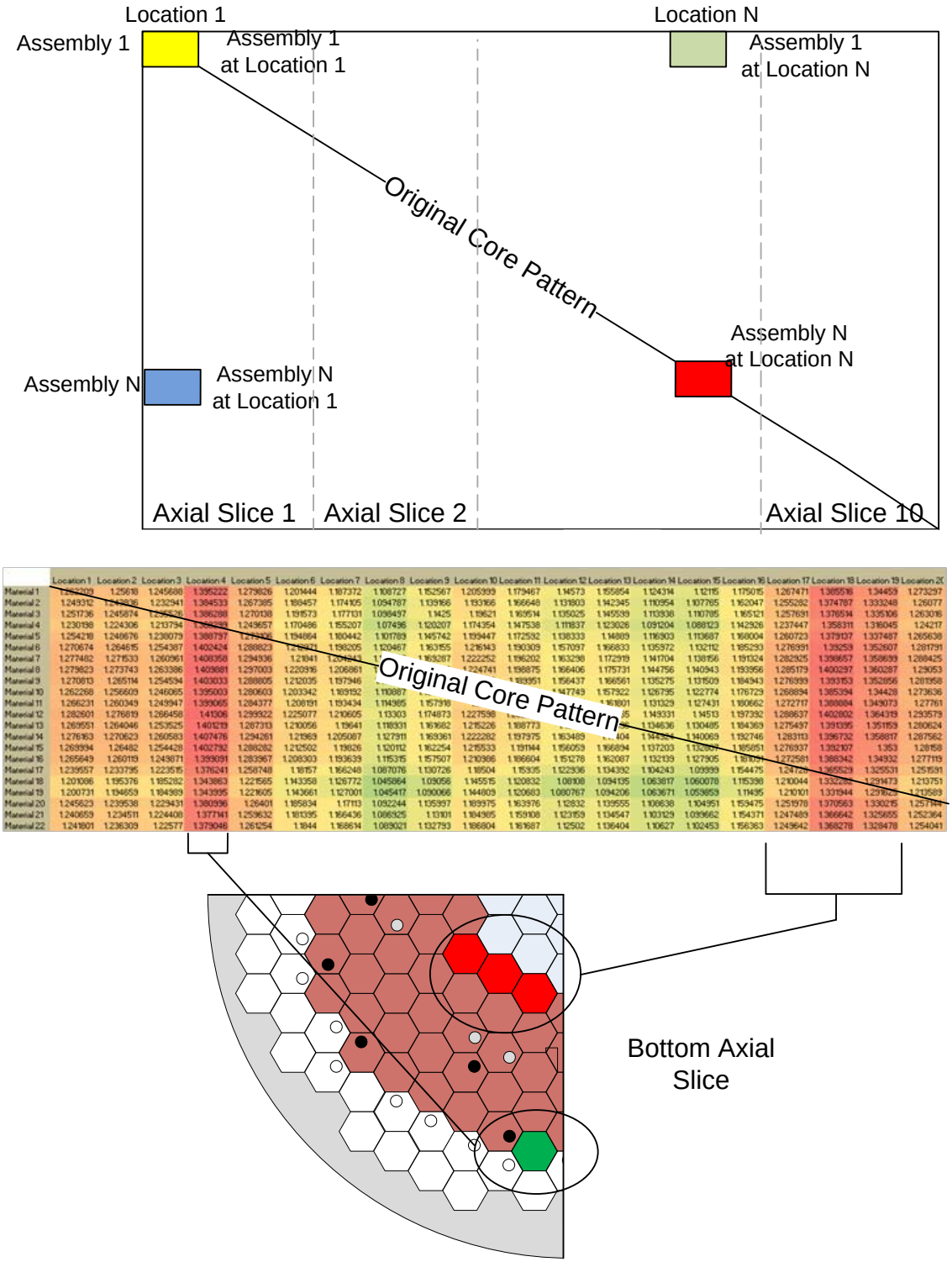

Fig. 24. Excess reactivity prediction

Figure 24 shows the location preference for all materials in location 4 and 18, these locations are next the inner reflector at the bottom of core, several mean paths away away from control rods. The prediction of excess reactivity in a fuel block allows for power profiles to be calculated without running of a neutronics code, this is true only for small permuation, as the permutations increase, data used to predict core behavior requires recalculation. Operation constraints, most important for core reloading, is the diminishing of power peaking, without power peaking reduction DB-VHTRs can exhibit power peaks of excess of 4. Current design requirements of power peaking have not been formalized for VHTRs, but it is believed that power peaks near 2 could be found to be acceptable due the robustness of VHTR safety and fuel design [Advance HTGR Systems, Yasuyoshi Kato]. Section IV, shows a demonstration of how the predictive algorithm with a constraint on power peaking produced an in-core acceptable fuel block shuffle, versus an arbitrary reload pattern.

To accomplish power peaking reduction, assemblies with lower excess reactivity can be placed into these locations or boron can be added to reduce peaking. Both these methods can have a large effect on system excess reactivity at BOL and EOL, in the case of an equilibrium cycle limitation of adding boron to only fresh fuel imposes a larger effect on excess reactivity due these assemblies being the major driver of system excess reactivity. To solve this problem the following algorithm is implemented to create two arrays similar as to those produced above to estimate system excess reactivity per unit mass:

$$RR_{\infty}(k2,k1)=\sum_{i=1}^{I}\left(\frac{RR_{\nu*\text{fiss,i,k1}}}{N_{i,k1}}N_{i,k2}\right)_{Fuel}-\sum_{i=1}^{I}\left(\frac{RR_{\alpha,\text{i,k1}}}{N_{i,k1}}N_{i,k2}+\frac{RR_{\gamma,\text{i,k1}}}{N_{i,k1}}N_{i,k2}+\ldots\right)_{Fuel}$$
$$-\sum_{i=1}^{I}\left(\frac{RR_{\alpha,\text{i,k1}}}{N_{i,k1}}N_{i,k2}+\frac{RR_{\gamma,\text{i,k1}}}{N_{i,k1}}N_{i,k2}+\ldots\right)_{BurnablePoison}$$

$RR_{\infty}(k2,k1)$ = Reactions produced for assembly k2 placed in the location of assembly k1
A positive RR_{∞} indicates excess neutrons being produced,
negative indicates a net neutron absorption

$Find\ \max(RR_{\infty}(k2,k1));\qquad I=k2;\qquad J=k1;$
$k2$ = highest reactive assembly
k1 = most preffered power production location

$RRx=RR_{\infty}(:,I);\qquad RRy=RR_{\infty}(J,:)'$
RRx = Sorted vector of reactive assemblies based on location k1
RRy = Sorted vector of assembly location based on assembly k2

$Shuffle_1=sort_{ascending}(RRy,RRx)$
$Shuffle_1$ = Highest excess reactive shuffle pattern (5)

$Shuffle_1$ is generally the highest reactive core, placing assemblies with the highest excess reactivity in preferred core fuel block location. At this point core excess reactivity can be estimated, based primarily on the summation $RR_{\infty}(Shuffle(:,1),Shuffle(:,2))$. In respect to meeting power peaking criteria, power peaking for each fuel block location can be estimated by calculating the following quantity.

$$\frac{RR_{\infty,CR}(Shuffle(:,1),Shuffle(:,2))}{mean(RR_{\infty,CR}(Shuffle(:,1),Shuffle(:,2))}=PP_{CR}(Shuffle(:,1),Shuffle(:,2))$$

$$\frac{RR_{\infty,SA}(Shuffle(:,1),Shuffle(:,2))}{mean(RR_{\infty,SA}(Shuffle(:,1),Shuffle(:,2))}=PP_{SA}(Shuffle(:,1),Shuffle(:,2)) \quad (6)$$

where array $RR_{\infty,SA}$ is for non control rod assemblies and $RR_{\infty,CR}$ is for fuel assemblies with control rods. Starting at the highest peaking fuel block which is:

$$RR_{\infty,SA}(Shuffle(1,1), Shuffle(1,2)) . \quad (7)$$

An adjustment has to be made, by addition of BP or by fuel block rotation, to meet the power peaking criteria. In the case of core shuffle permutation, implementation of the following method produces an estimated core that satisfies the selection criteria. In the case of rotated assemblies a criteria defined as permute criteria is called for. This criteria is based on excess neutron productions and directly relates to power peaking. It can range from an excessively large number, which would be more then the possible peaking in a core to a number of the actual maximum operation criteria, which for this dissertation is two. A second criteria is used for BP, by changing these numbers a core can be meet operation criteria solely on BP addition or fuel block rotation or a combination of both. Generally both is needed to ensure excess reactivity at BOL and the minimization of need BP. In the case of fuel block rotation the process is as follows:

1) Determine if $\frac{RR_{\infty,SA}(Shuffle(i,1), Shuffle(i,2))}{mean(RR_{\infty}(Shuffle(i,1), Shuffle(i,2))} > permutate\ criteria$
2) If Yes, Cycle through assemblies from highest to lowest to find an acceptable fuel block location

   while $RR_{\infty,SA}(Shuffle(i+j,1), Shuffle(i,2)) > criteria$
   $j = j+1$
   end

3) Shift assemblies from i to j down one preferred location move fuel block j+1 to location i. The location preference is based on shuffle pattern produced from the method at the beginning of this section
4) Recalculate $mean(RR_{\infty}(Shuffle(i,1), Shuffle(i,2))$, begin at i=1;

This shuffling algorithm is based on the concept that small permutation to the core shuffle pattern does not drastically change core-wide neutronics characteristics. At a predetermined permutation limit, the algorithm requires cross-section and spatial flux distribution be recalculated. This can be seen in Figure 25. The use of a neutronics code is used to determine if the core meets all criteria within a given error, if not, new

reactions rates are collected to produce a more updated RR array based on reactions rates for each location as done before, this iterative process is short and produces a core meeting the power peaking selection criteria. The other method of power peaking reduction by BP addition can be done. In this case, the known minimal BP addition has been estimated via the prior method, the reverse of this method can produce cores with either maximum BP additions or a hybrid between these two scenarios, i.e. a daughter between the two methods.

Beginning with the core arrangement produced above

5) Determine if $\frac{RR_{\infty,SA}(Shuffle(i,1),Shuffle(i,2))}{mean(RR_{\infty}(Shuffle(i,1),Shuffle(i,2))} < BPcriteria$

6) Cycle through assemblies from highest to lowest and calculate BP addition to meet the burnable poison criteria. Only fresh assemblies can have BP added.

while $RR_{\infty,SA}(Shuffle(i-1,1),Shuffle(i,2)) < criteria$

increase BP such that

$$\sum_{i=1}^{I}\left(\frac{RR_{\alpha,i,k1}}{N_{i,k1}}N_{i,k2}+\frac{RR_{\gamma,i,k1}}{N_{i,k1}}N_{i,k2}+\ldots\right)_{old} < \sum_{i=1}^{I}\left(\frac{RR_{\alpha,i,k1}}{N_{i,k1}}N_{i,k2}+\frac{RR_{\gamma,i,k1}}{N_{i,k1}}N_{i,k2}+\ldots\right)_{new}$$

$$RR_{\infty}(k2,k1)=\sum_{i=1}^{I}\left(\frac{RR_{\nu*fiss,i,k1}}{N_{i,k1}}N_{i,k2}\right)_{Fuel}-\sum_{i=1}^{I}\left(\frac{RR_{\alpha,i,k1}}{N_{i,k1}}N_{i,k2}+\frac{RR_{\gamma,i,k1}}{N_{i,k1}}N_{i,k2}+\ldots\right)_{Fuel}$$
$$-\sum_{i=1}^{I}\left(\frac{RR_{\alpha,i,k1}}{N_{i,k1}}N_{i,k2}+\frac{RR_{\gamma,i,k1}}{N_{i,k1}}N_{i,k2}+\ldots\right)_{BurnablePoison}$$

end

Steps 1 through 6 are repeated by changing the permute criteria and BP criteria until N shuffle patterns are produce. Each shuffle pattern can be run to determine BOL excess reactivity. If excess reactivity is above acceptable criteria, more BP should be added to reach a k-eff close to 1. BP addition is done by lowering the BP criteria shown in step 5. At the end of this process there will be N acceptable core shuffling permutations based on the number of time the permutation criteria have been changed. Each shuffle pattern can then be selected for a depletion run to determine which pattern produces the best

EOL metrics such as TRU destruction. This process is illustrated in Figure 25. From the prior estimated k! possible core configurations, this is an enormous reduction in permutations, requiring a neutronics code only to search from a few optimal solutions to find the likely domain optimal solution. The difference in EOL metrics from choosing any one daughter permutation is small, thus any solution could be used based on prior experience as the final solution.

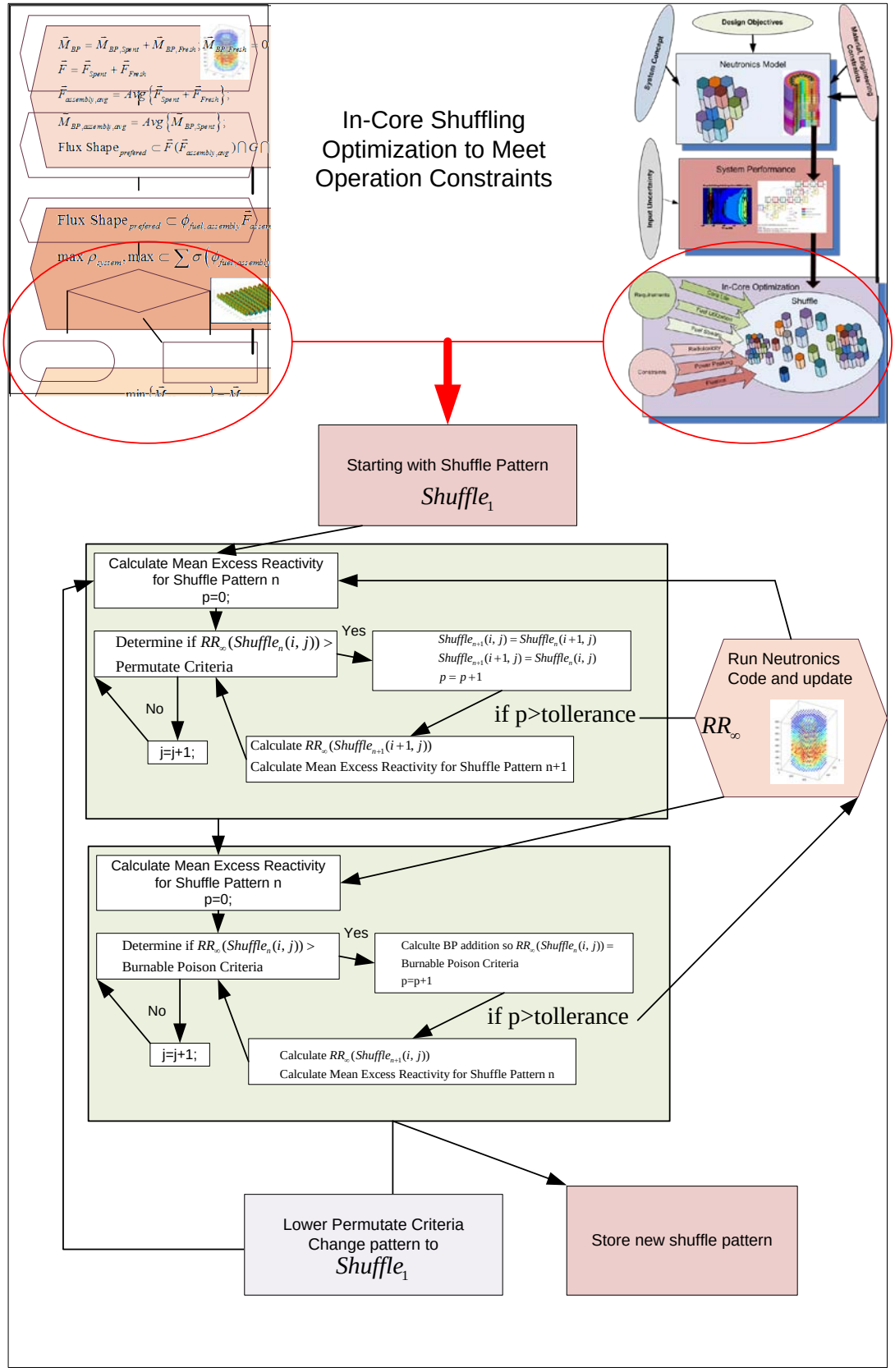

Fig. 25. Permutation subset algorithm of predictive 3D shuffling algorithm

IV. PERFORMANCE ANALYSIS OF DB-VHTR

In this section, sample studies of the VHTR operation domain for several core configurations are performed. To demonstrate validity of the developed DB-VHTR physics based shuffling algorithm, performance of several fuel compact configuration and fuel block loading patterns were evaluated through integral system performance characteristics including system excess reactivity and power peaking in individual assemblies. Fuel compact configuration refers to variations in packing fractions, kernel radius and number of individual fuels. Various packing fractions and kernel dimensions lead to different number of particles in each rod and fuel volume per compact. For a compact with same fuel volume but varying TRISO dimension and packing fraction produces variation in the number of particles in a single compact as shown in Table VII. The ability of HTGRs' to allow large variations of fuel physical parameters to influence the nuclear physics within the fuel kernel, will be demonstrated throughout this section.

Table VII. Kernel and Compact Packing Fraction Relationship to Particles per Compact

Packing Fraction	**Kernel Radius**	**TRISO Radius**	**Matrix Box Dimension**	**TRISOs/ Compact**	**Volume of Fuel/Compact**
[%]	[cm]	[cm]	[cm]		[cc]
50%	2.043E-02	3.665E-02	7.444E-02	15581	0.557
45%	2.216E-02	3.838E-02	8.074E-02	12211	0.557
40%	2.438E-02	4.060E-02	8.883E-02	9168	0.557
35%	2.737E-02	4.359E-02	9.970E-02	6484	0.557
30%	3.163E-02	4.785E-02	1.152E-01	4201	0.557
25%	3.829E-02	5.451E-02	1.395E-01	2367	0.557
20%	5.046E-02	6.668E-02	1.838E-01	1035	0.557
15%	8.090E-02	9.712E-02	2.947E-01	251	0.557

IV.A Operation with Single Composition Fuel Vector

A literature review on DB-VHTRs showed a wide variety of fuel designs including isotopics, number of different TRISO particles and particle dimensions[10,11,13,24]. The high fidelity DB-VHTR model developed for this dissertation allows for the user to specify a wide range of system designs, both in core configuration, fuel composition and compact design. The simplest DB-VHTR utilizes only one compact design composed of a Single-Fuel. In this design each fuel kernel throughout the core has identical isotopics. Recent research publications have proposed core designs with TRISO particles manufactured with different isotopics based on element preference. Such designs include placing only PuNp in a kernel, and/or AmCm. Additional designs propose adding of uranium and/or getter material to reduce the impact of free oxygen degradation of TRISO particles. These multi fuel vector variations can be distributed in a multitude of patterns throughout the core, including having unique blocks, unique compacts and/or mixed compacts. In this section, core configurations with one fuel composition are analyzed to determine their ability in DB-VHTR cores to efficiently destroy TRUs.

IV.A.1 BOL Studies for Single Composition Fuel

Initial analysis was focused on a LEU fueled three ring core that closely resembles the proposed NGNP core. This case was then expanded to three more additional configurations formed through additions of inner active core rings. Effects of a changing core configuration were analyzed using power production maps produced at each block location, as shown in Figure 1. Each dot shows an block location in Cartesian coordinates, with color and size of each dot representing power peaking magnitude.

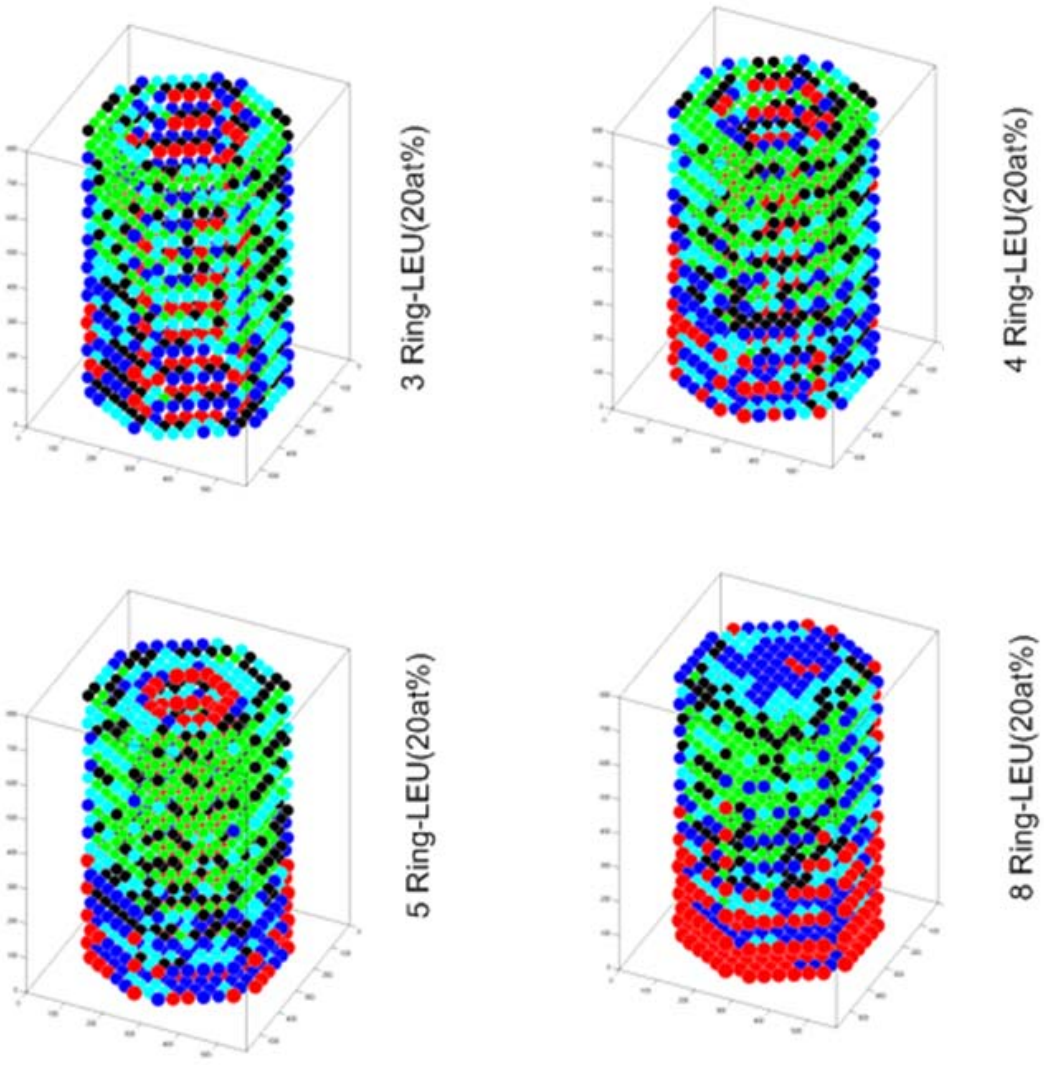

Fig 26. Power profile for LEU (20 at%) VHTR configurations

Figure 26 was demonstrates power peaking variation and preference in the four core configurations (3, 4, 5, and 8 Ring). The most drastic change between the four cores is the power peaking for a 8 ring core near the bottom reflector. The bottom reflector in a VHTR is thicker then the top, thus producing an excess of thermal neutrons by decreasing the leakage of thermal neutrons produced by the reflector. These core all contain 20% enriched LEU and burnable poison in the form of B4C.

Effect of TRISO dimension and compact packing fraction for each of the major core configurations were evaluated by analyzing system criticality at BOL. These cases were run for LEU configurations at varying kernel dimensions and packing fractions for 3, 4, and 5 Ring configurations at an enrichment of 20%. Table VIII shows the results of these cases.

Table VIII. Kernel and Compact Packing Fraction Effects on BOL LEU Single-Fuel Configurations

3 Ring		Packing Fraction				
		5%	10%	15%	20%	25%
Kernel Radius [µm]	150	1.22408	1.39347	1.4518	1.45801	1.45651
	200	1.37941	1.47251	1.47478	1.45479	1.43405
	250	1.44143	1.48816	1.46233	1.44514	1.39939
	300	1.4691	1.4895	1.45924	1.40662	1.38565
	350	1.50277	1.47645	1.43678	1.40418	1.35481
	400	1.51241	1.48421	1.41692	1.38172	1.35251
4 Ring		Packing Fraction				
		5%	10%	15%	20%	25%
Kernel Radius [µm]	150	1.32876	1.4715	1.50622	1.50341	1.48771
	200	1.46528	1.52328	1.51487	1.47916	1.45511
	250	1.51439	1.53051	1.48719	1.46321	1.4106
	300	1.53566	1.52517	1.48236	1.4176	1.38982
	350	1.55823	1.50496	1.44998	1.41059	1.35673
	400	1.55622	1.51348	1.42839	1.38185	1.32744
5 Ring		Packing Fraction				
		5%	10%	15%	20%	25%
Kernel Radius [µm]	150	1.39888	1.52143	1.54083	1.52854	1.51353
	200	1.51915	1.55762	1.540144	1.51681	1.46808
	250	1.56071	1.56234	1.50353	1.47557	1.41509
	300	1.57954	1.54845	1.49603	1.42228	1.39016
	350	1.59171	1.51968	1.46135	1.41256	1.35325
	400	1.58372	1.52924	1.43441	1.38318	1.32014

To illustrate how compact design effect system integral parameter of excess reactivity, a surface plots for varying packing fractions and kernel radius were produced or each core configuration in Table VIII. These surface plots are detailed in Figures 27-29.

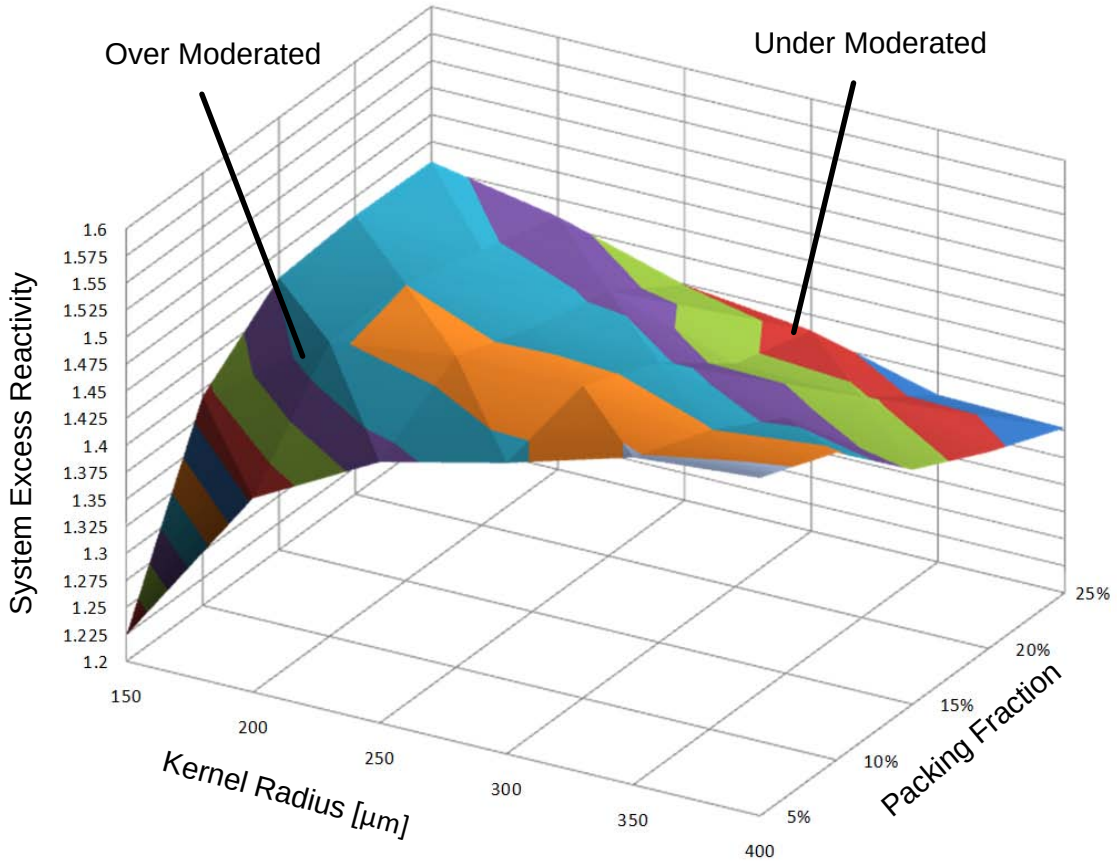

Fig. 27. Kernel and compact packing fraction effects on BOL LEU Single-Fuel three ring configuration

For a three ring LEU fuel core the effects of carbon to heavy metal (moderator to fuel) produced a peak excess reactivity of approximately 1.5. The complexity of the curve in Figure 27 is the resulting tradeoff between C/HM ratio (effected by both PF and Kernel radius) and resonance self shielding inside the kernel (kernel radius). Resonance self shielding is an effect were the mean free path of neutrons at resonance energy is much shorter than the average neutron. These neutrons will have a significant less chance of passing through the fuel kernel and most likely be absorbed before reaching the center of this kernel. The self-shielding effect makes the inner kernel invisible to neutrons at these energies. This effect will have a negative effect on system excess reactivity.

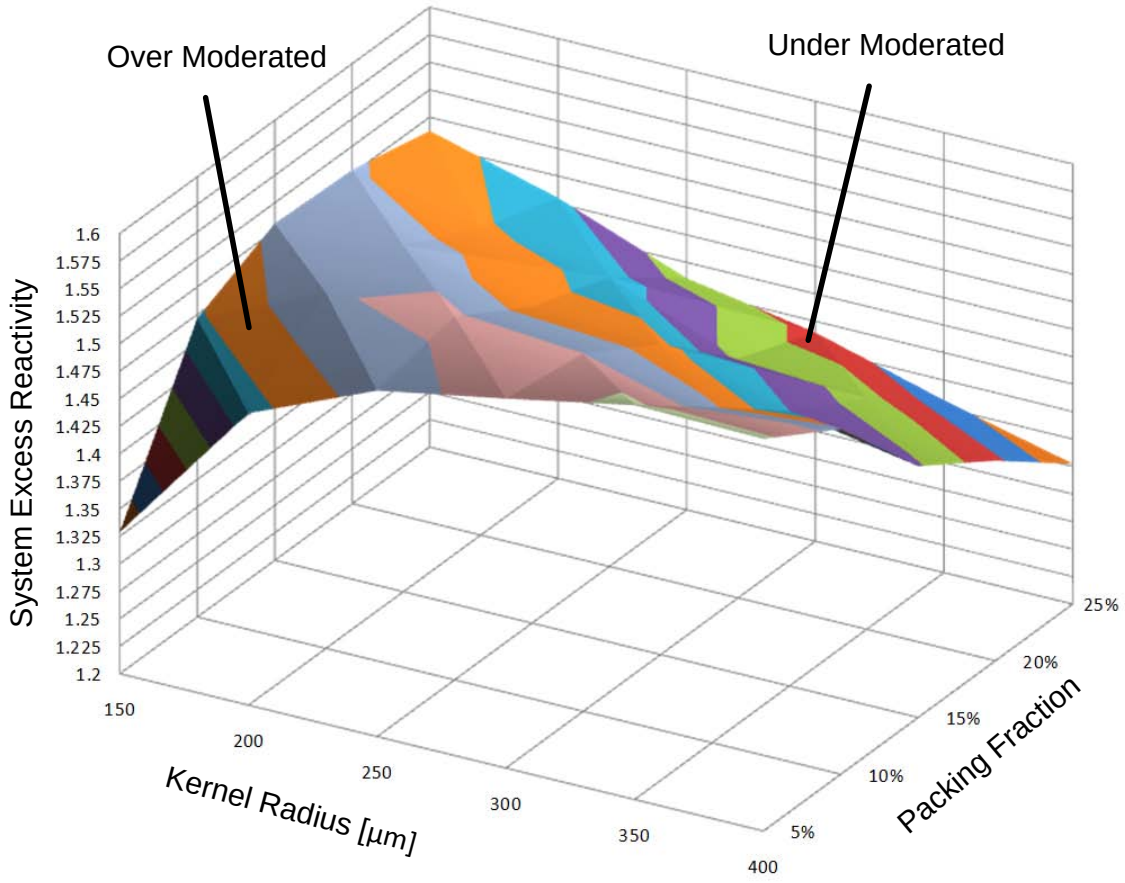

Fig. 28. Kernel and compact packing fraction effects on BOL LEU Single-Fuel four ring configuration

The effects discussed above can be seen in the four ring and five LEU fuel core. The curves as each ring is added shifts the peak excess reactivity peak toward smaller kernels. The result of this is not unexpected, for the reason of self shielding discussed above. As the central reflector is reduced with each ring addition, the average neuron energy in the active fuel ring increases, were resonance absorption is most likely to occur. The four and five ring cores are shown in Figure 28 and Figure 29 respectively.

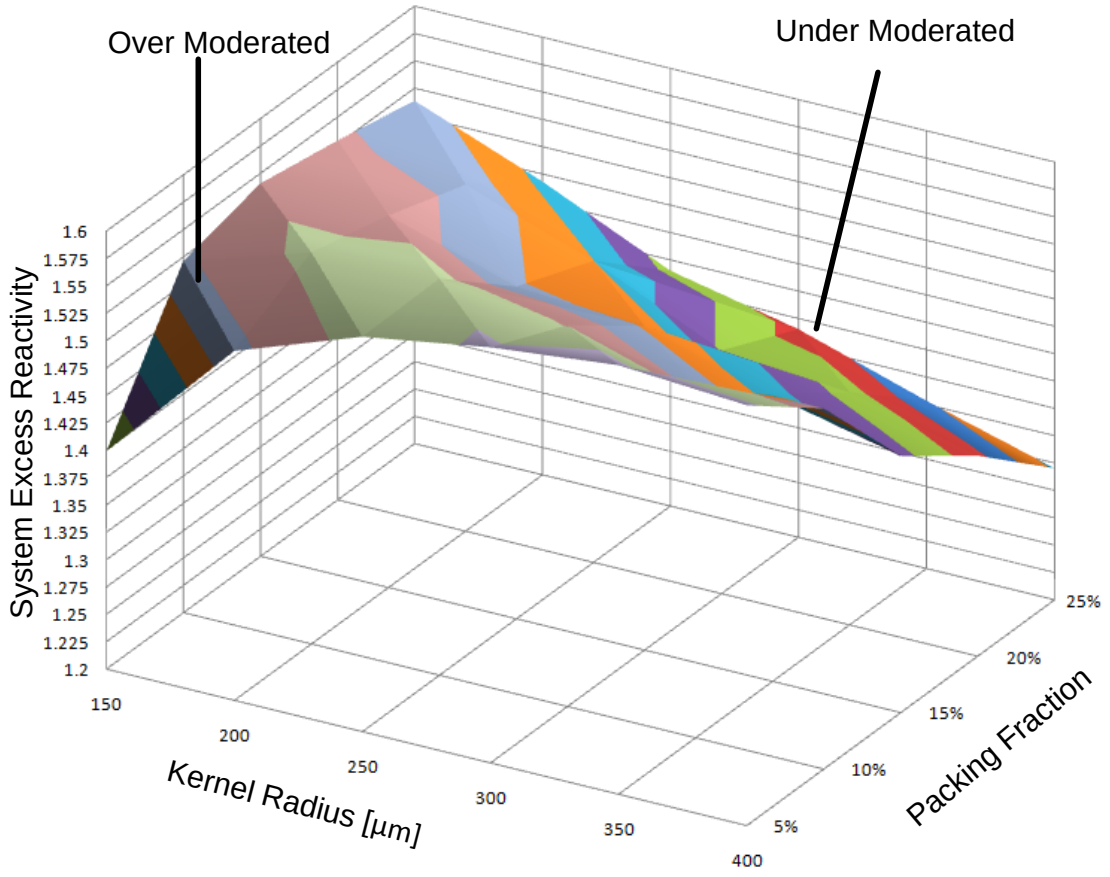

Fig. 29. Kernel and compact packing fraction effects on BOL LEU Single-Fuel five ring configuration

Effects of C/HM changes on LEU loaded cores are well documented by prior studies. Increase in system excess of reactivity is shown in Table IX as an additional ring is added for high C/HM fuels. As C/HM decreases the addition of an extra fuel ring diminishes. This result has not been well document and demonstrates the need for full core high fidelity models.

For comparison of how TRU cores behave compared to LEU cases, a base Single-Fuel TRU core power profile was created for each core configuration. These power profiles are shown in Figure 30.

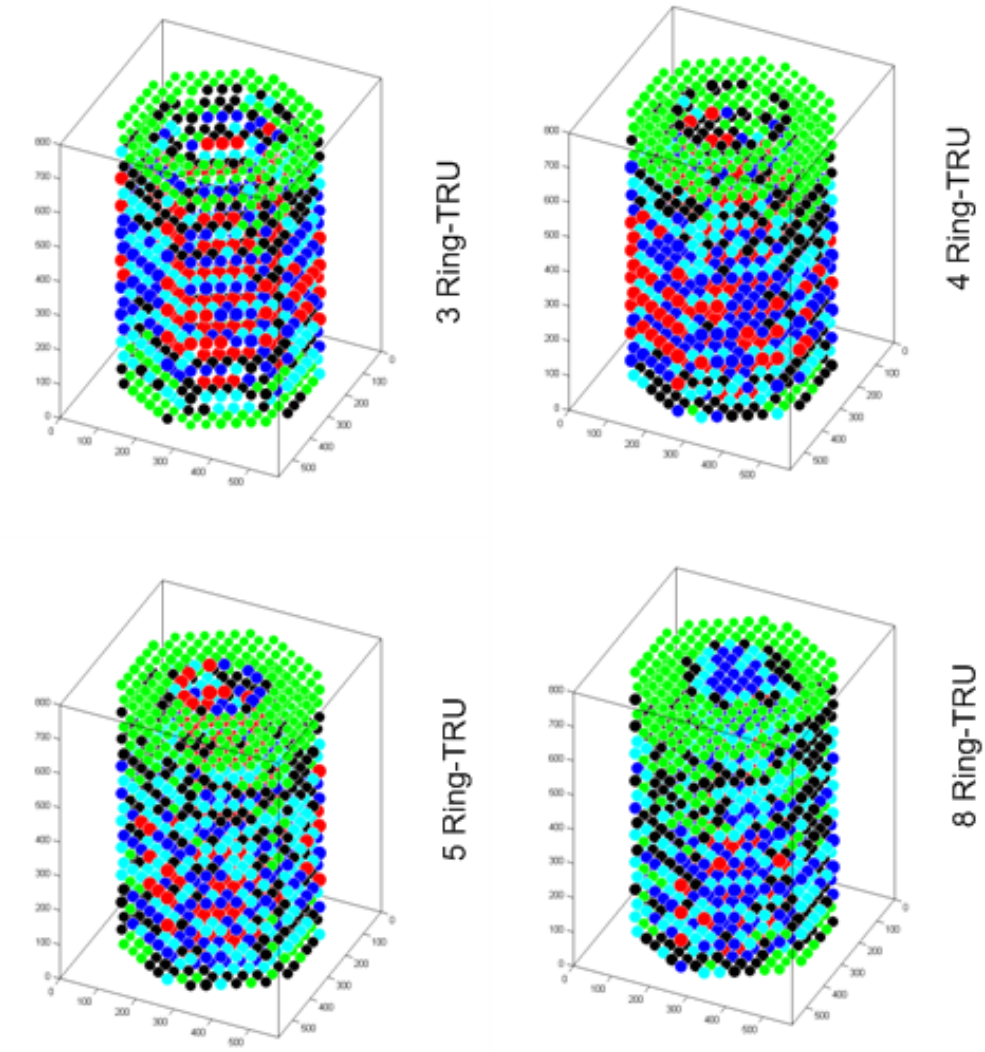

Fig. 30. Power profile for Single-Fuel particle type TRU VHTR configurations

Figure 30 does not readily show a difference in power profile from each core configuration, this is because power peaking for TRU cores tends to occur near the inner reflector and away from the outer reflectors, as shown in Figure 28. System reactivity was calculated for varying compact packing fractions and kernel radii. The effect of fuel parameter variation was calculated for the benchmark 5 ring DB-VHTR core configuration that will be used primarily for analysis in the dissertation.

Table IX. Kernel and Compact Packing Fraction Effects on BOL TRU Single-Fuel Configuration for a 5 Ring DB-VHTR

Packing Fraction [%]	**Kernel Radius [**µm]											
	150	175	200	225	250	275	300	325	350	375	400	425
15	0.9564	0.95935	0.96799	0.98099	0.98788	1.00831	1.02488	1.03544	1.03821	1.05642	1.06802	1.07865
17.5	0.95401	0.96296	0.97534	0.99322	1.01446	1.01852	1.0464	1.06333	1.07407	1.07617	1.09348	1.10745
20	0.95347	0.96914	0.98865	1.00731	1.03215	1.05194	1.05615	1.08683	1.10473	1.11268	1.11532	1.13013
22.5	0.95894	0.97651	1.00498	1.02708	1.04786	1.07563	1.08785	1.09794	1.12713	1.14268	1.14753	1.15136
25	0.96412	0.98964	1.01724	1.04318	1.06521	1.09166	1.11661	1.12151	1.14205	1.16522	1.17708	1.18016
27.5	0.97161	1.00469	1.0287	1.06511	1.0858	1.10714	1.13546	1.15158	1.15596	1.18068	1.19955	1.20826
30	0.9831	1.01424	1.04499	1.08046	1.10624	1.12569	1.15142	1.17602	1.18126	1.19187	1.21588	1.23003
32.5	0.99203	1.02549	1.06773	1.09138	1.1254	1.14611	1.16458	1.19009	1.20561	1.20941	1.22697	1.24786
35	1.00269	1.04024	1.08171	1.10581	1.14093	1.16359	1.18073	1.20294	1.22453	1.23648	1.23648	1.25976
37.5	1.00972	1.05625	1.09125	1.12535	1.15414	1.181	1.19772	1.23869	1.23869	1.25311	1.25311	1.2693

Analysis of Table IX shows a direct positive relationship between core heavy metal loading and BOL excess reactivity.

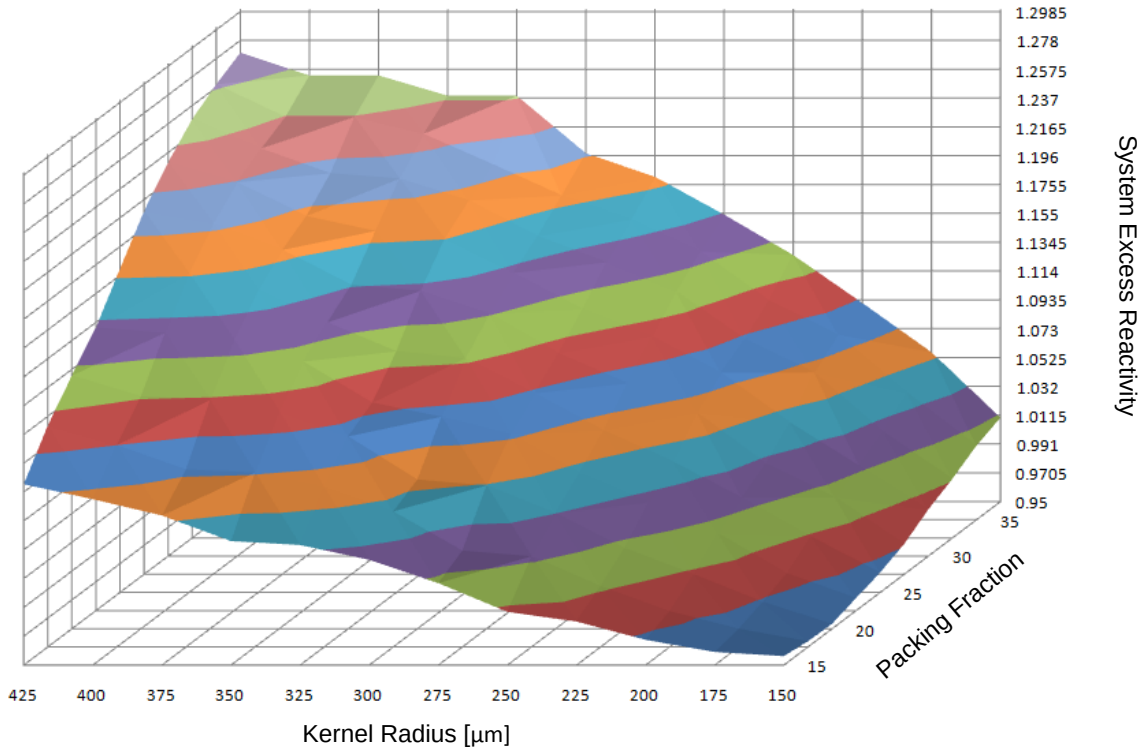

Fig. 31. Kernel and compact packing fraction effects on BOL TRU Single-Fuel configuration for a 5 ring DB-VHTR

As stated above, system reactivity was calculated or varying compact packing fractions and kernel radii for a five ring DB-VHTR with a Single-Fuel. The results of these calculation produced the surface plot shown in Figure 31. The curve in Figure 31 differs from those produced for LEU cores in intensity of resonance self shielding and is almost entirely a function of C/HM. A linear inverse relationship between C/HM and system excess reactivity is demonstrated in this curve.

Behavior of DB-VHTRs and LEU VHTRs tend to have different initial BOL core behavior. Though both LEU and TRU fuels both experience peaking from excess thermal neutrons, TRU cores also peak from excess fast neutrons. This can be best seen in the 8 Ring TRU core when compared to the same core loaded with LEU.

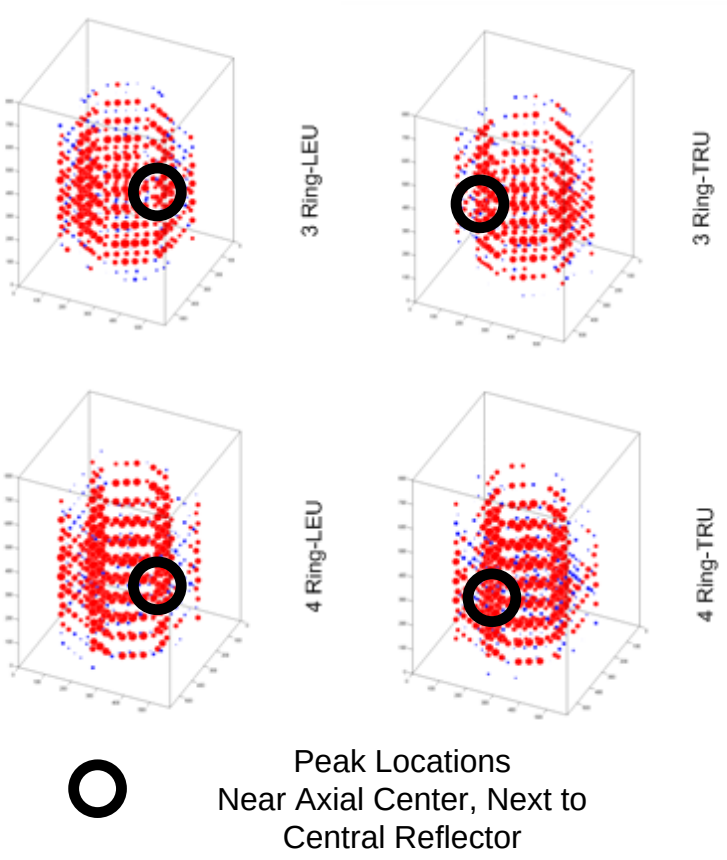

Fig. 32. Power peaking for LEU & TRU VHTR configurations a

Figure 32 shows that hot spots for both LEU and TRU cores tend to occur near the same location, those near the reflectors. What is not shown in these plots is in TRU loaded cores the power peaking is not nearly as drastic as that in LEU cores. LEU responds much more readily to thermal neutrons, those assemblies located near the reflectors grab most of these particles before they have a chance to see the inner assemblies.

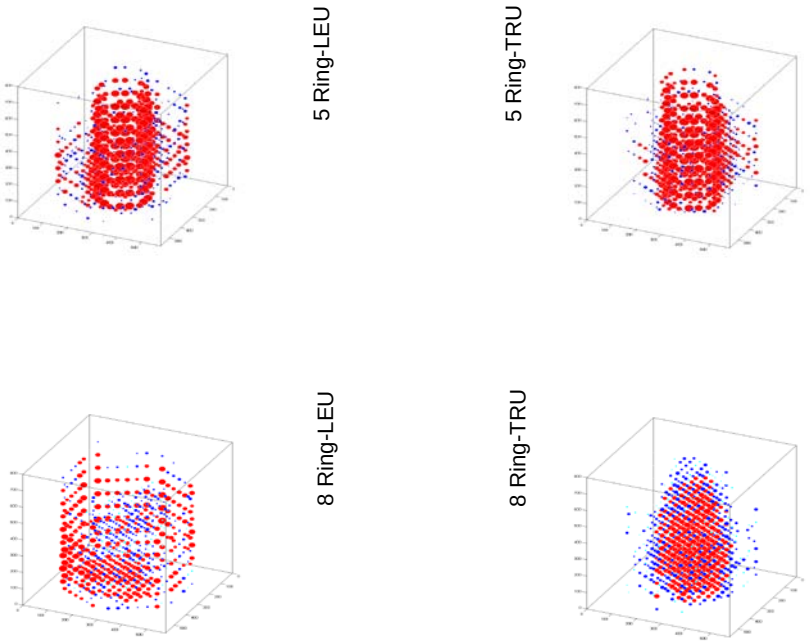

Fig. 33. Power peaking for LEU & TRU VHTR configurations b

As stated before, the most dramatic difference in BOL TRU and LEU cores can be seen in Figure 33, by comparing an 8 Ring LEU and TRU fueled core. In this case all power is being produced in opposite regions of the core. For an LEU core power is produced at the bottom and outer reflector while the TRU core produces power entirely in the core center.

IV.A.2 Random Shuffling vs. Non-Shuffling Performance for Single-Fuel Composition

IV.A.2.a 3D Random Shuffle

A comparison was made for different fuel compact configurations for non-shuffled cores and randomly shuffled cores. Initial configurations were chosen based on BOL criticality studies, such that core life was either approximately 1.10 and 1.05, as well as a reference design for the HTTR (300 micron 30% PF) and the VHTR configuration (425 micron and 17.5% PF). All randomly shuffled cores were shuffled with the same initial source tape so as not to introduce any noise to comparison between random shuffle and non-shuffled cases. Source tape files contain initial source points for the monte carlo calculations.

The random shuffle process is described in Section III. The basic premises of the random shuffle requires a random combination produced in Matlab, using the command randperm(n), which returns a random permutation of the integers 1:n. This command is based on a random number generator that produces uniformly distributed pseudorandom numbers. For each configuration the random stream is set to the same initial seed to insure each random shuffle is the same, so as to not create the possibility of results based on different core shuffles. Since the randperm command is based on a uniform random number generator, there is equal chance for a block to be moved to another location.

Plots were produced showing Burn Up, Power Peaking, and TRU Destruction through time. Comparing cases shown in Tables X and XI; show approximately the same average EOL metrics for each individual block and for the core as a whole. The effects of a random shuffle on these cases appear to be only reflected in the spread between max and minimum values of burnup and TRU destruction. This reflects that non-shuffled fuel experiences higher or lower power production based on where the block is located. In the cases of a random shuffle core, where the core was shuffled randomly every nine

months, the change of block location allows a more even core burn. To further analyze this phenomenon, Figure 34 was produced.

Figure 34 shows how TRU destruction for non-shuffled cores have a pattern similar to that of BOL power profiles for the same system. The randomized shuffling pattern removes this pattern while minimizing variation in block to block TRU destruction. It is apparent from the studies of a Single-Fuel TRU systems, that shuffling does not necessarily improve EOL metrics but does decrease the variability of block EOL metrics. Furthermore, the average TRU destruction does not necessarily fall in the range of a DB-VHTR. Cause of this can be attributed to the resonance shelf shielding effects of large particles when combined with high capture cross-sections from higher actinides.

These results though expect in some degree are not widely reflected in literature review of DB-VHTRs, the magnitude of this results in the need of multiple fuel types. This fuel will be explained later in this section.

The largest TRU destruction was approximately 15 atom% for a shuffled core. This core also had the longest core life and had the largest tons of SNF loaded into the core. With a proper shuffling algorithm, it is expected that an increase in atom destruction of TRU istopes could be produced, but will fall outside the touted destruction rates of over 50% for DB-VHTR systems. The major factor for the low destruction rates of TRUs for these Single-Fuel systems is resonance self shielding of Am and Cm to the fission reaction for Pu-239 and Pu-241.

Table X. EOL Metrics for Non-Shuffled TRU Single-Fuel Configuration 5 Ring DB-VHTR

Kernel Radius	**Packing Fraction**	**Core Life Time**	**Core BU**	**Block Max Burnup**	**Block Min Burnup**	**Max Power Peaking**	**Min Power Peaking**	**Average TRU Destruction**	**Max TRU Destruction**	**Min TRU Destruction**
µm	*%*	*days*	*MWd/MTHM*	*MWd/MTHM*	*MWd/MTHM*	*X/avg.*	*X/avg.*	*at%*	*at%*	*at%*
425	17.5	3375	190.607	347.437	125.737	2.6592	0.25416	12.458	21.199	8.709
400	17.5	2835	166.831	330.232	91.609	2.4888	0.26904	11.020	19.269	7.486
375	20	3375	185.865	344.047	105.59	2.7984	0.24384	12.166	20.574	8.376
300	30	4725	219.814	370.82	155.262	2.7096	0.29592	14.157	22.509	9.740
300	17.5	1350	104.264	216.15	68.982	2.856	0.33096	6.925	13.341	4.269
275	27.5	3240	180.051	317.434	117.368	2.8272	0.33984	11.651	19.892	8.133
275	20	1485	107.197	221.1	69.875	2.7144	0.36648	7.332	14.488	4.674
250	30	3105	173.689	319.178	114.7605	2.5992	0.183816	11.420	19.821	7.899
225	32.5	2835	165.959	317.597	106.927	2.9016	0.212448	10.967	19.579	7.443
225	25	1350	102	225.19	61.971	2.6904	0.25728	6.778	12.988	4.523
200	37.5	2700	162.228	293.646	104.361	2.8848	0.25824	10.561	18.911	7.054
200	30	1350	99.136	208.26	56.6	2.7552	0.2784	6.597	13.284	4.151
175	37.5	1755	122.209	237.424	75.294	2.6832	0.37032	8.288	15.499	5.662
150	37.5	135	7.841	17.86	4.738	2.6064	0.48768	0.802	1.818	0.483

Table XI. EOL Metrics for 3D Random Shuffled TRU Single-Fuel Configuration 5 Ring DB-VHTR

Kernel Radius	**Packing Fraction**	**Core Life Time**	**Core BU**	**Block Max Burnup**	**Block Min Burnup**	**Max Power Peaking**	**Min Power Peaking**	**Average TRU Destruction**	**Max TRU Destruction**	**Min TRU Destruction**
µm	*%*	*days*	*MWd/MTHM*	*MWd/MTHM*	*MWd/MTHM*	*X/avg.*	*X/avg.*	*at%*	*at%*	*at%*
425	17.5	3375	190.594	227.981	160.44	2.8224	0.29112	12.449	14.736	10.410
400	17.5	2970	178.249	224.195	146.254	2.8032	0.27192	11.535	14.817	9.522
375	20	3510	196.589	232.108	170.387	2.748	0.2496	12.639	15.102	10.641
300	30	4860	228.953	265.215	192.727	2.7432	0.15216	14.557	18.120	12.552
300	17.5	1350	104.264	142.352	80.756	2.8512	0.42096	6.927	10.507	5.094
275	27.5	3375	185.384	225.025	162.957	2.7216	0.223824	12.127	15.201	9.670
275	20	1620	121.15	166.966	94.964	2.988	0.30543	8.004	11.990	5.512
250	30	3240	184.572	238.967	158.772	2.844	0.3492	11.917	15.433	9.530
225	32.5	2700	160.279	191.108	135.04	2.784	0.28368	10.434	13.119	8.050
225	25	1350	102.013	139.791	75.902	2.9112	0.36768	6.789	9.936	5.019
200	37.5	2835	167.969	205.467	140.496	2.8056	0.30384	11.082	14.585	8.694
200	30	1485	106.022	146.545	78.911	2.9184	0.34872	7.258	9.731	5.377
175	37.5	1755	122.206	154.399	90.939	3.024	0.219888	8.280	11.937	6.442
150	37.5	135	7.841	17.86	4.738	2.6064	0.48768	0.802	1.818	0.483

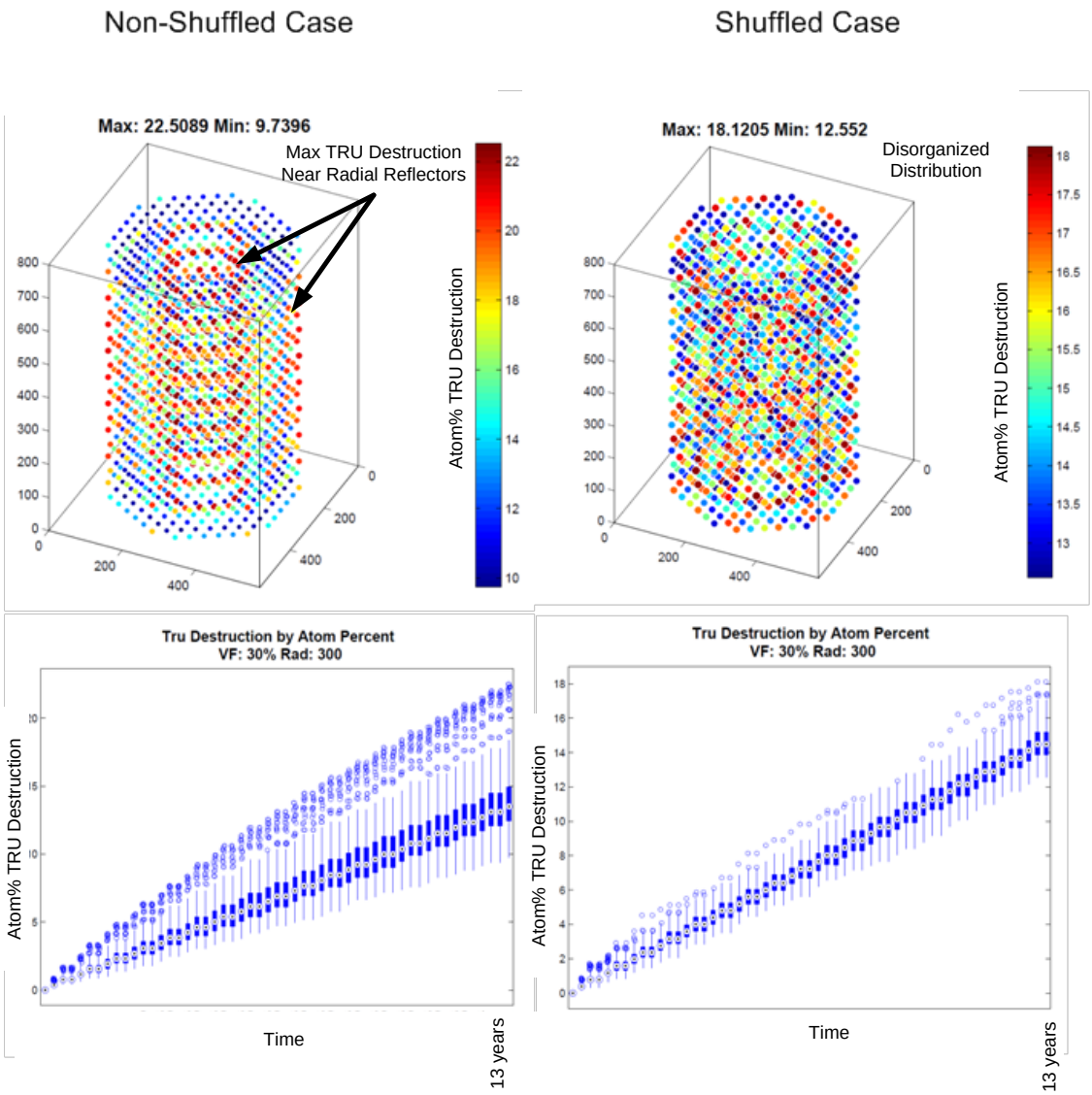

Fig. 34. Effects of a random 3D shuffle on TRU destruction profile at EOL

Figure 35 shows the immediate effect of power production when shuffling occurs. Not only does a smooth power profile not appear after a random shuffling, but power peaking can be increased by the movement of fresher fuel into preferred power production locations. This core contained no BPs, the addition of BPs can be used to offset some power peaking issues but without a proper shuffling algorithm, neither scenario would be within operation constraints.

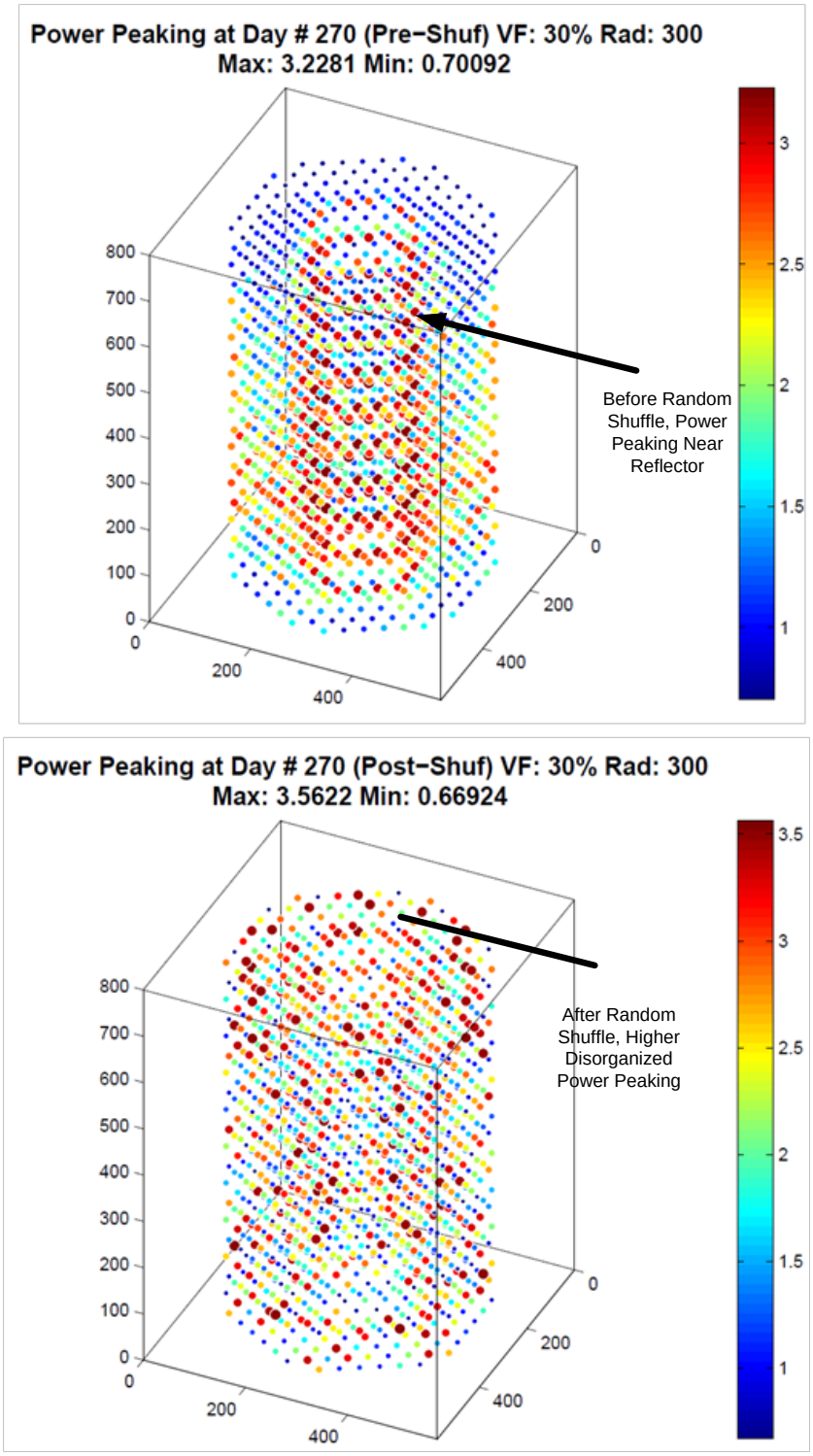

Fig. 35. Effects of a random 3D shuffle on TRU destruction profile near BOL

IV.A.2.b 2D Random Axial Only Shuffle

The 3D random shuffle was deconstructed into two components, radial and axial random shuffles. This was done to determine if axial movement or radial movement produced any characteristics that could either be avoided or taken advantage of in an intelligent 3D shuffle.

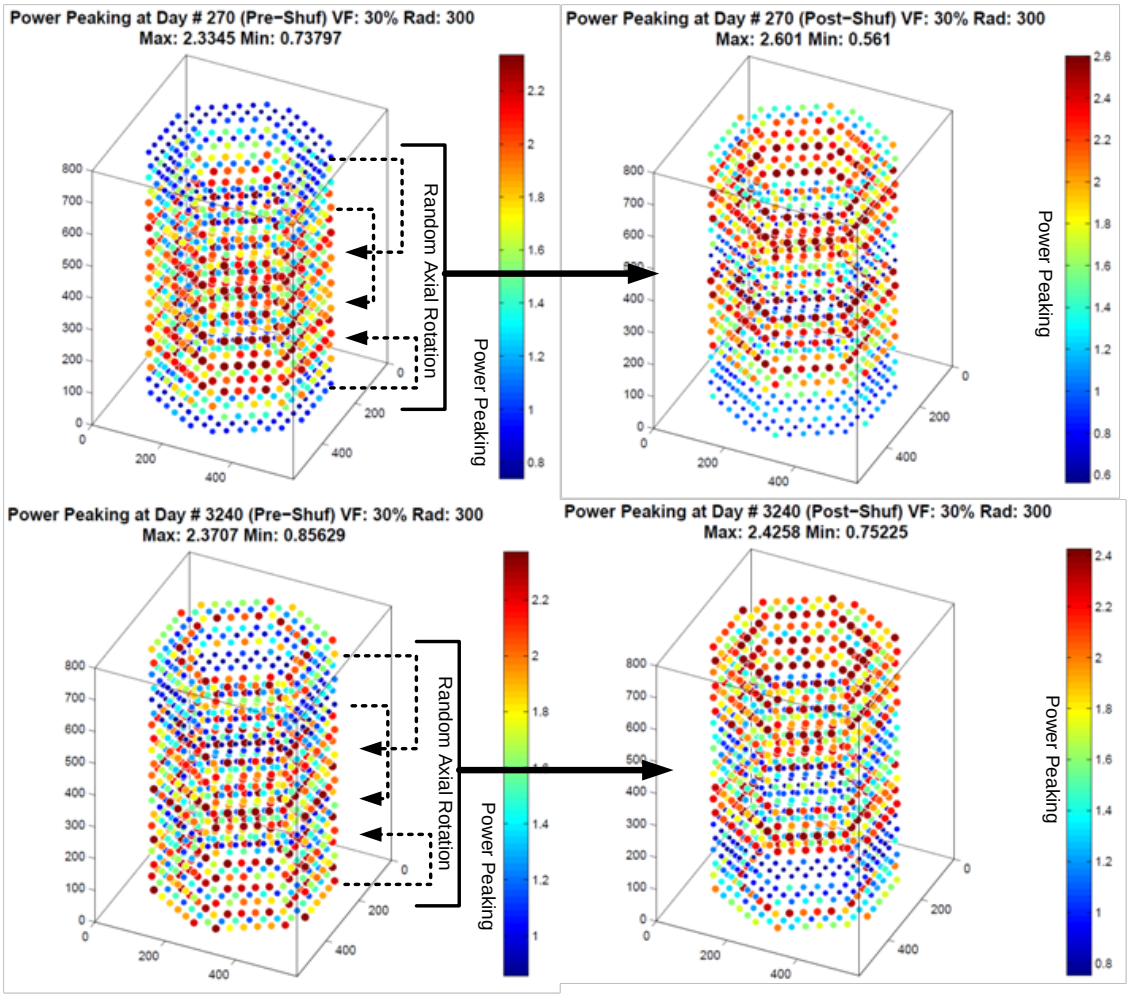

Fig. 36. Random axial only shuffling of a 3 ring TRU single composition fuel

Figure 36 shows the power peaking profile of a 3D random shuffle after the first shuffle step at day 270 and again near end of life at approximately 9 years. Of interest is the striation pattern of an axial shuffling in respect to power peaking.

The bright red layers shown in Fig. 12 are assemblies that have lower burnup then the average block. These assemblies have spent less time near the center of the core and thus when they approach the center of the core the excess fissile nuclides will cause an above average fission density. When comparing the power profile from BOL to EOL, a noticeable lack of power peaking at the top of bottom of the core has become less pronounced. This demonstrates that fresh fuel cannot be simply hidden from preferred power producing location due to the large mean free path of neutrons in graphite moderated systems.

IV.A.2.c 2D Random Radial Only Shuffle

The second component of the 3D random shuffle is a radial only random shuffle. Figure 37 shows the power peaking profile of this shuffling method after the first shuffle step at day 270 and again near end of life at approximately 9 years. Of interest is that the striation pattern of a random axial shuffling method is not seen in the radial method but rather a power profile seen near the beginning of life is still evident after the first shuffle on day 270. Not as apparent but still shown at day 3,240 before the last shuffle is a decrease in power production near the top of the core. This last axial layer still has not significantly added to core power, at EOL without producing power these fuel assemblies are largely underutilized. A proper shuffling pattern should decrease the variation between high burnup assemblies and low burnup assemblies, by doing so several EOL metrics will be improved.

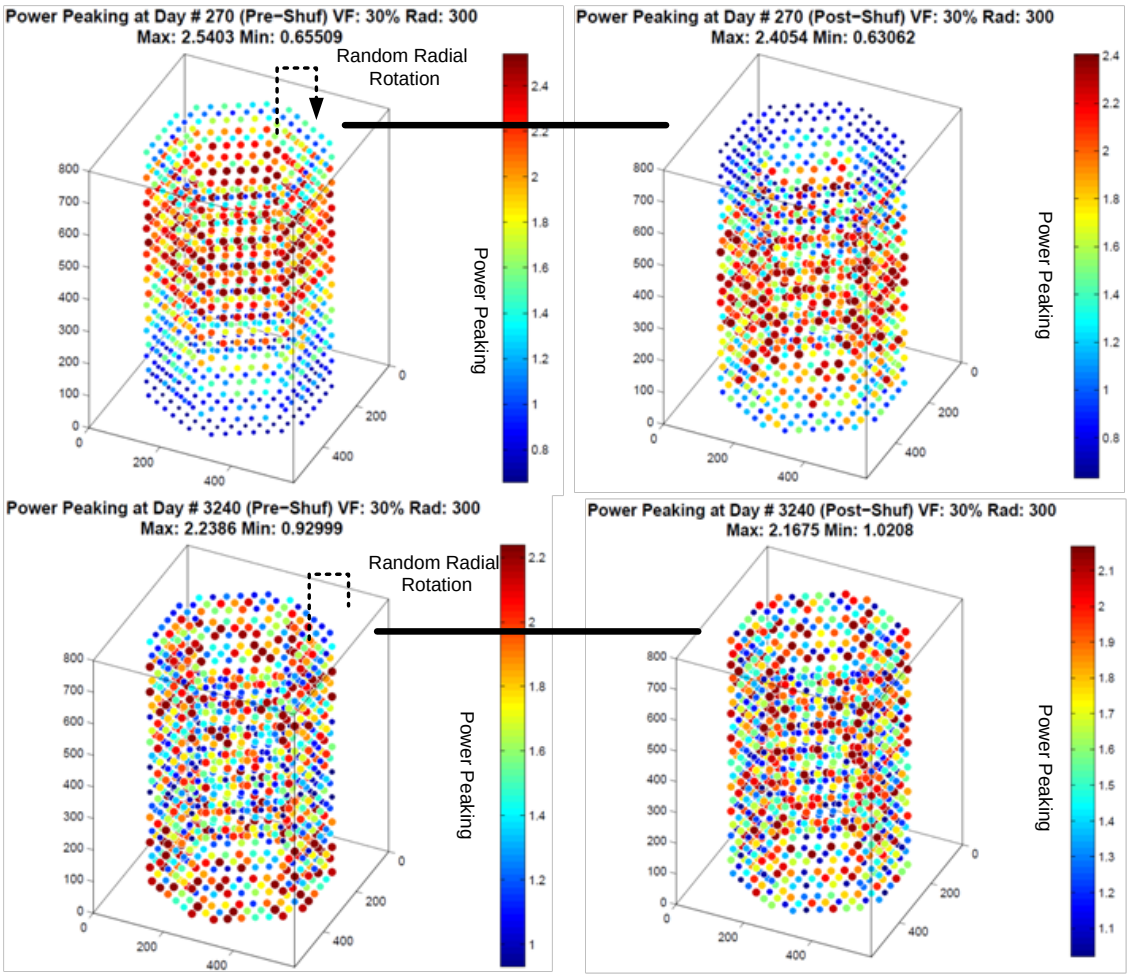

Fig. 37. Random radial only shuffling of a 3 ring TRU single composition fuel

Figure 38 compares the 3D TRU destruction of all three random methods; radial, axial and 3D. Additionally shown are box plots for total atom destruction for each corresponding method. The variation of TRU destruction throughout the core is related to the effectiveness of a shuffling algorithm to utilize fuel. The axial only 3D TRU destruction plot shows a radial variation of TRU destruction with preference of assemblies located near the inner reflector. The radial only shows a variation axially with the most TRU destruction occurring near the center of the active core. Finally no distinct pattern can be seen the 3D random 3D TRU destruction plot. Also shown is peak TRU destruction is the least (~18%) in this case while the minimum destruction is the greatest near 11%. Comparison of the box plots shows that this decrease in TRU destruction variation is true throughout core life. Outliers are shown in each box plot if they lie more then 2.7 standard deviations away from the mean. Standard box plot quartile ranges apply to those shown in Figure 38. As the distance between max and min destruction occurs more outliers are produced as demonstrated in the order of radial, axial and 3D random shuffle. Large minimum outliers increase power peaking if these assemblies were to be located in power producing regions of the core. This situation has to be accounted for in a proper shuffling algorithm.

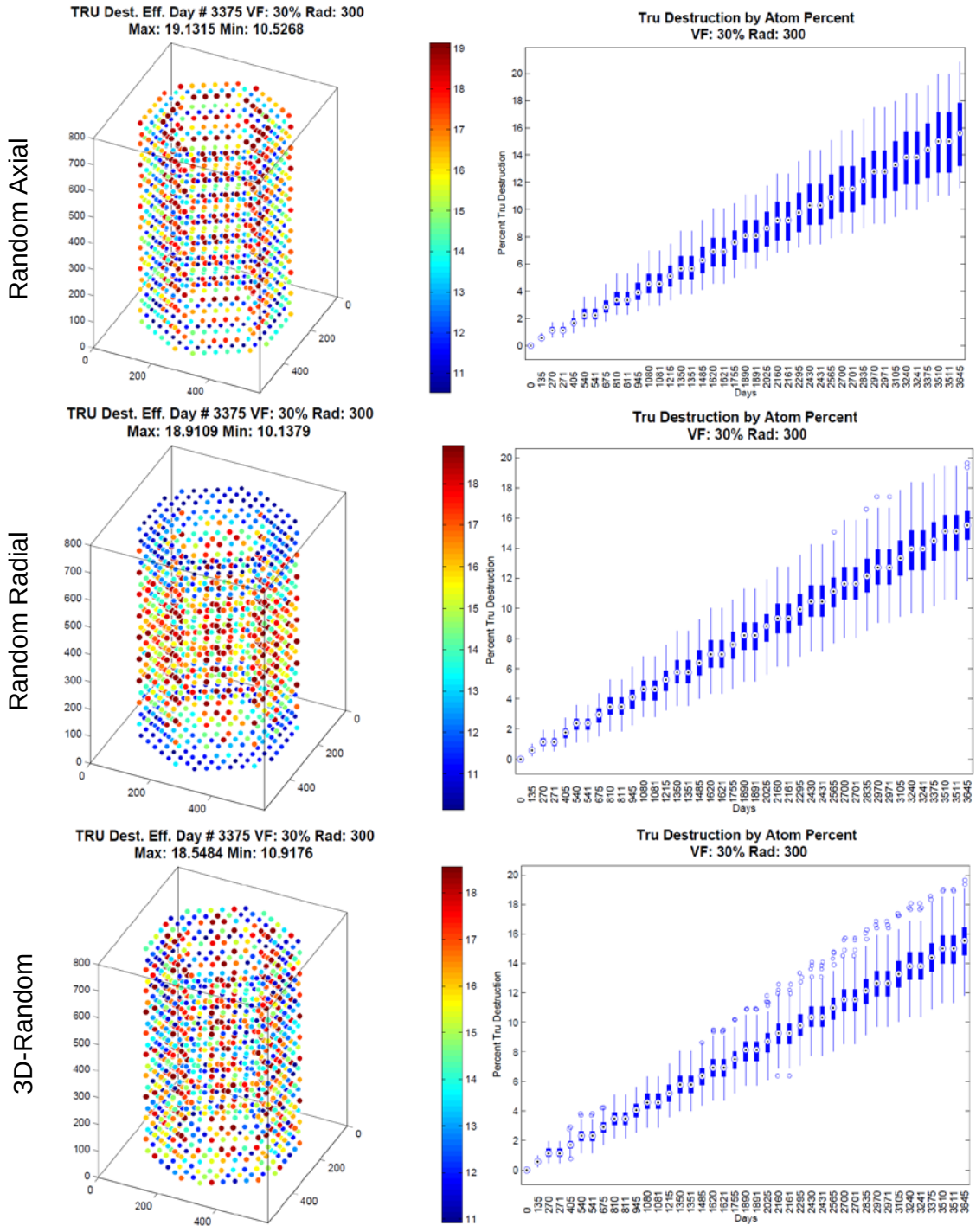

Fig. 38. Comparison 3 ring TRU single composition fuels in 3 random shuffling schemes

IV.B Operation with Two-Fuel Compositions

The inherent flexibility of HTGR's fuel type, allow for the possibility of creating variation in TRISO isotopics to reduce effects of resonance absorption. Current research has proposed of using a driver fuel and a transmutation fuel to increase system excess reactivity, TRU destruction, and negative temperature reactivity feedback. Negative temperature reactivity feedback is produced by several TRU isotopes, most noteably Am-241, Np-237 and Pu-240 to counteract the positive temperature reactivity feedback of Pu-239. The addition of these istopes also benefits by decreasing the need for rare earth burnable poisons such as Er-167. The use of TRU istopes for this purpose increases the system neutron economy through core life, benefiting total TRU destruction.

IV.B.1 BOL Block Selection for Two-Fuel Compositions

At this point it has been discovered that a full TRU vector fuel with isotopics corresponding from LWR SNF does not produce favorable TRU destruction, at max producing 15 atom% destruction. From a literature review, current efforts do not

propose a Single-Fuel but several fuels or at least the removal of Am and Cm, an effort was made to find an acceptable block for TRU destruction to test and develop a 3D intelligent shuffling algorithm. Furthermore a choice was made to have a fuel that would not be reprocessed such that after manufacturing TRISO particles, the block in its integrity would be placed for disposal or sent to a fast reactor for further TRU destruction. Furthermore constraints placed on the block design include combining Pu and Np as a Single-Fuel and Am and Cm as another fuel. These fuels would then be placed in a distributed pattern inside the block. The amount of each fuel would allow for a constant ratio of isotopics to be maintained, such that the ratio of any one isotope to another would be constant, thus reducing the buildup of anyone element at a reprocessing facility. Additionally, due to the small abundance of Am and Cm in LWR SNF, U238 was also allowed to be added. Due to the speed of BOL criticality studies for a single block a complete forward iterative method was used for mapping possible block domains. A general schematic of how block designs were produced is shown in Figure 39.

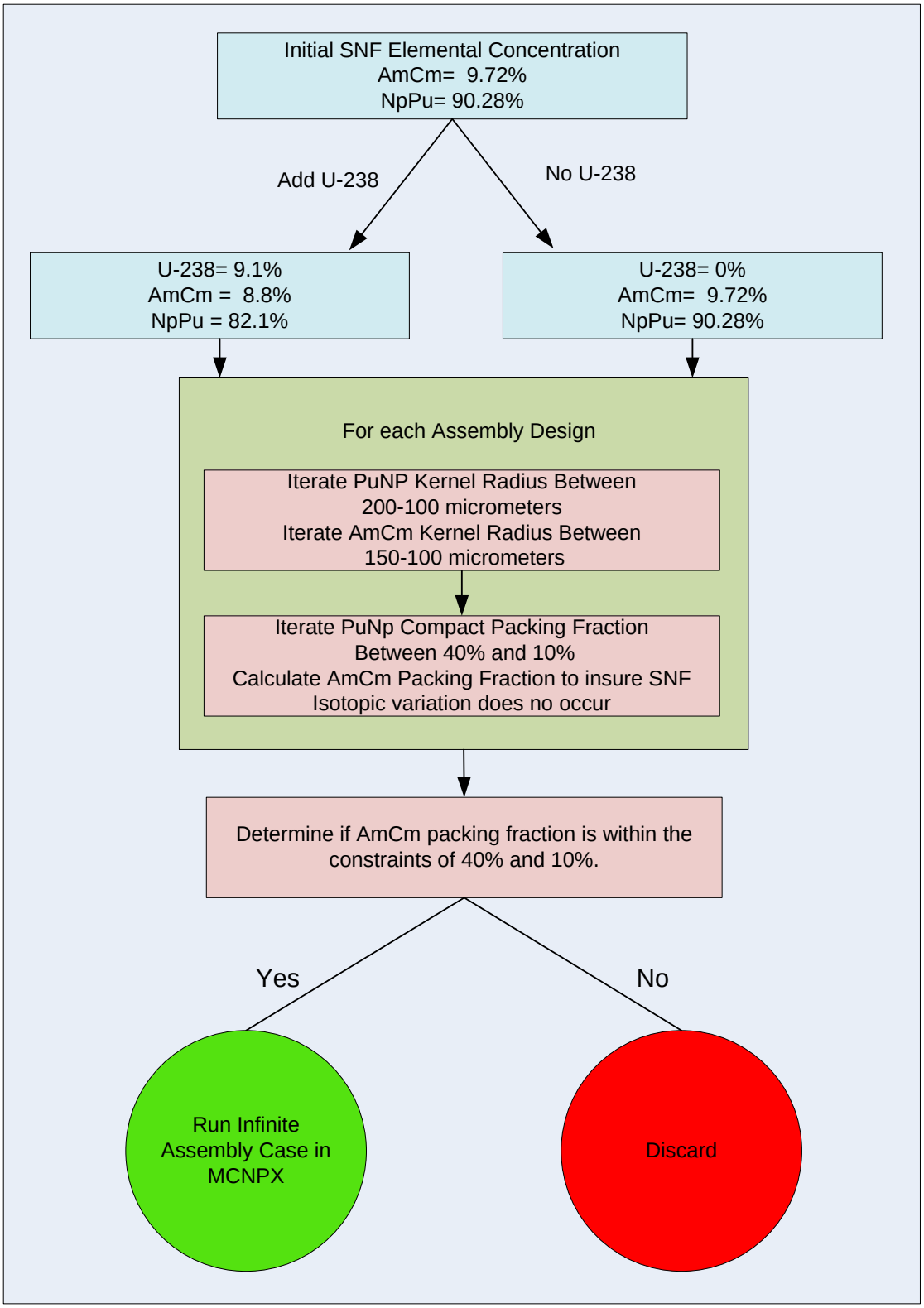

Fig. 39. Block design iterative process

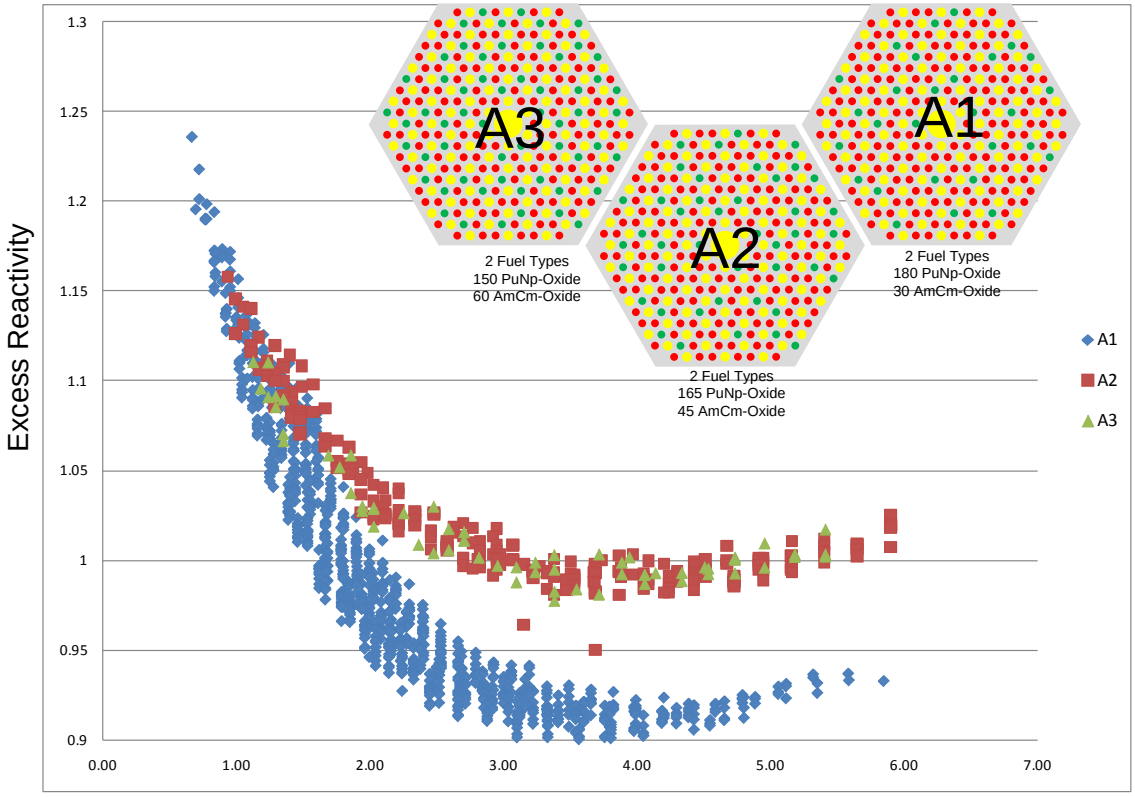

Fig. 40. BOL excess reactivity vs. mass TRU loading for 3 block designs

Nearly 3000 block designs were evaluated to determine BOL excess reactivity. Three of the block designs produced a significant number of BOL results which are shown in Figure 40. Excess reactivity was plotted against the relative loading of TRU in each block. Block design 1, A1, produced the largest number results followed in order by design 2, A2, and design 3, A3. A3 and A2 have produced comparable curves with nearly all designs with a k-eff more then 1. A1, with the most results, produced a curve that not only peaked much higher excess reactivity then the other two designs as well as the least reactive design. Each of the BOL criticality files used the same source tape and a total of 25000 active neutron histories were used to calculate k-eff with an error ~+/- 0.004. Each case took approximately five minutes, for a total of 216 computational hours.

Since each block case is a function of several parameters, driver fuel packing fraction and kernel radius, transmutation fuel packing fraction and kernel radius, U-238 addition, and block design, a multi-dimension analysis should be used to analyze the results. To facilitate this the following 4D Cartesian plots were produced. In Figure 41 all block cases producing results, including those with the addition of U-238, are plotted. The plot compares kernel radius of both driver and transmutation rod for the x-y coordinates and relative loading of TRU/block, which is a function of both block design and packing fractions, for the z coordinate. Data points were colored to excess reactivity, producing the fourth dimension.

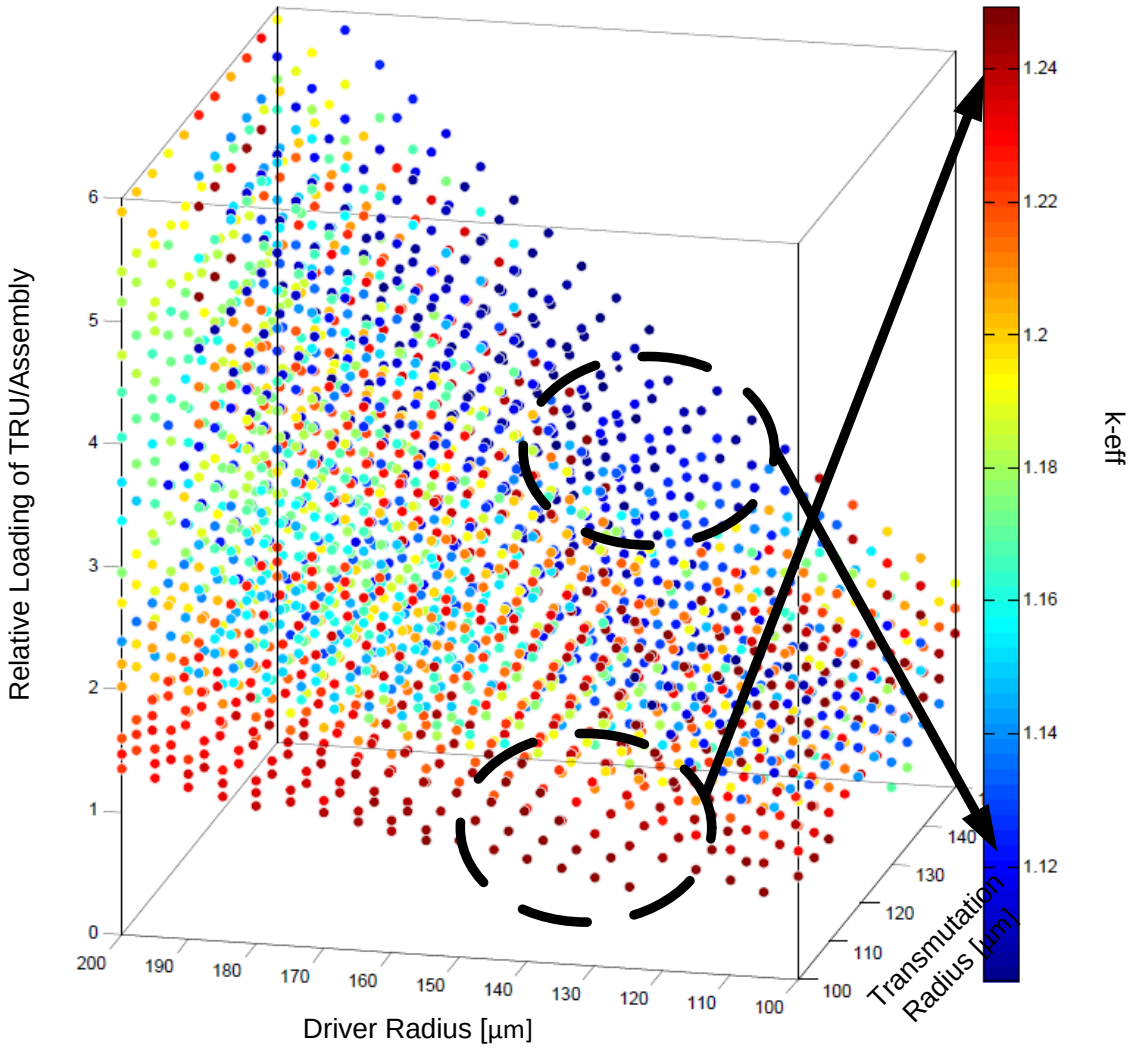

Fig. 41. 4-D scatter plot for block loading designs

The analysis of Figure 41 shows several high k-eff of assemblies with low TRU loadings, much like Figure 40 shows. Furthermore the hottest assemblies seem to be with smaller kernel radius, kernel that have the least resonance self shielding. These two observations are not true over the entire design domain, with several high k-eff assemblies spread throughout the domain. To help distinguish effects of each variable used to produce the plot sub plots were produced, starting with Figure 42. Figure 42 shows only assemblies of design one and no U-238 addition are plotted. Several distinct surfaces appear become apparent, each of these surfaces corresponds to a driver packing fraction. A trend is of increase driver radius causing a decrease in excess reactivity is observed, with a smaller effect seen for high TRU-loading assemblies beginning to regain some reactivity. Furthermore, as TRU loading increases the amount excess reactivity decreases.

In terms of core life, the higher TRU loading the longer the core can operate. The tradeoff of larger TRU loading causes an increase of resonance absorption by generally requiring the need to increase kernel radius. These two effects counteracts each other, a judgement of core life can not be predicted based soley on BOL studies due to the complexity of nuclear phsyics occurring in TRU kernels. With respect of TRU destruction, a direct correlation cannot be made to core life, thus requiring the need for the depletion of test assemblies to map the performance domain of DB-VHTRs.

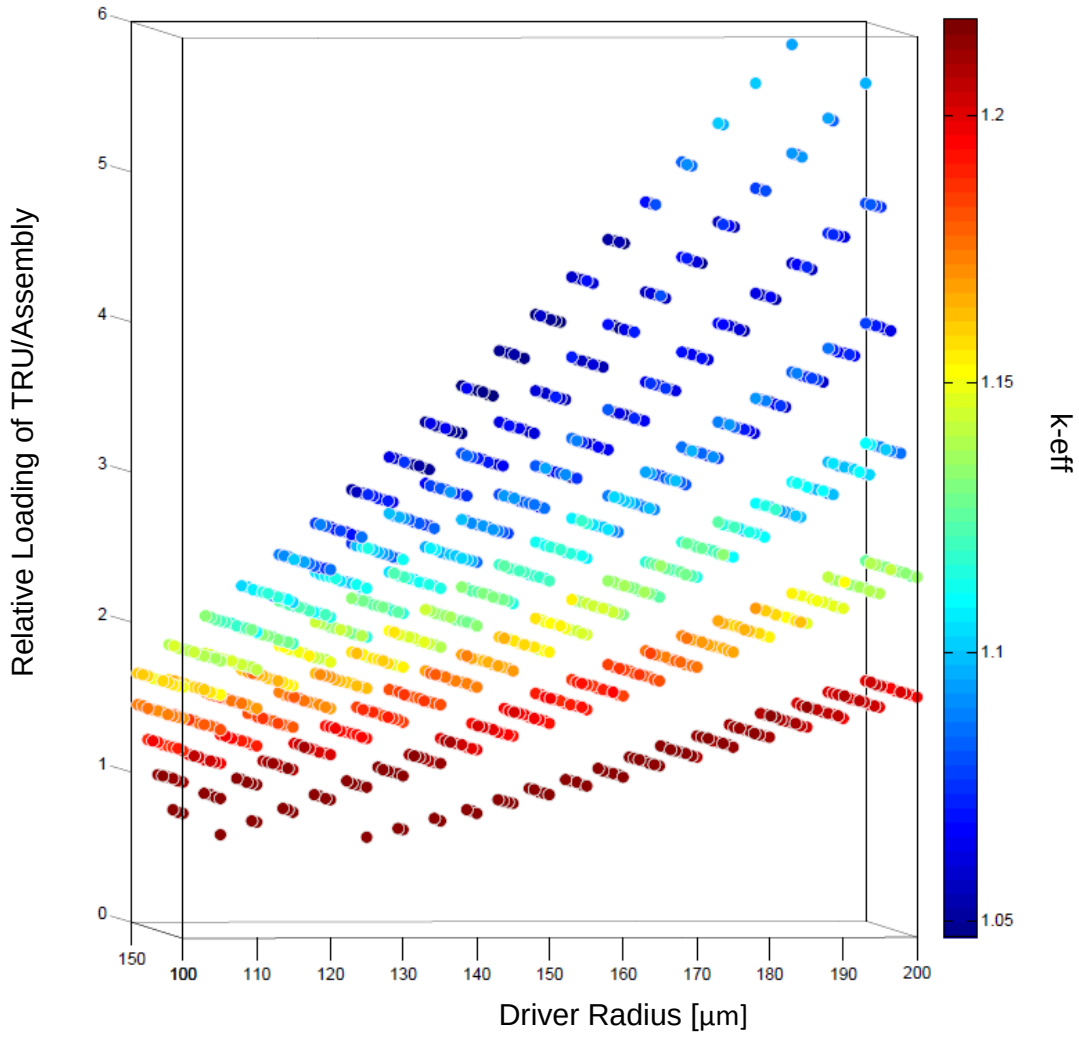

Fig. 42. 4-D scatter plot for block design A1 containing, with no U-238 added to fuel composition

Only block design 1 is shown in Figure 42. Figure 43 is showing all 3 block designs. The addition of these two designs show several cases that have gained reactivity as the TRU loading increases in contrast as that is seen with block design 1. It assumed that the amount of TRU in these systems have led to a significant change the neutron spectrum shift toward higher energy neutrons. This effect is most pronounced to larger driver kernel radius and smaller transmutation fuel kernel radius. These driver compacts would have a low packing fraction while having transmutation rods with a higher

packing fraction. This effect shows similarities to that of the Single-Fuel design core earlier in this section, where for some time larger kernel radii produce more excess reactivity.

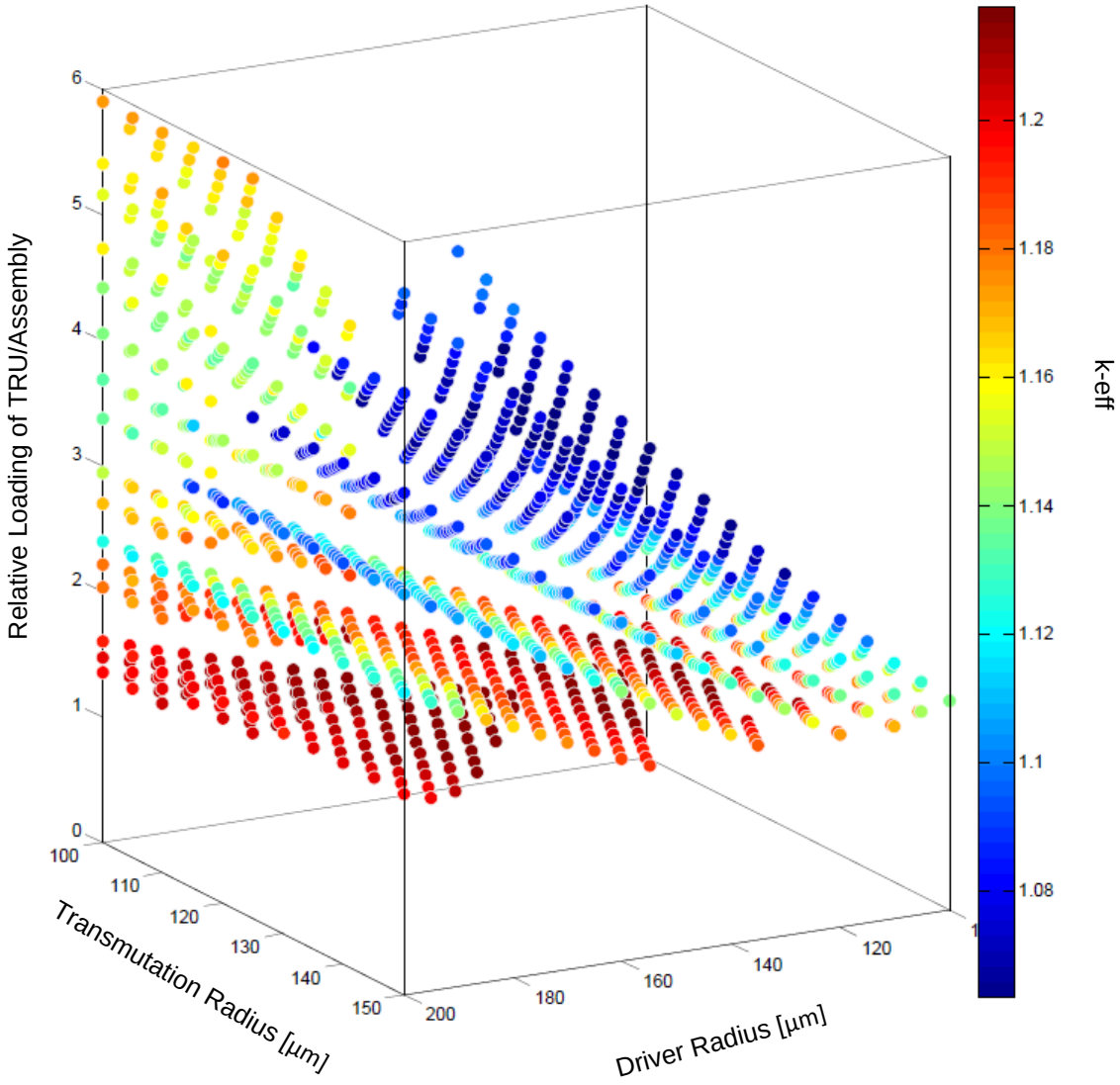

Fig. 43. 4-D scatter plot for block designs containing no U-238

The investigation of U238 addition to the LWR SNF fuel feed produced results shown in Figure 44. All block designs are plotted in the figure and shows a much larger degree of noise associated to each driver packing fraction curve. Furthermore a distinct pattern of assemblies exhibiting high excess reactivity is not clearly seen, but rather they appear to group in regions of the design domain. The most discernable pattern is a shifting of assemblies that have high excess reactivity from the region of the design domain with lower driver radii for low loading of TRU to the region of high TRU loading and large kernel radii.

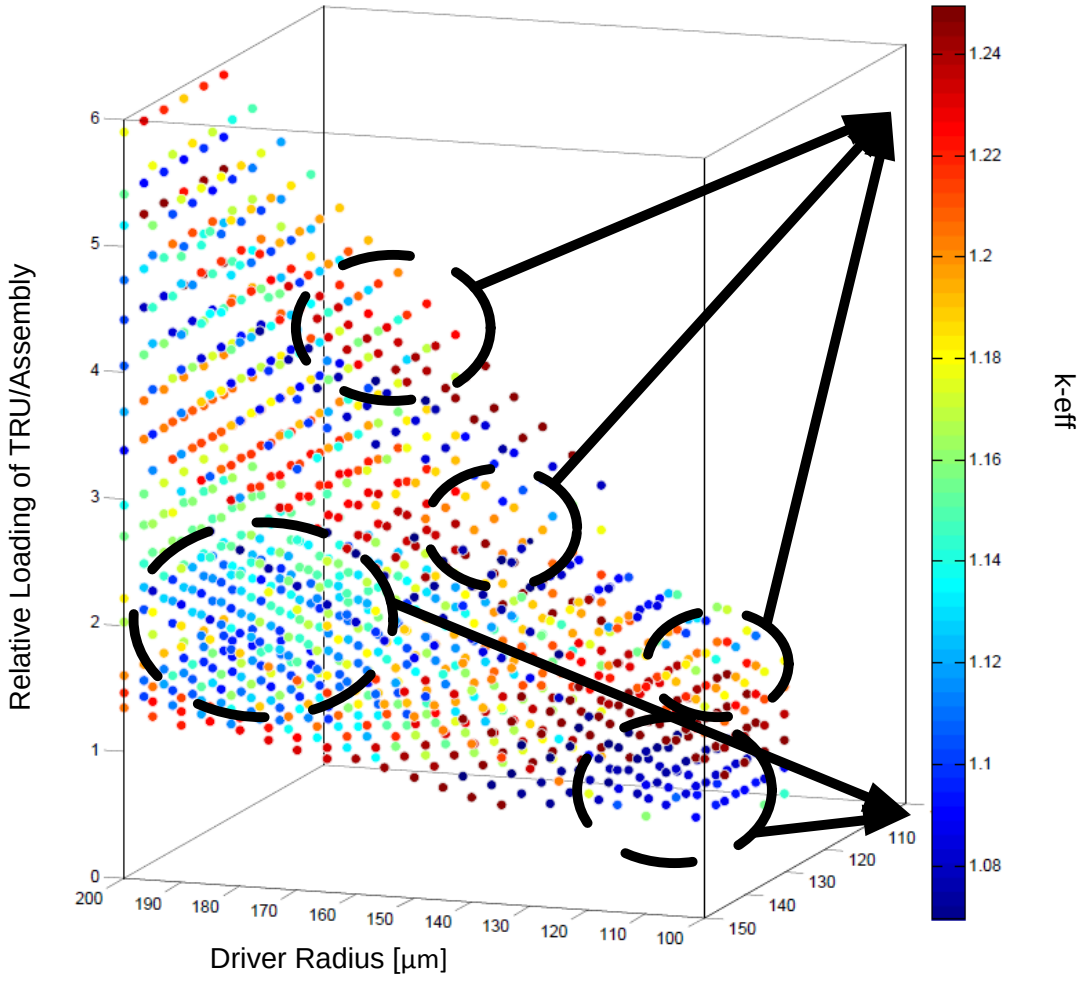

Fig. 44. 4-D scatter plot for block designs containing U-238 in the fuel composition

IV.B.2 In-Core Block Selection for Two-Fuel Compositions

Selections of 122 block designs produced in the prior section were chosen for depletion based on excess reactivity. No cases were chosen with U238 addition. This choice was made in part to simplify the block selection process. The full details of these cases are provided in the appendix, a selection of these cases is shown in Table XII. These 25 cases produced the highest burnup of all 122 cases. The higher the burnup the higher the TRU destruction.

Each case was run at a fractional power for a five ring DB-VHTR operating at 600 MWth, 0.42683 MWth. A total of 500,000 neutron histories were use for each depletion step. A total run time of 28 hours is needed for each case, with a total of 145 computation days for all cases. The highest burnup case produced a burnup of over 55% TRU destruction, mostly from the destruction of the Pu isotopes, specifically Pu-239. This highest burnup case was selected for full core depletion model used for the shuffling algorithm in the next section. This block has a driver kernel radio of 100 μm and a transmutation fuel kernel radio of 100 μm. The packing fraction in the driver compact is 30% and the packing fraction for the transmutation rod is 19.38%. It is of block type 1.

Table XII. EOL Block Depletion Cases

Driver Kernel Radius [μm]	**Transmutation Kernel Radius** [μm]	**Relative TRU Loading**	**Driver Burnup** [GWd/MTHM]	**Transmutation Rod Burnup** [GWd/MTHM]	**Core Life** [years]
100	100	1.1	576.2	95.0	3.1
100	125	1.3	569.7	92.1	3.1
110	105	1.1	567.6	93.0	3.0
110	110	1.1	566.6	92.5	3.0
100	115	1.3	565.4	94.2	3.1
100	105	1.2	564.4	91.0	3.1
115	130	1.3	562.7	100.7	3.3
115	105	1.1	563.1	96.0	3.3
110	115	1.1	562.5	87.7	3.0
100	120	1.3	562.0	80.6	3.1
110	100	1.0	561.2	85.7	3.0
115	110	1.2	556.9	99.3	3.3
100	110	1.2	557.9	88.2	3.0
115	120	1.2	556.6	86.8	3.3
105	125	1.4	555.9	85.5	3.4
115	115	1.2	553.7	99.1	3.2
110	120	1.2	555.9	76.9	3.0
130	100	1.0	554.3	90.6	3.1
135	130	1.2	553.3	92.2	3.4
130	115	1.1	550.1	94.9	3.1
115	100	1.1	550.3	91.2	3.2
130	120	1.1	551.0	76.9	3.1
155	110	0.9	548.2	88.5	2.9
135	110	1.1	546.9	91.5	3.3
165	100	1.0	547.0	87.3	3.0

IV.C Demonstration of the Developed Shuffling Algorithm

The block loading and compact design selected in the prior section was used for a full core model. This block loading and compact design produced favorable TRU destruction in the range of DB-VHTR performance domain. It allows the shuffling algorithm developed for this dissertation to be tested on a representative DB-VHTR. This full core model is similar to that used for a Single-Fuel, except instead of an OTTO cycle, an estimated equilibrium cycle was produce. The product of this cycle was done solely for the production of an estimated equilibrium core. This estimated equilibrium core was needed to add variability in fuel/BP isotopics to test the shuffling algorithm. The isotopics for the estimated equilibrium cycle was produced from a core using the same block design as that selected in the prior selection and burned without shuffling until the core reached a sub-crtical state, approximately 3 years. It was assumed the equilibrium cycle would be similar to that of a LWR core with 1/3 of the assemblies that have experienced the highest burnup removed at each core reload. During this 3 year OTTO cycle, the 1/3 highest burned assemblies isotopics were found at year 1 and year 2 to be used as once burn and twice burn assemblies for the equilibrium cycle respectively. An illustration of this is shown in Figure 45. Additionally this core used control rods at half active core height to increase variability of core power producing location.

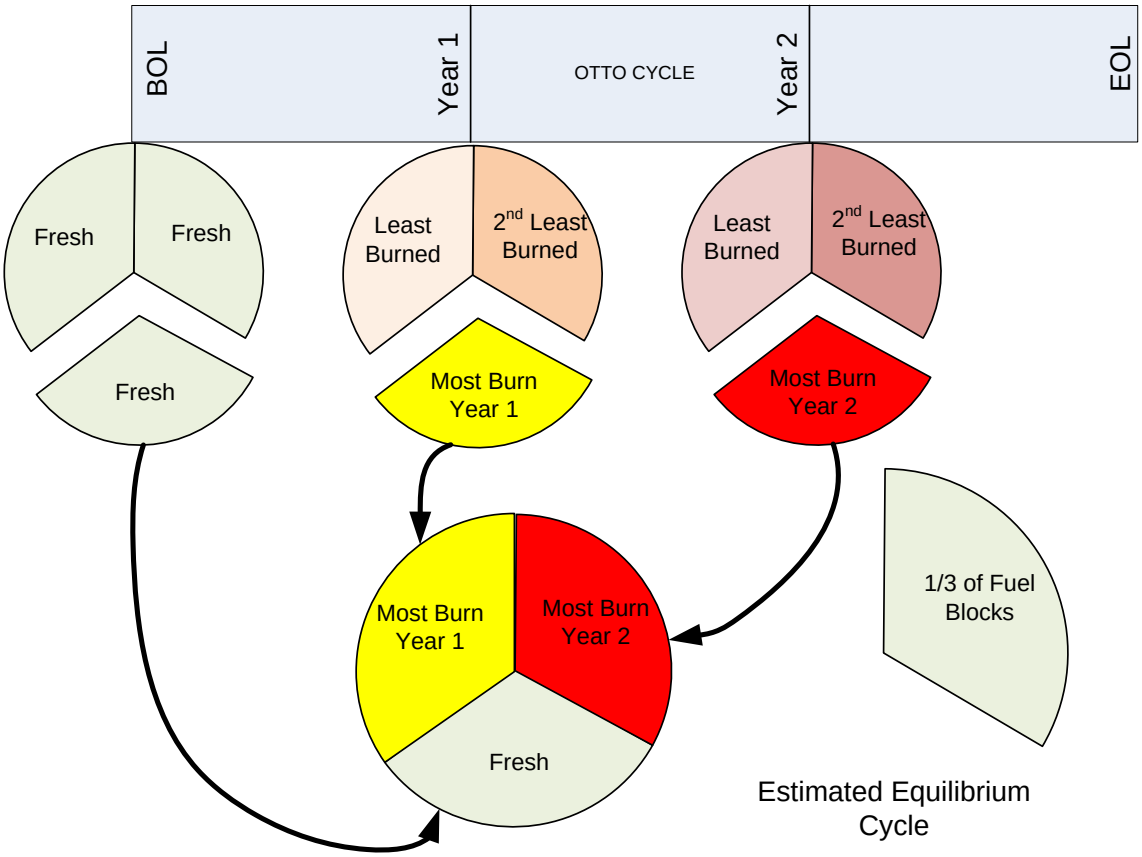

Fig. 45. Development of equilibrium cycle for shuffling algorithm development

IV.C.1 Sample Shuffling Patterns

In this section a results from the physics based shuffling algorithm developed are analyzed. BOL power peaking was set as the only operational constraint for core shuffling. This allowed for only the analysis of BOL characteristics of a shuffled core, thus removing the need for high computational time depletion cases models. A depletion model is needed for determining when the next core shuffle has to occur. This is done by simply checking in-core operation constraints at each burnup step, such as neutron fluence and max burnup. These in-core constraints do not effect core shuffling, but instead core life. This is solely because the algorithm already places blocks with

high burnup in locations that produce little power. As shown in Figure 38 of Section III the shuffling process requires updating the cross-sections and spatial flux profile to ensure proper shuffling. Several permutations were done without updating the spatial flux and cross-section to determine the importance of this step. A selection of these permutations is shown in Figure 46. Each of these cases were developed with a permutation constraint of 3 and a BP constraint of 2, thus the maximum power peaking should be 2 as shown in section III Figure 38.

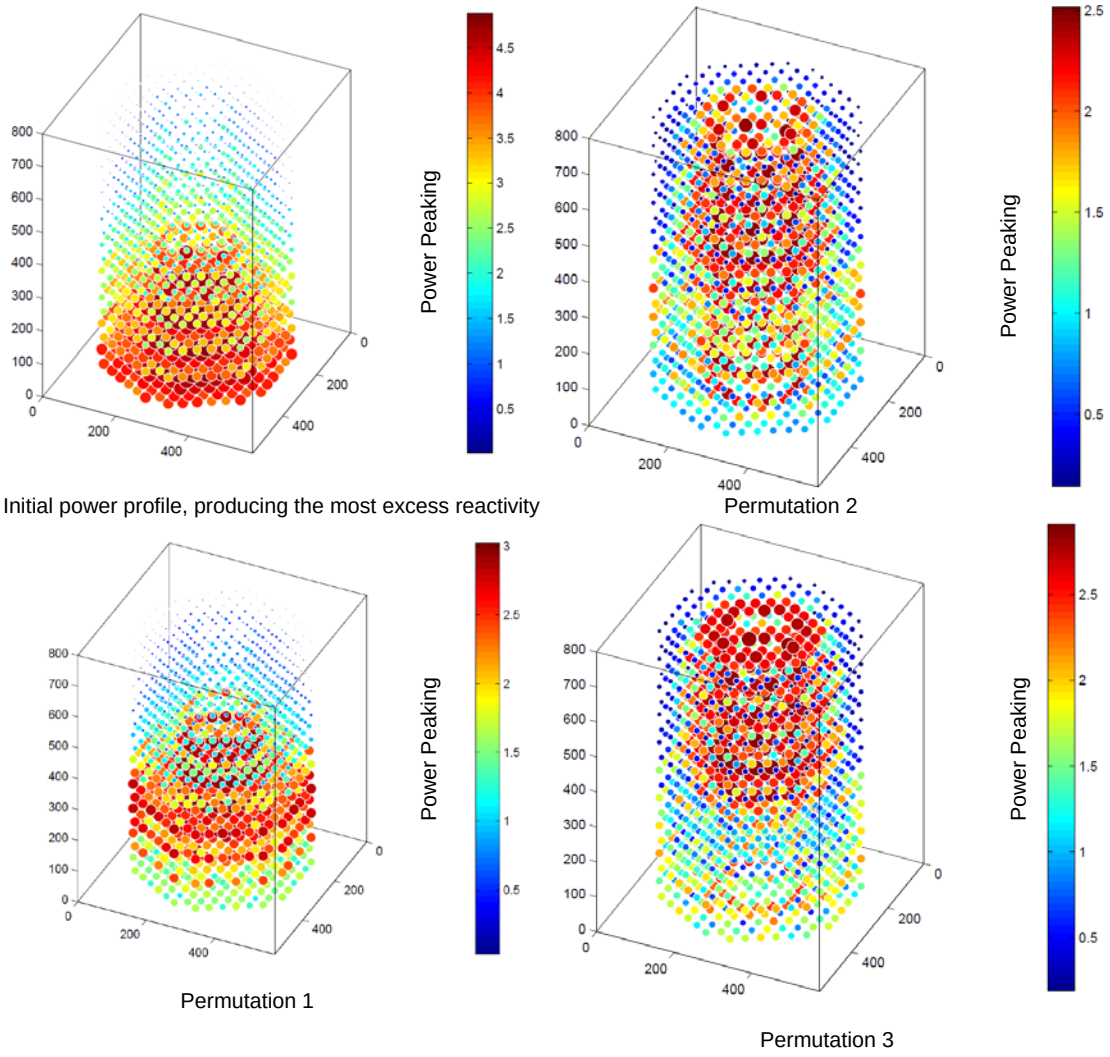

Fig. 46. Shuffling permutations without spatial flux and cross-section updating

Figure 46 shows that without updating the nuclear data, undesired results are produced. As the algorithm shuffles fresh blocks into less power producing locations, the grouping of fresh blocks causes a change in the spatial power profile. This is the result of the large mean free path of neutrons in the graphite moderated system. In the final permutation the freshest blocks are located near the top of reactor very close to control rods, which are at half active core height. These blocks still produce a large excess of power compare to the average block but the neutron economy of the system is sacrificed due to the proximity of the control rods. This system had a k-eff below 1.

Allowing for the updating of the spatial flux profile the following power profile is produce. The spatial flux and cross-section were only updated once for this model but it shows an immediate reduction in power peaking. The algorithm still has a power peaking maximum of 2, which this shuffle core only slightly exceeds. This is shown in Figure 47.

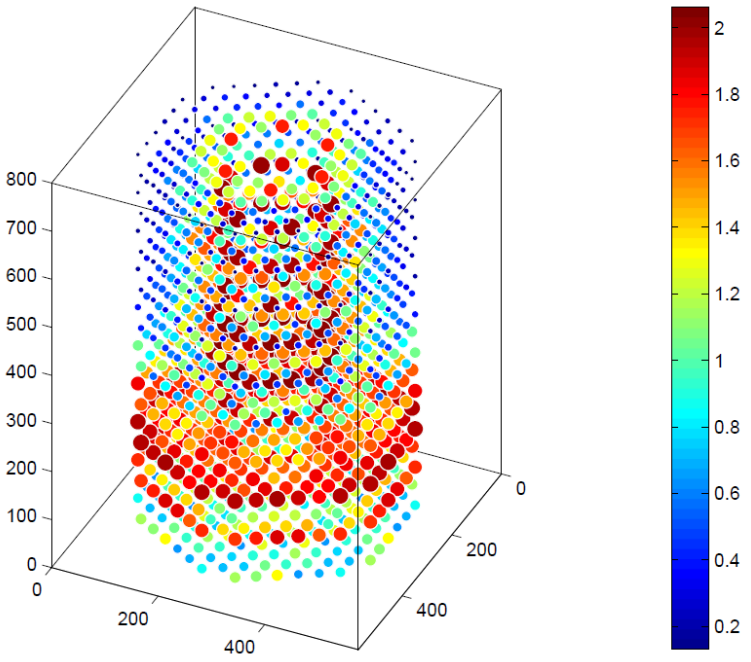

Fig. 47. Shuffling permutation with single spatial flux and cross-section update

To compare the results of an arbitrary shuffling pattern, a shuffle pattern done interactively is compared to one produced after a single update, to one produce from a random shuffle, and the initial most reactive block. The interactively produced shuffle patter was produced by placing the freshest fuel in the second ring from the outside, then moving the fuel after the first burn to the most outward ring and finally placing the fuel blocks that have been in the core for two burn periods in the inner most rings. This is shown in Figure 48. The arbitrary shuffling patter is produced from a random 3D block shuffle.

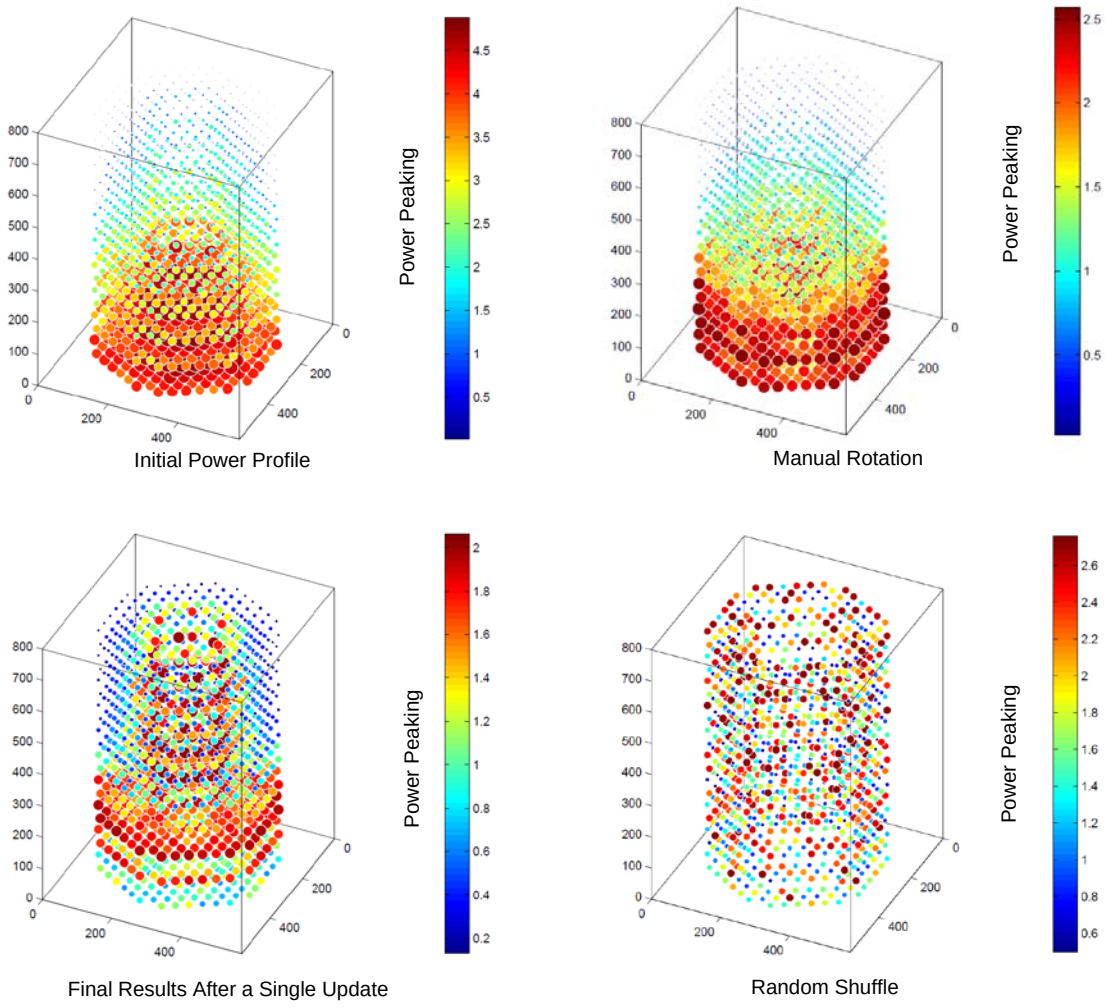

Fig. 48. Comparison of shuffling algorithms

The effect of control rods is seen in each subplot except the random shuffle. The random shuffle core did not have control rods. The interactive shuffling method was produce with a basic rotational scheme, but without knowledge of control rod height, power peaking occurs in regions of the core not affected by the rotation. Only the shuffling scheme from the propose shuffling algorithm produces a core that meets the operation constraint that any fuel block will produce no more then 2 times the average block power. As can be seen, by using a predictive method of 3D block excess reactivity any number of constraints can be met, if possible, by the simple permutation process and nuclear data updating used by the proposed shuffling algorithm.

V. CONCLUSIONS AND RECOMENDATIONS

In this dissertation, a physics based 3D multi-directional reloading algorithm for prismatic DB-VHTR was developed and tested to meet DB-VHTR operation constraints utilizing a high fidelity neutronics model. The argument for DB-VHTR deployment in adapted open cycles and closed cycles due to their inherit ability to quickly destroy a large percentage of TRUs isotopes in a single pass was demonstrated. Reduction of TRUs in a DB-VHTR utilizing a full vector of TRUs from LWR SNF was shown for both a single and Two-Fuel composition core. Single fuel composition cores utilizing a full vector of TRUs, was shown to approach an average destruction of 15%, furthermore core life's to obtain this destruction rate were in excess of 12 years at 600 MWth. Two-Fuel composition cores, utilizing elemental separation of the TRU vectors into a stream of NpPu and AmCm were shown to have possible destruction rates in excess of 50% over a core lifetime of three years. The neutronics code MCNPX was used for physic calculations in this dissertation, and required the development of a high fidelity automated model that allows design flexibility and metric tracking.

Taking advantage of the 3D DB-VHTR model, a physics-based reloading algorithm and the corresponding computational sequence for shuffling fuel in prismatic HTGRs was developed. The reloading algorithm includes detailed mapping of the DB-VHTR performance domain of several fuel compact designs and fuel block loading patterns. It required an automated sequence based on given constraints and nuclides vectors to meet defined performance objectives. Total TRU destruction and core life were accounted for as performance objectives. Operational differences of TRU fuel DB-VHTRs and LEU fuel VHTRs were compared finding excess reactivity to be a larger function of C/HM in LEU VHTRs compared to total fuel loading for TRU fueled DB-VHTRs. Single fuel system domain for a single fuel vector was searched for possible use in DB-VHTRs based on a computation scheme utilizing BOL whole core neutronic calculations with MCNPX. Performance of the BOL domain from multi-dimensional permutations were evaluated.

Utilizing the high fidelity 3D model of a DB-VHTR and the reloading algorithm, sample studies were performed for DB-VHTR behavior under shuffling conditions to demonstrate performance of the developed algorithm and take advantage of the algorithm to provide unique physics insight into DB-VHTRs and their ability to destroy TRUs recovered from LWR spent fuel. Depletion of whole core high fidelity DB-VHTR neutronic model in OTTO mode of several single fuel permutations utilizing the depletion ability of MCNPX were executed to evaluate effects of a non-intelligent random 3D shuffling scheme on in-core metrics and EOL metrics. These permutations were compared to non-shuffled cases and showed no major improvement of total TRU destruction, but decrease in TRU destruction variation on a single assembly basis. The in-core metric of power peaking was shown to be worsened in shuffled cases. The effects of a radial and axial only random shuffle were compared to whole 3D random cases for a single fuel DB-VHTR model.

The Two-Fuel system domain for a single fuel vector was searched for possible use in DB-VHTRs based on a computation scheme utilizing BOL infinite assembly neutronic calculations with MCNPX. Performance of the BOL domain from multi-dimensional permutations of Two-Fuel assemblies were evaluated using a 4D plotting scheme that characterized TRU mass loading, kernel dimensions and BOL excess reactivity. Addit ion of U238 into the LWR SNF TRU fuel feed was analyzed. This analysis showed complex inter-dependencies of resonance self shielding of each fuel type and whole system TRU mass loadings. Depletion of selected assembly permutation based on BOL neutronics studies of the Two-Fuel systems, showed possible tradeoffs in core life and TRU-destruction, with shorter core life and smaller fuel kernels producing higher destruction and shorter core life.

The need of a proper shuffling algorithm that considers effects of small core permutations in meeting operation constraints was demonstrated. Effects of non-intelligent shuffling algorithms were compared to that developed for this dissertation. Utilizing a Two-Fuel assembly permutation from within the Two-Fuel system domain

for a single fuel vector evaluated earlier in the dissertation, the developed shuffling algorithm for this dissertation was tested. The need of neutronic data updating during the shuffling process was shown. A single neutronic data update was shown to improve the shuffling algorithm effectiveness.

The general nature of the code system developed for the use of this dissertation's developed shuffling algorithm demonstrated the large DB-VHTRs design domain affects the small acceptable performance domain. The large computational time from MCNPX depletion and BOL calculation hinders the swath of the operational domain's optima solution search. It is recommended that the use of a faster neutronics code such as a diffusion code should be use to increase the speed of this search. Such a code would have to be benchmarked to ensure that it accurately predicts the complex behavior of DB-VHTR assembly movement and multi-dimensional fuel permutations. Furthermore, fuel selection should have selection criteria based on fuel handling constraints, such as heat production and neutral particle radiation emission.

REFERENCES

1. L. Baetsle, “Application of Partitioning/Transmutation of Radioactive in Radioactive Waste Management,” Nuclear Research Centre of Belgium, Mol, Belgium (2001).

2. “The Atomic Energy Act of 1982,” As Amended. Nuclear Regulatory Legislation, 107th Congress; 1st session, (June 2002) Office of the General Counsel. US Nuclear Regulatory Commission.

3. Nuclear Energy Research Advisory Committee and the Generation IV International Forum, “Generation IV Roadmap Fuel Cycle Assessment Report,” US DOE (2002).

4. M. Richard, “Final Environmental Impact Statement,” Department of Energy, Office of Civilian Radioactive Waste Management, Washington, D.C., DOE/EIS-0250 (2002).

5. DOE, “Report to Congress: Spent Nuclear Fuel Recycling Program Plan,” Department of Energy, Washington, D.C. (2006).

6. “Fuels and Materials for Transmutation: A Status Report,” NEA No. 5419, (2005).

7. T. Taiwo and R. Hill, “Summary of Generation-IV Transmutation Impacts,” Nuclear Energy Division, Argonne National Laboratory (2005).

8. Nuclear Energy Agency, “Accelerator-driven Systems (ADS) and Fast Reactors (FR) in Advanced Nuclear Fuel Cycles,” Nuclear Development-NEA (2002).

9. P. V. Tsvetkov, “Utilization of Minor Actinides as a Fuel Component for Ultra-Long Life VHTR Configurations: Designs, Advantages and Limitations: First Year Report,” Texas A&M University, College Station, Texas (2006).

10. S. Bays, H. Zhang, and M. Pope, “Deep Burn Fuel Cycle Integration: Evaluation of Two-Tier Scenarios.” Report INL/EXT-09-15915, INL, (2009).

11. L. Taylor, “Fort Saint Vrain HTGR (Th/U carbide) Fuel Characteristics for Disposal Criticality Analysis.” Report DOE/SNF/REP-060 (2001).

12. L. Demick, and D. Vandel, “Next Generation Nuclear Plant Pre-Conceptual Design Report.” Report INL/EXT-07-12967 (2007).

13. C. Rodriguez, A. Baxter, D. Mceachern, M. Fikani and F. Venneri, “Deep-Burn: Making Nuclear Waste Transmutation Practical.” *Nuclear Engineering and Design*, **222**(2-3): 299-317 (2003).

14. T. Kim, T. Taiwo, R. Hill and W. Yang, “A Feasibility Study of Reactor-Based Deep-Burn Concepts.” Report ANL-AFCI-155 (2005).

15. G. Bruna, R. Labella, and C. Trakas, “Uncertainty Analysis and Optimization Studies on the Deep-Burner-Modular Helium Reactor for Actinide Incineration,” PHYSOR, ANS (2004).

16. N. Kodochigov, Yu. Sukharev, E. Marova, N. Ponomarev-Stepnoy, E. Glushkov, et al., “Neutronic Features of the GT-MHR Reactor.” *Nuclear Engineering and Design*, **222**(2-3): 161-171 (2003).

17. P. MacDonald, “NGNP Preliminary - Point Design Results of the Initial Neutronics and Thermal-Hydraulics Assessments,” Report INEEL/EXT-03-00870, (2003).

18. I. Das and J. Dennis, “A Closer Look at Drawbacks of Minimizing Weighted Sums of Objective for Pareto Set Generation in Multicriteria Optimization Problems,” *Structural Optimization*, **14**(1)**,** 63-69, (1997).

19. D. Dumitrescu, Crina Groşan and Mihai Oltean, “Evolving Continuous Pareto Regions,” *Evolutionary Multiobjective Optimization: Theoretical Advances and Applications*, 167-199, (2005).

20. M. Ehrgott, J. Figuerira, and S. Greco, “Mutiobjective Programming, in Multiple Criteria Decision Analysis: State of the Art Surveys,” *International Series in Operations Research & Management Science*, **78**, 1-1045 (2005).

21. C. Grosan, A. Abraham, and M. Nicoara, “Search Optimization Using Hybrid Particle Sub-Swarms and Evolutionary Algorithms,” *International Journal of Simulation Systems, Science & Technology*, **6**(10-11), 60-79, 2005.

22. A. Messac and C. Mattson, “Generating Well Distributed Sets of Pareto Points for Engineering Design Using Physical Programming,” *Optimization and Engineering*, **3**(4), 431-450, (2002).

23. A. Messac, A. Yahaya, and C. Mattson, “The Normalized Normal Constraint Method for Generating the Pareto Frontier,” *Structural and Multidisciplinary Optimization*, **25**(2) : 86-98, (2003).

24. A. Quist, R. Geemert, J. Hoogenboom, T. Illes C. Roos and T. Terlay, “Application of Nonlinear Optimization to Reactor Core Fuel Reloading,” *Annals of Nuclear Energy* **26**: 423-448 (1999).

25. S. Bandyopadhyay, S. Saha, U. Maulik, and K. Deb, “A Simulated Annealing Based Multiobjective Optimization Algorithm: AMOSA,” *IEEE Transactions on Evolutionary Computation*, **12**(3), 269-283 (2008).

26. Y. Kim and V. Francesco, "Optimization of One-Pass Transuranic Deep Burn in a Modular Helium Reactor." *Nuclear Science and Engineering*, **160**, 59-74, (2008).

27. A. Talamo and G. Waclaw "Incineration of Light Water Reactors Waste in High Temperature Gas Reactors: Axial Fuel Management and Strategy for Transmutation of Americium and Curium." *Nuclear Science and Engineering*. **156**(2), 244-266, (2007).

28. A. Chipperfield and P. Fleming, "Multi-Objective Gas Turbine Engine Controller Design Using Genetic Algorithms," IEEE *Transactions on Industrial Electronics*, **43**, 583 - 587 (1996).

29. M. Doumpos, Y. Marinakis, M. Marinaki, and C. Zopounidis, "An Evolutionary Approach to Construction of Outranking Models for Multicriteria Classification: The Case of the ELECTRE TRI Method," *European Journal of Operational Research*, **199**, 496-505 (2009).

30. S. Peigin and B. Epstein, "Multi-Constrained Aerodynamic Design of Business Jet by CFD Driven Optimization Tool," *Aerospace Science and Technology*, **12**, 125-134 (2008).

31. J. Wang, J. Zhang, and X. Wei, "Evolutionary Multi-Objective Optimization Algorithm with Preference for Mechanical Design," Report LNAI 3930, (2006).

32. F. Caldas and R. Schirru, "Parameterless Evolutionary Algorithm Applied to the Nuclear Reload Problem," *Annals of Nuclear Energy*, **35**, 583-590 (2008).

33. R. Domingos and R. Schirru, "Particle Swarm Optimization in Reactor Core Design," *Nuclear Science and Engineering*, **152**, 197-203 (2006).

34. S. Jiang, A. K. Ziver, J. N. Carter, C. C. Pain, A. J. H. Goddard, S. Franklin, and H. J. Phillips, "Estimation of Distribution Algorithms for Nuclear Reactor Fuel Management Optimization," *Annals of Nuclear Energy*, **33**, 1039-1057 (2006).

35. Y. Kim, C. K. Jo, and J. M. Noh, "Optimization of Axial Fuel Shuffling Strategy in a Block-Type VHTR," *Transactions of Amer. Nucl. Soc./European Nucl. Soc.*, **97**, 406-407 (2007.)

36. A. M. M. de Lima, R. Schirru, and F. Silva, "A Nuclear Reactor Core Fuel Reload Optimization Using Artificial Ant Colony Connective Networks," *Annals of Nuclear Energy*, **35**, 1606-1612 (2008).

37. J. L. Montes, J. L. Francois, J. J. Ortiz, C. Martin-del-Campo, and R. Perusquia, "Local Power Peaking Factor Estimation in Nuclear Fuel by Artificial Neural Networks," *Annals of Nuclear Energy*, **36**, 121-130 (2009).

38. S. Seker, E. Turkcan, E. Ayaz, and B. Barutcu, "Artificial Neural Networks for Dynamic Monitoring of Simulated-Operating Parameters of High Temperature Gas-Cooled Engineering Test Reactor (HTTR)," *Annals of Nuclear Energy*, **30**, 1777-1791 (2003).

39. S. Yilmaz, K. Ivanov, S. Levine, and M. Mahgerefteh, "Application of Genetic Algorithms to Optimize Burnable Poison Placement in Pressurized Water Reactors," *Annals of Nuclear Energy*, **33**, 446-456 (2006).

40. A. Talamo and W. Gudowski, "A Deep Burn Fuel Management Strategy for the Incineration of Military Plutonium in the Gas Turbine-Modular Helium Reactor Modeled in a Detailed Three-Dimensional Geometry by the Monte Carlo Continuous Energy Burnup Code." *Nuclear Science and Engineering*, **153,** 172-183, (2006).

41. T. K. Kim, T. A. Taiwo, R. N. Hill, and W. S. Yang, "A Feasibility Study of Reactor-Based Deep-Burn Concepts," ANL Report ANL-AFCI-155 (2005).

42. C. Rodriguez, A. Baxter, D. McEachern, M. Fikani, and F. Venneri, "Deep Burn: Making Nuclear Waste Transmutation Practical," *Nuclear Engineering and Design*, **222**, 299-317 (2003).

43. R. M. Versluis, F. Venneri, D. Petti, L. Snead, and D. McEachern, "Project Deep-Burn: Development of Transuranic Fuel for High-Temperature Helium-cooled Reactors," *Proc. 4th Intern. Top. Meeting on High Temperature Reactor Technology*, Washington D.C., USA HTR2008-58325 (2008).

44. A. Alajo, "Impact of PWR Spent Fuel Variations on TRU-Fueled VHTRs," MS Thesis, Department of Nuclear Engineering, Texas A&M University (2007).

45. "Report to Congress on Advanced Fuel Cycle Initiative: The Future Path for Advanced Spent Fuel Treatment and Transmutation Research," Report 03-GA50439-06, U.S. DOE (2003).

46. C. W. Forsberg, "Refueling Options and Considerations for Liquid-Salt-cooled Very High-Temperature Reactors," ORNL Report ORNL/TM-2006/92 (2006).

47. T. Hertzler, "Technical and Regulatory Review of the Rover Nuclear Fuel Process for Use on Fort St. Vrain Fuel," Report EGG-WTD-10550, Office of Environmental Restoration and Waste Management, U.S. DOE (1993).

48. L. L. Taylor, "Fort Saint Vrain HTGR (Th/U Carbide) Fuel Characteristics for Disposal Criticality Analysis," DOE/SNF/REP-060, Office of Environmental Management, U.S. DOE (2001).

49. A. Talamo and W. Gudowski, "Studies of a Deep Burn Fuel Cycle for the Incineration of Military Plutonium in the GT-MHR Using the Monte-Carlo Burnup Code," *Proc. PHYSOR 2004-The Physics of Fuel Cycles and Advanced Nuclear Systems: Global Developments*, Chicago, Illinois, April 25-29, 2004, on CD-ROM. (2004).

50. G. Brunna, R. Labella, C. Trakas, A. Baxter, C. Rodriguez, and F. Venneri, "Uncertainty Analysis and Optimization Studies on the Deep-Burner-Modular Helium Reactor (DB-MHR) for Actinide Incineration," *Proc. PHYSOR-2004 - The Physics of Fuel Cycle and Advanced Nuclear System: Global Developments*, Chicago, Illinois, April 25-29, 2004, on CD-ROM. (2004).

51. A. Talamo, W. Gudowski, and F. Venneri, "The Burnup Capabilities of the Deep Burn Modular Helium Reactor Analyzed by the Monte Carlo Continuous Energy Code MCB," *Annals of Nuclear Energy*, **31,** 173-196 (2004).

52. A. Talamo, W. Gudowski, J. Cetnar, and F. Venneri, "Key Physical Parameters and Temperature Reactivity Coefficients of the Deep Burn Modular Helium Reactor Fueled with LWR's Waste," *Annals of Nuclear Energy*, **31,** 1913-1937 (2004).

53. G. Baccaglini, S. Ball, T. Burchell, B. Corwin, T. Fewell, et al, "Very High Temperature Reactor (VHTR) Survey of Materials Research and Development Needs to Support Early Deployment," INL Report INEEL/EXT-03-00141 (2003).

54. T. Burchell, R. Bratton, and W. Windes, "NGNP Graphite Selection and Acquisition Strategy," ORNL Report ORNL/TM-2007/153 (2007).

55. D. L. Hanson, "Screening Tests for Selection of VHTR Advanced Fuel," Report PC-000510, General Atomics (2003).

56. C. K. Jo, Y. Kim, and J. M. Noh, "Minimization of the Reactivity Swing by Burnable Poisons in VHTR," *Transactions of Amer. Nucl. Soc./European Nucl. Soc.*, **97**: 402-403 (2007.)

57. P. E. MacDonald, "NGNP Preliminary Point Design-Results of the Initial Neutronics and Thermal-Hydraulics Assessments," INL Report INEEL/EXT-03-00870 Rev. 1 (2003).

58. P. M. Mills, R. Soto, and G. Gibbs, "Next Generation Nuclear Plant Pre-Conceptual Design Report," NGNP Project, INL Report INL/EXT-07-12967 Rev. 1 (2007).

59. W. E. Windes, T. D. Burchell, and R. Bratton, "The Next Generation Nuclear Plant Graphite Program," *Proc. 4th Intern. Conf. on HTR Technology (HTR2008)*, Washington D.C., USA, paper HTR2008-58138, 1-7, ASME, INL Report INL/CON-08-14693 (2008).

60. J. K. Wright and W. R. Lloyd, "Analysis of Potential Materials for the Control Rod Sleeves of the Next Generation Nuclear Plant," ORNL Report INL/EXT-06-11614 (2006).

61. C. Rodriguez, A. Baxter, D. McEachern, F. Venneri, and D. Williams, "Deep Burn Transmutation of Nuclear Waste," *Proc. Intern. Conf. on HTR Technology (HTR2002),* 1-5 (2002).

62. C. Rodriguez, A. Baxter, D. McEachern, M. Fikani, and F. Venneri, "Deep Burn: Making Nuclear Waste Transmutation Practical," *Nuclear Engineering and Design*, **222**, 299-317 (2003).

63. A. Talamo and W. Gudowski, "Incineration of Light Water Reactor Waste in High-Temperature Gas Reactors: Axial Fuel Management and Efficiency of Americium and Curium Transmutation," *Nuclear Science and Engineering*, **156**, 244-266 (2007).

64. Y. Kim, C. K. Jo, and J. M. Noh, "Optimization of Axial Fuel Shuffling Strategy in a Block-Type VHTR," *Transactions of Amer. Nucl. Soc./European Nucl. Soc.*, **97**, 406-407 (2007).

65. Y. Kim and F. Venneri, "Optimization of One-Pass Transuranic Deep Burn in a Modular Helium Reactor," *Nuclear Science and Engineering*, **160**, 59 -74 (2008).

66. H. A. Abbass and R. Sarker, "The Pareto Differential Evolution Algorithm," *Intern. Journal on Artificial Intelligence Tools*, **11**(4), 531-552 (2001).

VITA

Tom Goslee Lewis III received his Bachelor of Science, Master of Science and Doctorate of Philosophy degree in nuclear engineering from Texas A&M University in 2005, 2007 and 2010, respectively. He worked at the Yucca Mountain Project in Las Vegas, Nevada starting in May 2007 and leaving August 2008 to finish his PhD.

Dr. Lewis may be reached at 414 East 27th Street, Houston, TX 77008. His email is tglewis3@gmail.com.